10-29-2018

Analysis of Fluvial Scroll Bar Development With Surface Wave Inversion: False River, Louisiana

Blake Odom
Louisiana State University and Agricultural and Mechanical College

ANALYSIS OF FLUVIAL SCROLL BAR DEVELOPMENT WITH SURFACE WAVE INVERSION: FALSE RIVER, LOUISIANA

A Thesis

Submitted to the Graduate Faculty of the
Louisiana State University and
Agricultural and Mechanical College
In partial fulfillment of the
requirements for the degree of
Master of Science

in

The Department of Geology and Geophysics

by
Blake Odom
B.S., Washington and Lee University, 2016
December 2018

In memory of Barbara Lumsden.

ACKNOWLEDGEMENTS

I thank Dr. Juan Lorenzo for his unyielding patience, sagely advice, and geophysical MacGyverism. Throughout our time together I have truly learned what it means to be a scientist. I also thank my committee members Dr. Peter Clift and Dr. Kory Konsoer for your guidance and input during my research.

Thank you to my fellow brothers-and-sisters-in-arms in the department: Martial Morrison, Nathan Benton, Derek Goff, Abah Omale, Adam Gostic, and Liz Olson.

Finally, I'd like to thank my parents, family, and friends without whose support I would not have been able to achieve this Master's.

TABLE OF CONTENTS

ABSTRACT

The development of ridge-and-swale scroll bar topography of meandering river point bars is not well understood. We hypothesize that scroll bars formed during lateral accretion by the landward migration of transverse bars. To explore this, we relate the scroll bar topography to the internal sedimentary structure. We acquire, invert, and interpolate three pseudo-2D shear wave velocity profiles in two regions of the False River point bar, a Mississippi river oxbow lake in Pointe Coupee Parish Louisiana. Prior studies provide electrical conductivity well logs and cores as well as SH seismic reflection images along the same seismic surveys. LiDAR elevation data provide maps of the ridge-and-swale topography bisected by the seismic surveys. The uppermost 10-15 meters of point bar sediments cannot be well-imaged by reflection seismic processing techniques. From the same seismic data acquired for reflection processing, we extract surface wave signals for dispersion interpretation. The dispersion data are then inverted using a direct-search nearest neighbor algorithm. We then interpolate the inversion results to create pseudo-2D shear wave velocity profiles that image the uppermost 12 meters of sediment. Well log and core data are then correlated with these velocity profiles during interpretation. This study finds that velocity layers dip in two directions away from the crests of scroll bar ridges, parallel to the ridge and swale topography in both overbank sediments and the underlying IHS zone. We interpret this finding as evidence attributing False River scroll bar development to the landward migration of transverse bars, as this parallel sedimentary architecture suggests a stratigraphic link between the IHS and surface topography. A competing model for scroll bar development that attributes individual scrolls to single low-frequency high-discharge flooding events does not suggest this stratigraphic link.

CHAPTER 1. INTRODUCTION

1.1. Research Problem and Purpose

Despite being a heavily studied reach of the Mississippi River, the topographic morphology of floodplain features such as scroll-bars are poorly understood (Lewin & Ashworth 2014). Past studies of preserved point-bar architecture in outcrop often cannot resolve the very uppermost strata of these complexes nor paleo-topographic features like scroll-bars (Durkin et al, 2017). Numerical and experimental studies addressing scroll-bar development have been successful in re-creating these features, but a lack of two-dimensional subsurface information of modern scroll bar topography remains (van Dijk et al, 2013; van de Lageweg 2014).

The purpose of this thesis is to constrain the near surface fluvial architecture of locations within the False River point bar in False River, Louisiana in order to understand scroll-bar development. I specifically seek to examine the relationship between surface topography and sub-surface architecture obtained from surface wave inversion.

1.2. Scroll Bar Development

The specific processes responsible for the creation of ridge and swale topographies on point bars are not fully understood (Lewin and Ashworth, 2014). Although characteristic of meandering rivers and widely observable in fluvial settings across the globe in varying climate and geological regions, a comprehensive and uniformly applicable model does not exist (Nanson and Croke, 1992). Instead, two different models attempt to explain the phenomena. Both are valid and observable, yet each fails to explain alternative conditions that are also known to form scroll-bars in other river systems with varying scale, seasonal discharge, vegetation, and sediment load (Baar, 2013).

The first model is known as the discharge-model, or flood stage model (Hickin, 1974). This model states that secondary currents deliver rapidly eroding cutbank sediment to the inner bank during high-discharge, low-frequency events. At the inner bank, this sediment is deposited where bank shear stress is low in the flow separation zone. When the river discharge decreases back to more normal stages, this deposited sediment is left behind as an 'initial ridge' which is then colonized by vegetation, while low-stage erosion steepens the stream-ward side of the deposit (Figure 1.1) (Leclerc and Hickin, 1997; Nanson, 1980). Subsequent major flood events will create a new ridge stream-ward, thus explaining this topography seen on point bars. In this model, it is important to note that the channel width is constantly maintained, as cutbank erosion occurs, so too does lateral, stream-ward migration of the point bar. Strick (2016) presents the same model with a more detailed hydrodynamic representation (Figure 1.2). The multiple iterations of this flood-stage scroll model describe the scrolls as fundamentally vertically accreted, fine grained, suspended-load products.

However reasonable this mechanism, experimental work conducted with physical models have initiated scroll-bar development in sand tanks where discharge was maintained constant (van de Lageweg et al., 2014). It is also important to note that the model somewhat relies on the presence of vegetation to preserve the ridges, whereas scroll bars are known to develop in completely arid, near vegetation-less systems (Pyrce and Ashmore, 2005). Although clearly not applicable to all fluvial environments, the flood-stage model is often used because it was the first offered model to the scroll bar problem (Baar, 2013).

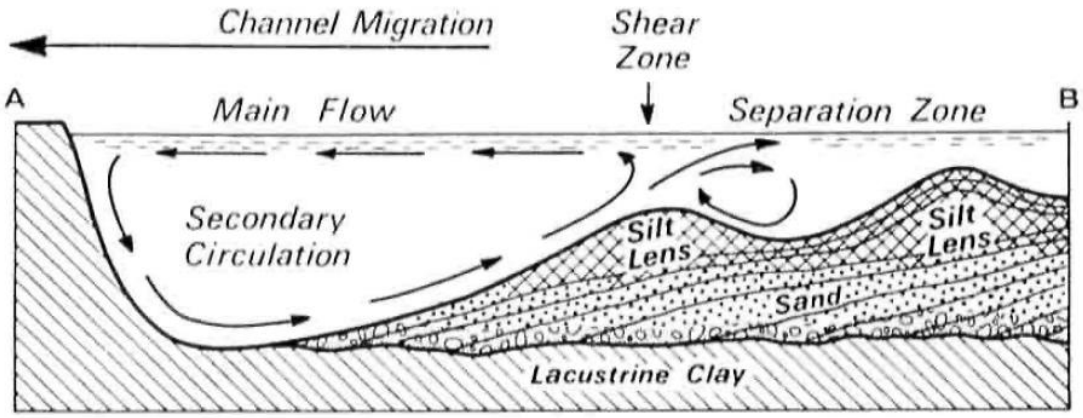

Figure 1.1. Flood stage model of scroll bar development. In this model, the fine-grain dominated ridges are the products of secondary circulation during low-frequency, high discharge events. The ridge to the left is the one being formed by low bed shear stress zone, while the right ridge was previously formed by a prior flood event. From (Nanson, 1980).

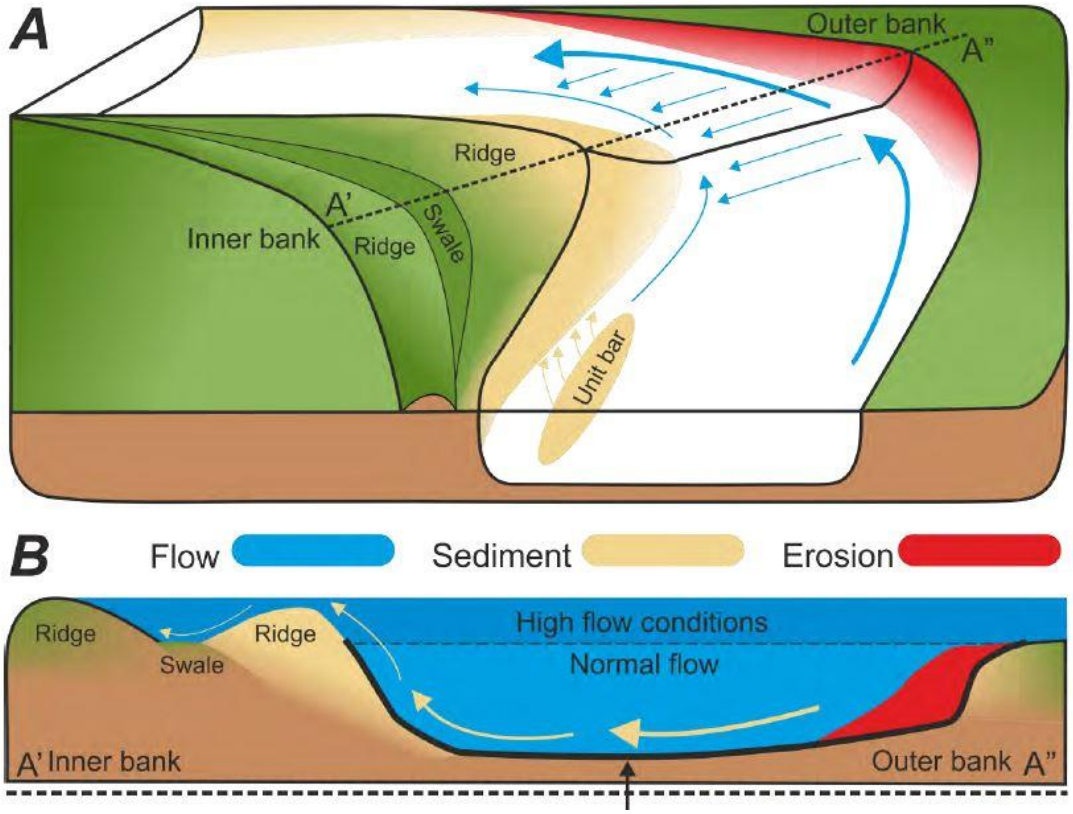

Figure 1.2. Recasting of flood-stage model of scroll bar development. A. 3-D model of basic point bar development B. Secondary current flow lines indicate the hydrodynamic basis for the deposition of the ridges during high flow conditions. Erosion occurring on the cutbank or 'outer bank'. From (Strick, 2016) adapted from (Nanson, 1980).

A second approach describes scroll bars as forming from the downstream, landward migration of transverse bars or unit bars (Jackson, 1976; Kleinhans and van den Berg, 2011; Sundborg, 1956; van de Lageweg et al., 2014). In these models, mid-channel sandy unit bars migrate toward the inner-bank because of a dominant secondary flow (Figures 1.3, 1.4). Often aided by debris from trees and other material, these bars will eventually become part of the point bar complex itself as ridges, with the swales forming as a result of non-deposition in zones of extremely low bed shear stress where even sediment deposition is not possible (Sundborg, 1956). In this model the scrolls are more products of the lateral accretion of the point bar (Figure 1.5). It is important to note that the physical models utilized in these experiments do not scale up consistently (Froude scaling) (Kleinhans, 2010). These models also typically involve vegetation maintaining the ridges to a certain degree also (Jackson, 1976). However, aside from vegetation not being necessary for scroll bars to appear in extremely arid environments, Nanson (1980) demonstrates that scrolls can develop both up and downstream.

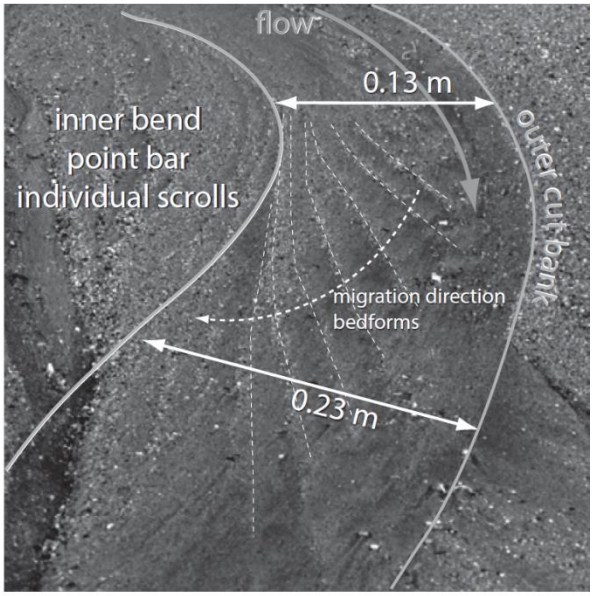

Figure 1.3. Photograph of scroll bar development observed in sand table experimentation. In-channel bedforms were observed migrating downstream and toward the inner bend forming a scrolled floodplain when both discharge and sedimentation were held constant. (van de Lageweg et al., 2014)

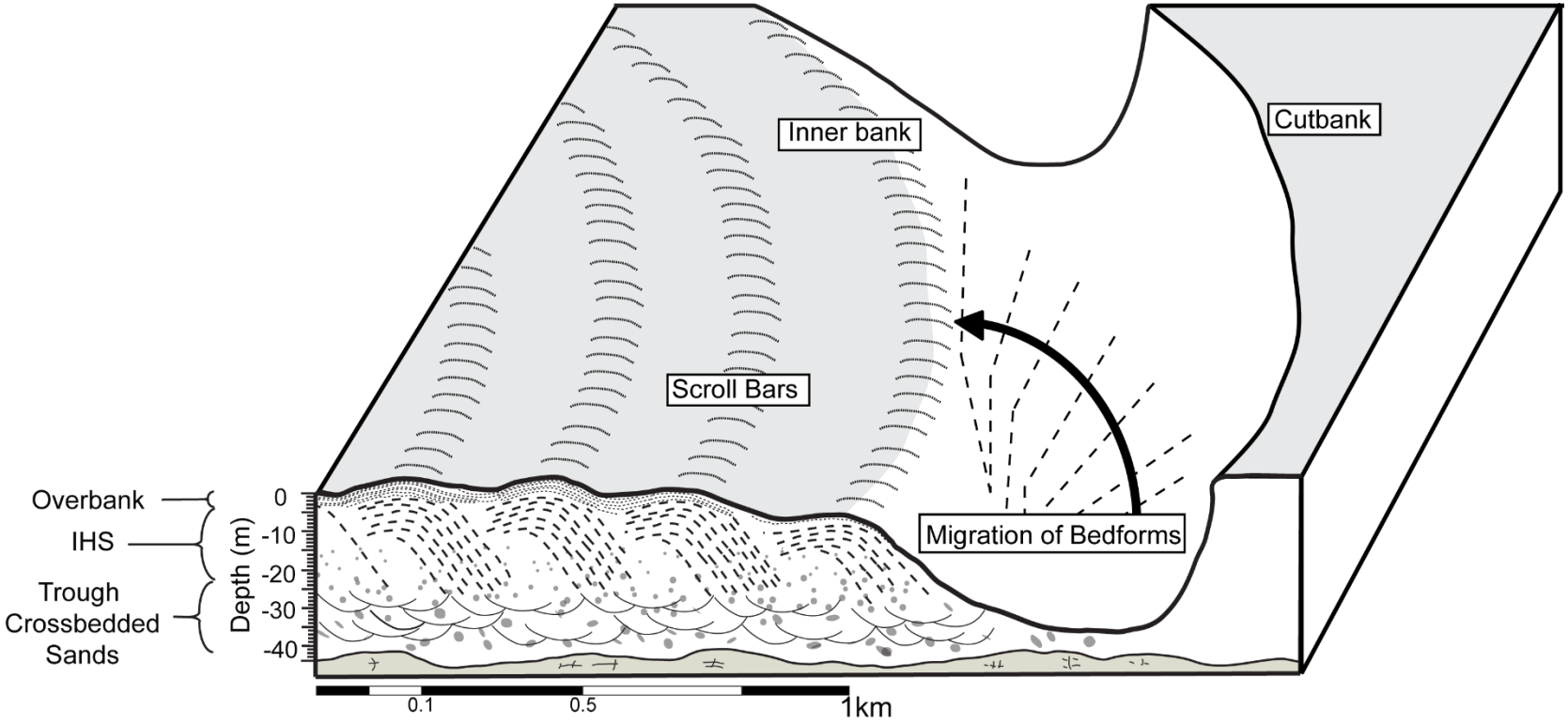

Figure 1.4. A simplified 3D cartoon that illustrates the features shown in Figure 1.3. In-channel bedforms migrate towards the inner bank to form individual scroll bars, the evidence of which can be seen in the cross-sectional view of a point bar. Scales of channel width, scroll bar spacing, and the depth of stratal sections are matched to False River based on well interpretations and map lengths.

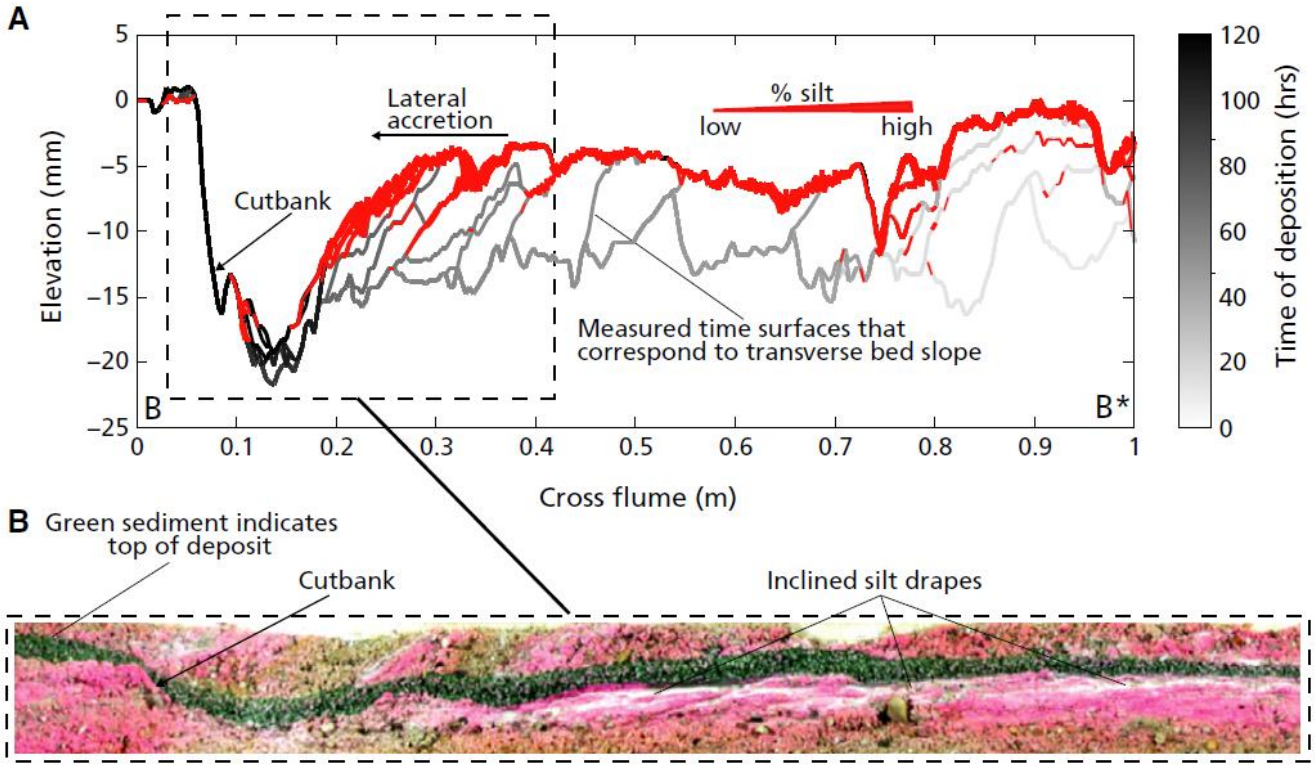

Figure 1.5. A simplified interpretation (A) and a sediment peel (B), from transverse bar migration developed scroll bars. The whiter sediments represented finer grained materials, while the pinkish materials are the result of pink dye used in the water during the experiment. From the experiment it was inferred that the inclined silt drapes corresponded to the transverse beds that migrated to build the scroll bar ridges themselves. These scroll bars were formed while discharge and sediment were kept constant, while outer bank erosion was manually stimulated by removal of materials to cause lateral migration (van de Lageweg et al., 2014).

Spatial analysis of Lower Mississippi ridge and swale topography and geometry also support this model. Utilizing aerial photography and Lidar elevation maps of 10 larger point bars in the immediate vicinity of the False River point bar, spatial analysis reveals a very close link between river channel width and scroll bar periodicity and spacing (Strick et al., 2018). Scroll bar periodicity calculated within these point bars averages 25% of the river channel width, suggesting a strong relationship between the maintenance of river channel width equilibrium and scroll formation (Figure 1.6). During the experimental observation of transverse bar migration forming scroll bars, the same relationship is calculated (van de Lageweg et al., 2014). A scroll development model that credits flood-stage as the driver shouldn't appear to be linked to channel width as strongly as discharge seasonality. Additionally, 19 other rivers across the world considered in the study showed scroll periodicity falling between 20-60% of the river channel, itself suggesting that rivers must migrate a minimum distance to facilitate scroll formation (Figure 1.7) (Strick, 2016).

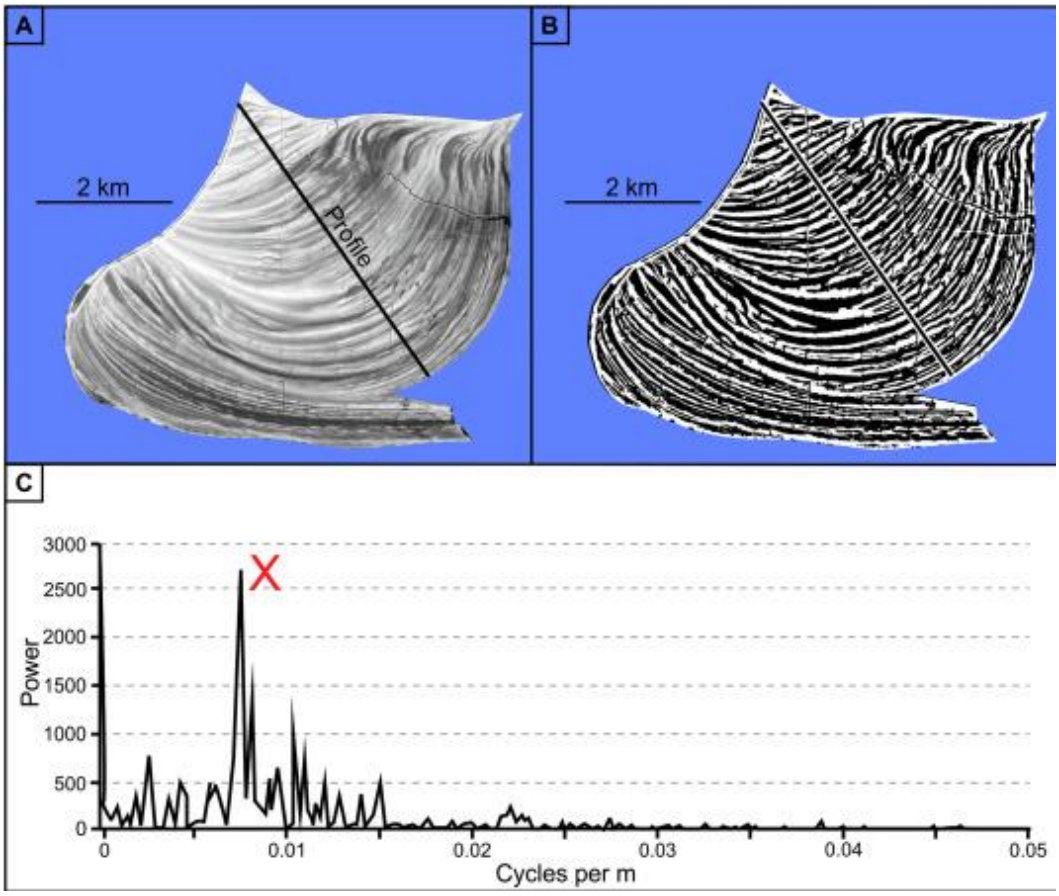

Figure 1.6. (A) meander bend on the lower Mississippi Lidar image. (B) binary output of the same lidar map using Atuomatic Local Thresholding segmentation where white=ridge and black=swale. (C) Frequency power spectrum derived from the binary profile. The red X marks a peak equal to a spacing of a scroll every 173 meters (Strick et al., 2018).

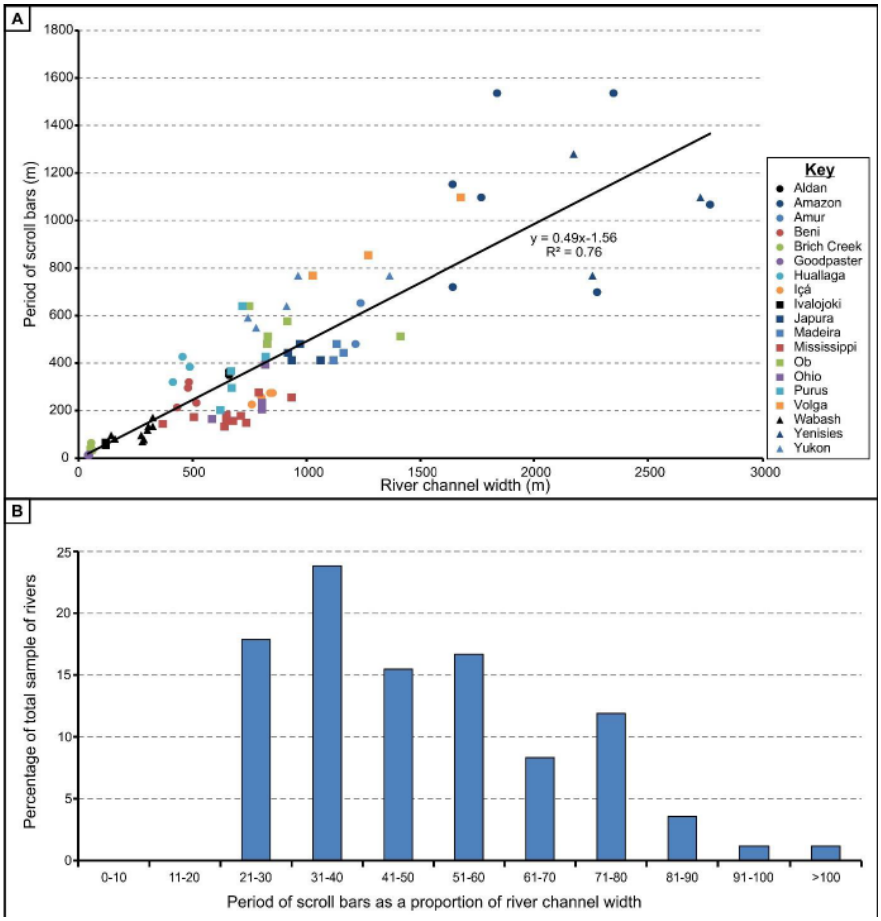

Figure 1.7. Relationship between scroll bar period and adjacent river channel for 19 different rivers from Fourier transform of point bar planform features. (B) Histogram of scroll bar period and the percentage of river channel width the spacing is equal to. (Strick et al., 2018)

For a continental scale meandering river such as the Mississippi, only the flood stage model and transverse bar model offer potential explanations for scrolled floodplains. In order to evaluate the validity of both of these models in the context of Mississippi scrolled floodplains, an analysis of the sedimentary architecture below the surface could offer an evaluation of the processes described in the models (Figure 1.8). Studies addressing the subsurface architecture beneath these scrolls are also fairly rare, especially for systems like the Mississippi (Strick et al., 2018).

Table 1.1. Comparing main scroll bar development models.

	Flood Stage Vertical Accretion of Ridges	Landward Migration Of Transverse Bars
Description	•Low-frequency, high magnitude flood events •High stage increases outer bank erosion •Deposition of initial ridge in low bed shear zone via secondary currents •Exposed as a ridge during more average stage height	•During lateral accretion, channel maintains width by inner bank accretion •In channel oblique transverse bars migrate downstream and landward to form scroll bar ridges
Associated Issues	•Experimental observations of scroll formation in constant discharge scenarios	•Has been mainly observed experimentally in non Froude-scaled physical models
Sources	•Hickin (1974) •Nanson (1980)	•Jackson (1976) •Sundborg (1956) •van de Lageweg et al. (2014) •Strick and Lewin (2018)

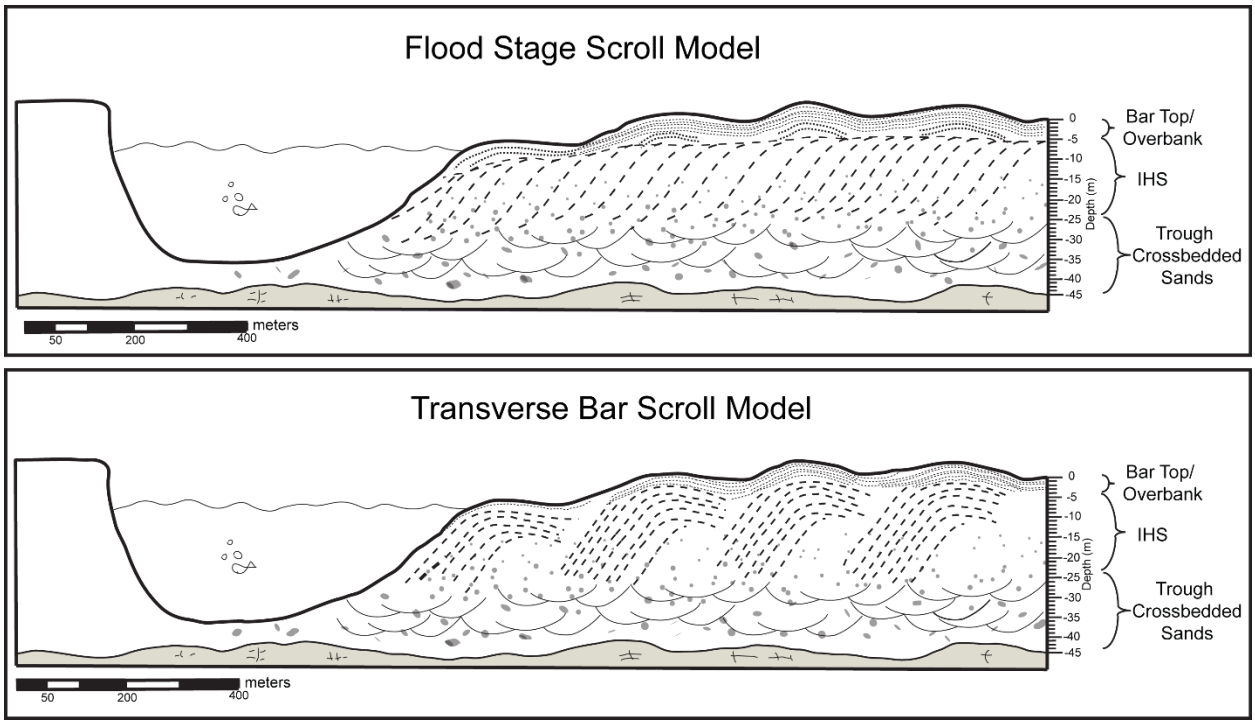

Figure 1.8. TOP scaled sketch of the Flood stage scroll bar model using point bar subfacies depths from well information (Olson, 2017). BOTTOM scaled sketch of the transverse bar scroll model. Top model section is based on figure by (Nanson, 1980).

1.3. Study Location: False River, Louisiana

Once the main channel of the Mississippi River, the modern False River is an oxbow lake in Point Coupee Parish, on the western side of the modern channel. Included in the well-known 1947 map of past Mississippi River channels, the oxbow lake is commonly understood as having cutoff from the main channel of the river around the year 1720 (Fisk, 1947). Historical information, including land ownership plots around the lake, provide this specific timing for when False River became a non-navigable part of the Mississippi River (Sternberg, 1956). The point bar structure known locally as "the island" is also covered by the Louisiana Statewide LiDAR project, providing high-resolution elevation data of the ridge and swale topography (Cunningham et al., 2018). Given the availability of recently-collected seismic and well data, False River presents a unique opportunity to study fluvial topography and the underlying subsurface architecture (Figure 1.9) (Benton, 2018; Gostic, 2018; Olson, 2017). Reflection seismic surveys conducted at two sites, the Woody and Bueche study areas compliment wire-line logs and sediment cores taken from wells along transects orthogonal to the lateral migration of the point bar and the paleo-thalweg.

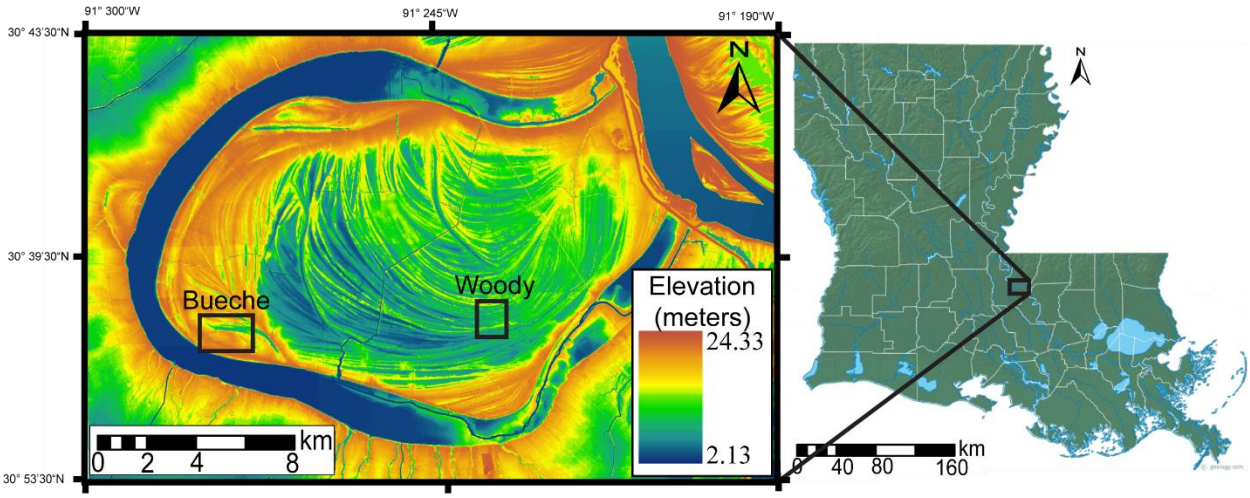

Figure 1.9. A LiDAR location map of False River oxbow lake and point bar. The characteristic ridge and swale scroll bar topography is very identifiable in LiDar images. Seismic survey and well locations Bueche and Woody are highlighted here. (Cunningham et al., 2018). Physical features map of Louisiana on right from geology.com.

1.4. Surface Wave Inversion: Multi-Channel Analysis of Surface Waves (MASW)

The inversion of surface waves is a useful tool in shallow geophysics that enables velocity information to be gained in the near-surface. Exploiting the dispersive characteristic of surface waves to travel at different frequencies for different wavelengths in a layered media, inversion yields 2-dimensional depth shear velocity profiles. Both for the Woody and Bueche seismic surveys acquired in stages between 2016-2017, more conventional reflection seismology processing is only able to image the subsurface below around 10 meters in depth (Benton, 2018; Gostic, 2018; Morrison, 2017). This limitation of seismic reflection imaging is because of the presence of surface waves, which are typically muted or filtered out as noise during reflection processing. Given the importance of the top 10 meters of subsurface architecture when studying scroll bars and surface topography for a large river such as the Mississippi river, surface wave inversion techniques can exploit this seismic 'noise' to develop a shallow seismic velocity structure (Socco et al., 2010).

1.5. Hypotheses and Expectations of Shear Velocity Profiles

Mississippi River scroll bars develop during low-frequency, high discharge events when secondary circulation creates a vertically accreted finer grained ridge on top of coarser upper bar sands. Shallow subsurface shear velocity models should thus show a physical distinction between the initial ridge and overlying overbank deposits and velocity layers with a single dip direction in the IHS zone. Velocity layering geometry should not be parallel to the the topographic expression of the scroll ridge at depths into the IHS zone, as these strata bear no stratigraphic link to the scroll itself (Figure 1.10).

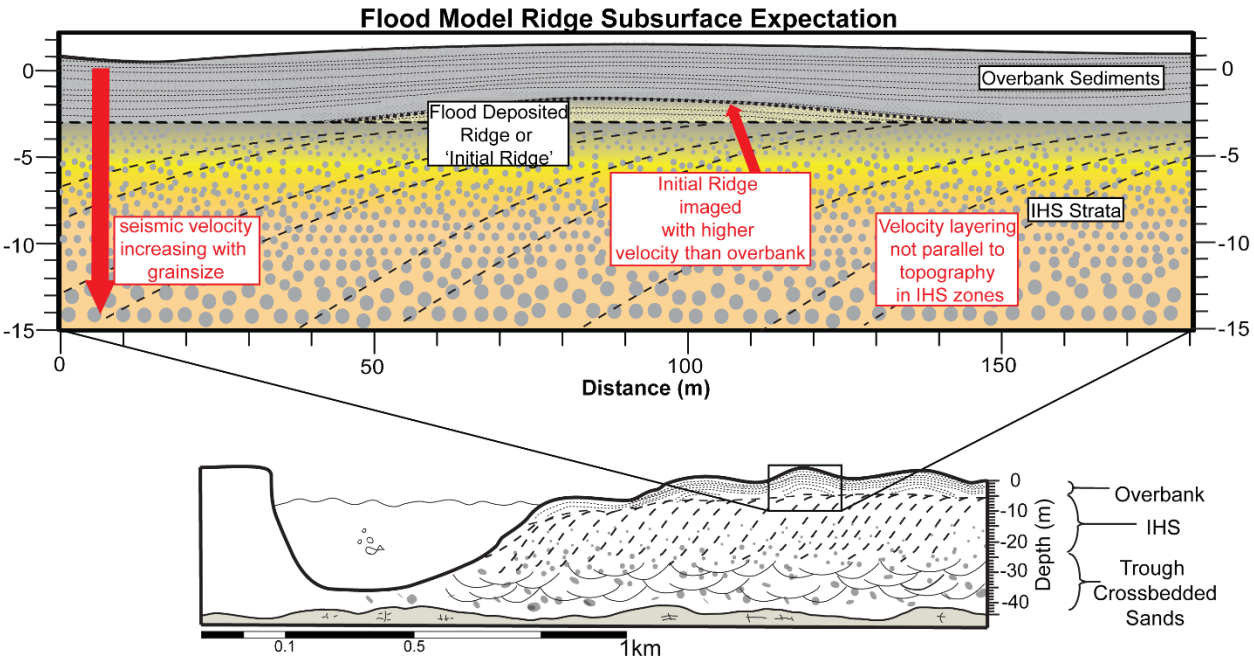

Figure 1.10. Expectations of shear wave velocity profiles of False River if scroll bars were formed during low frequency high discharge events by secondary currents. The flood-deposited initial scroll ridge or silt lens as indicated by the models should be physically distinct from the overlying overbank deposition, while velocity layering below 4 meters of depth in the IHS zone should not be parallel the topographic expression of the scroll ridge.

Mississippi River scroll bars develop from the downstream migration of transverse and unit bars that create a ridge and swale successions during lateral accretion of the point bar. Shallow subsurface shear velocity models should thus reveal a smoother transition from overbank deposits to the underlying coarser IHS strata. In addition, surface topographic expression would be parallel to velocity layering in the IHS zone, as IHS layering dips in two directions (Figure 1.11).

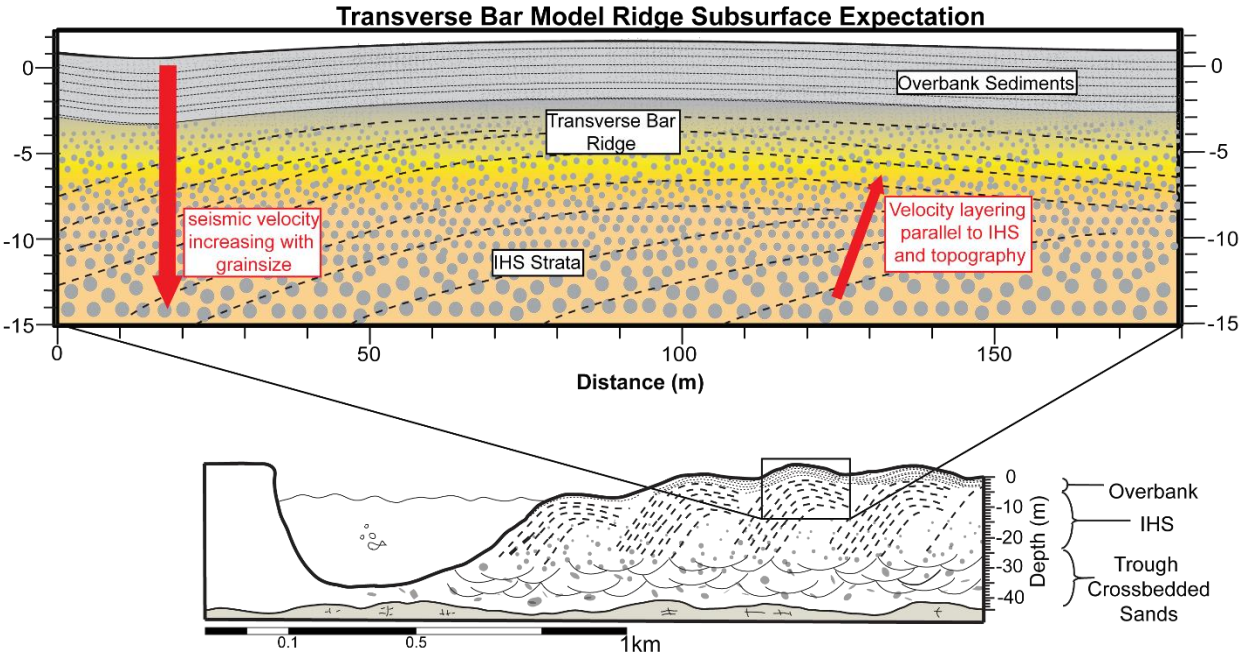

Figure 1.11. Expectations of shear wave velocity profiles of False River if scroll bars were formed by the landward migration of transverse bars. Velocities should gradually increase with depth and grainsize, while velocity layering at depth should be parallel to topography, as the formation of the scroll ridges are linked to the same processes that formed the IHS during lateral accretion.

CHAPTER 2. SURFACE WAVE INVERSION THEORY

2.1. Love Wave Dispersion Phenomenon

The dispersive property of surface waves is the chief characteristic exploited by surface wave inversion. Unlike body waves, in which all frequencies travel at the same phase velocity, for surface waves velocity varies with frequency. If a vertical source is used with vertical component geophones, the main surface wave sampled will be Rayleigh, while Love waves are produced and sampled by horizontal sources and horizontal component geophones such as those used in this study. Unlike Rayleigh waves, which are the product of P-wave and vertical shear wave retrograde particle motion, Love waves are formed by the total internal reflection of multiple horizontally polarized shear waves (Bullen and Bolt, 1985) (Figure 2.1). Love waves are not dependent on Poisson's ratio and cannot exist in a homogeneous half space, but require at least a layer overlying a half space of higher velocity in order to exist (Figure 2.2) (Safani et al., 2005). Because of this, Love waves are always dispersive, and are independent of P-wave velocity (Aki and Richards, 1980). This dispersion phenomena, in which single Love wave frequencies travel at a velocity that is dependent on the shear wave velocity of a layer is what allows for inversion to produce shear wave velocity profiles.

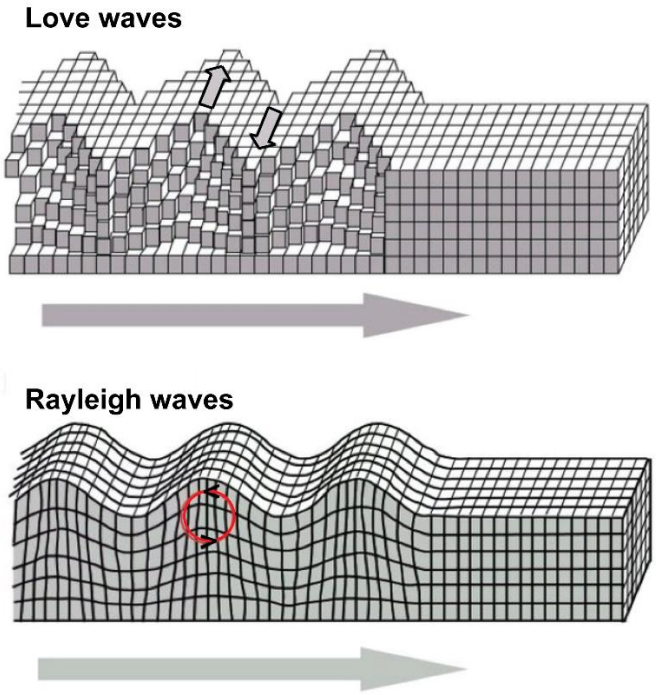

Figure 2.1. Love wave displacement (top) is parallel to the surface and perpendicular to propagation direction. Rayleigh wave displacement (bottom) is conversely perpendicular to the surface and parallel to propagation, resulting in retrograde particle motion (indicated by the red motion circle). From (Fowler, 2005).

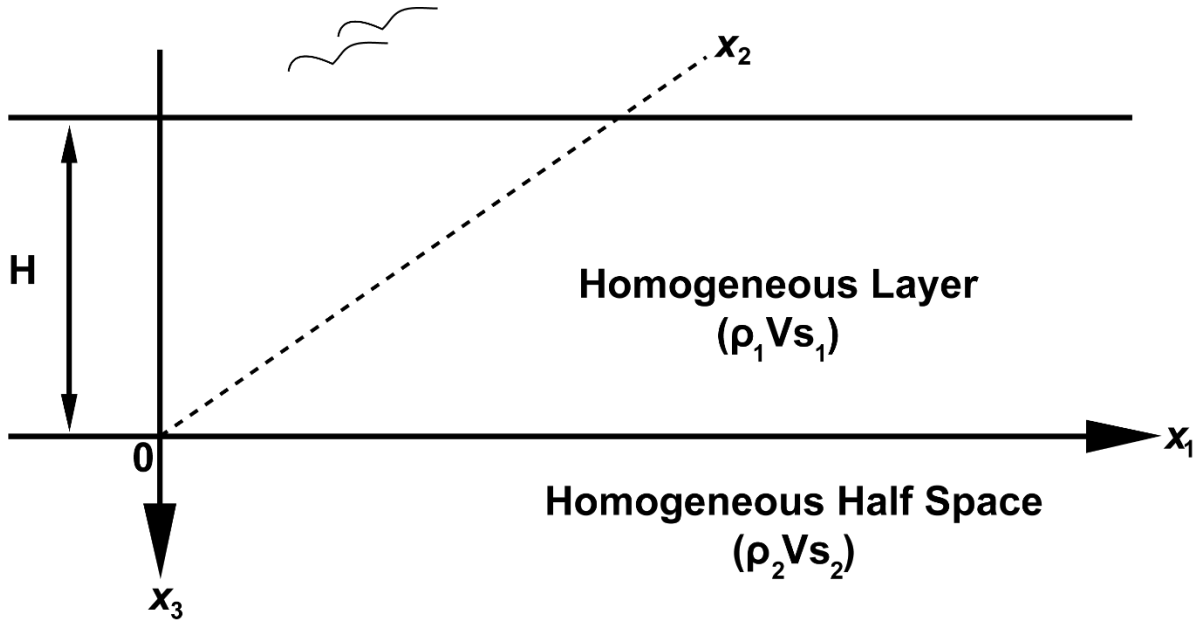

Figure 2.2. Graphical representation of the simplest layered earth model necessary for the existence of Love waves. A homogenous layer of height H over a homogeneous and infinite Half space of higher shear velocity (Vs_2). Adapted from (Bullen and Bolt, 1985).

Love wave dispersion can be represented mathematically by first representing the Love wave displacement as a plane wave in Cartesian coordinates:

$$\mathrm{u}(x_1, x_2, x_3, t) = (\,0, h(x_3)e^{\mathrm{i}(kx_1-\omega t)}, 0\,) \tag{2.1}$$

where u is displacement, i is the imaginary unit, ω is frequency, *k* is wavenumber, *t* is time, and the unknown function $h(x_3)$ that describes the vertical decay of the wave (Boschi, 2012). Being that wavenumber relates to the wavelength (λ) and phase velocity (*c*):

$$k = \frac{2\pi}{\lambda} = \frac{\omega}{c} \tag{2.2}$$

Considering an elastic medium and the equation of motion:

$$\rho \frac{\partial^2 u_i}{\partial t^2} = \frac{\partial \tau_{ji}}{\partial x_j} \tag{2.3}$$

where ρ is density (Aki and Richards, 1980). Because only displacement in the x_2 can be considered according to (2.1), the motion equation can be satisfied thus:

$$\rho \frac{\partial^2 u_i}{\partial t^2} = \mu \left(\frac{\partial^2 u_2}{\partial x_1^2} + \frac{\partial^2 u_2}{\partial x_3^2}\right) \tag{2.4}$$

where μ serves as the shear modulus (Boschi, 2012). In a simplified 2-layer earth model in which a homogenous layer of density and shear velocity (ρ_1, Vs_1) overlies a homogenous half space of (ρ_2, Vs_2) where Vs_2>Vs_1, (1) can be placed into the equation of motion (2.3):

$$\frac{\partial^2 h(x_3)}{\partial x_3^2} = \left(k^2 - \frac{\omega^2}{\partial_i^2}\right) h(x_3) \tag{2.5}$$

where *i* = 1,2 for the half space and overlying layer. By using constants, the Love wave displacement equation (2.1) for this 2-layer scenario can be expressed as:

$$\mathrm{u}(x_2,t) = \left[A_i e^{-\sqrt{k^2-\omega^2/Vs_i^2}x_3} + B_i e^{-\sqrt{k^2-\omega^2/Vs_i^2}x_3}\right] e^{i(kx_1-\omega t)}\ (i = 1,2) \qquad (2.6)$$

where the constants A_i, B_i, ω, and k can be further defined using a series of boundary equations. The eigenvalue problem of (2.6) when simplified from exponential into trigonometric terms:

$$tan\left(H\omega\sqrt{1/\beta_1^2 - 1/c^2}\right) = \frac{\mu_2\sqrt{1/c^2-1/Vs_1^2}}{\mu_1\sqrt{1/\beta_1^2-1/c^2}} \qquad (2.7)$$

where H indicates the height of the first layer in the model (Lay and Wallace, 1995). Named the love wave dispersion equation, (2.7) has solutions for real numbers as $Vs_1 < c < Vs$. For a single frequency (ω) value, (2.7) can yield multiple, yet finite solutions called modes (Figure 2.3). For the n=0 solution, this is referred to as the fundamental mode. The fundamental mode is the lowest velocity for any given frequency, and is the most often used mode in surface wave inversion because it consistently yields the lowest relative error and is the easiest to identify (Xia et al., 2003). Additionally, higher order modes typically correspond to weaker peaks. (Song et al., 2007) (Xia et al., 2003). Because of the phenomena demonstrated by these equations, Love waves are always dispersive because they can only exist if there is at least a low velocity layer over a higher velocity half space (Lay and Wallace, 1995).

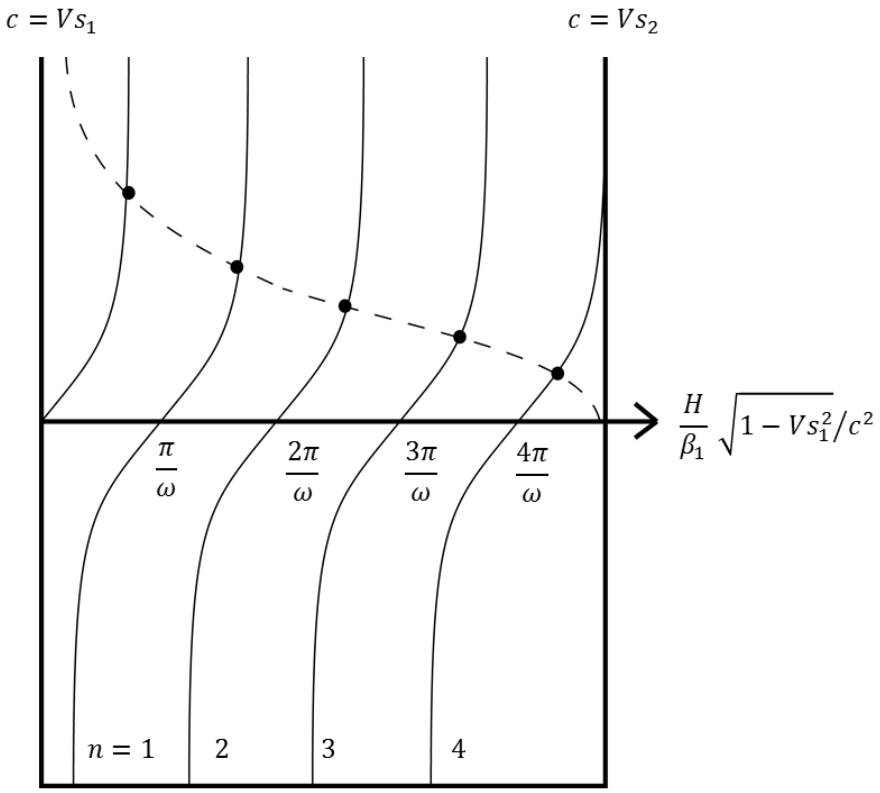

Figure 2.3. A graphical visualization of the love wave dispersion equation (2.7). The left and right boundary conditions for real numbers of the phase velocity (c) being between the velocity of the overlying layer (Vs_1) and the half space (Vs_2). The dashed line represents solutions to the equation, with intersections identifying potential phase velocity values (c) at frequency ω. Each solution is indicated by an n= mode, beginning with the fundamental mode at n=o at the left side of the plot. Figure adapted from (Aki and Richards, 1980).

To relate this phase velocity (c) of the Love wave to the shear velocity (Vs) first the relation of the shear modulus as:

$$\mu = \rho Vs^2 \tag{2.8}$$

can be used to compute the partial derivative of the phase velocity with respect to shear wave velocity:

$$\left[\frac{\partial c}{\partial Vs}\right]_\omega = \left[\frac{\partial c}{\partial \mu}\right]_\omega \left[\frac{\partial \mu}{\partial Vs}\right]_\rho = \frac{\rho Vs}{2k^2 I_1 g(\omega)} \left[k^2 A_1 + \left(\frac{dA_1^2}{dx_3}\right)\right] \tag{2.9}$$

where *g(ω)* refers to the group velocity, and I_1 refers to the first energy integral (or $1/2 \int_0^\infty \rho(x_3) A_1^2 \, dx_3$) (Safani et al., 2005). For Rayleigh waves, the phase velocity of a

surface wave is estimated to be around 92 percent of the shear-wave velocity, with adjustments made to the assumed Poisson's ratio, the percentage remains around 90 (Stokoe, 1994). Love wave phase velocity is entirely dependent on the shear wave velocity, density, and thickness of layer. This dispersive nature of Love waves, enables inversion to calculate highly accurate vertical shear velocity profiles from surface wave data (Figure 2.4) (Xia et al., 2012).

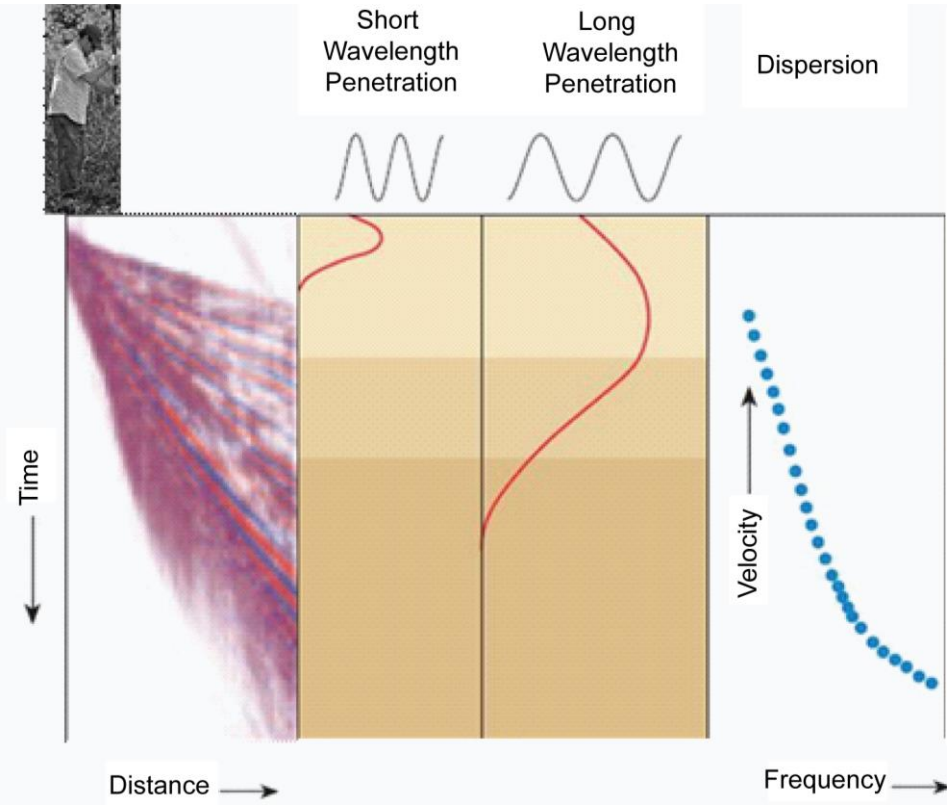

Figure 2.4. A simplified representation of surface wave dispersion. The actual surface wave energies generated by the source (top left corner) contain multiple waves of different wavelength that will travel at the average velocity of the surrounding media at a travel speed that is the average from the surface to 1/2 to 1/3 of the wavelength. This relationship is plotted as a dispersion curve (middle right), which can be inverted for a velocity model product (right). Adapted from (Bagaini et al., 2010)

2.2. Nearest Neighbor Inversion Method

A form of direct-search-inversion, the Nearest Neighbor Algorithm generates forward models of subsurface velocity data that could produce the dispersion results calculated from reflection seismic data (Sambridge, 1999; Wathelet, 2008) (Wathelet, 2008). The approach involves genetic algorithms guiding random sample generation by the results from previous samples given a set of parameters (Sen and Stoffa, 1991) (Lomax and Snieder, 1994). A direct-search inversion in the case of surface wave inversion is based on the continued calculation and reduction of misfit. In surface wave inversion, this misfit is defined as:

$$misfit(\omega) = \sqrt{\sum_{i=0}^{n_f} \frac{\left(c_{picked} - c_{calculated}\right)^2}{\sigma_i^2 n_f}} \qquad (2.10)$$

where (c_{picked}) is the interpreted input phase velocity for each frequency (ω), and ($c_{calculated}$) is the product of the new forward model. The σ represents uncertainty and n_f is the total number of frequency samples considered. The equation examines the difference between the interpreted or picked phase velocity and the calculated or modeled phase velocity that each correspond to the same frequency (Wathelet, 2008). In a direct-search type inversion, thousands of forward models are generated based on how iterative minor changes to subsequent models effects the misfit (Sambridge, 1999). (Figure 2.5) shows a visualized example of surface wave inversion. The 1D vertical V_s profiles generated by different forms of the basic inversion approach can be interpreted geologically alone, or can be interpolated to create pseudo 2D V_s models of the subsurface.

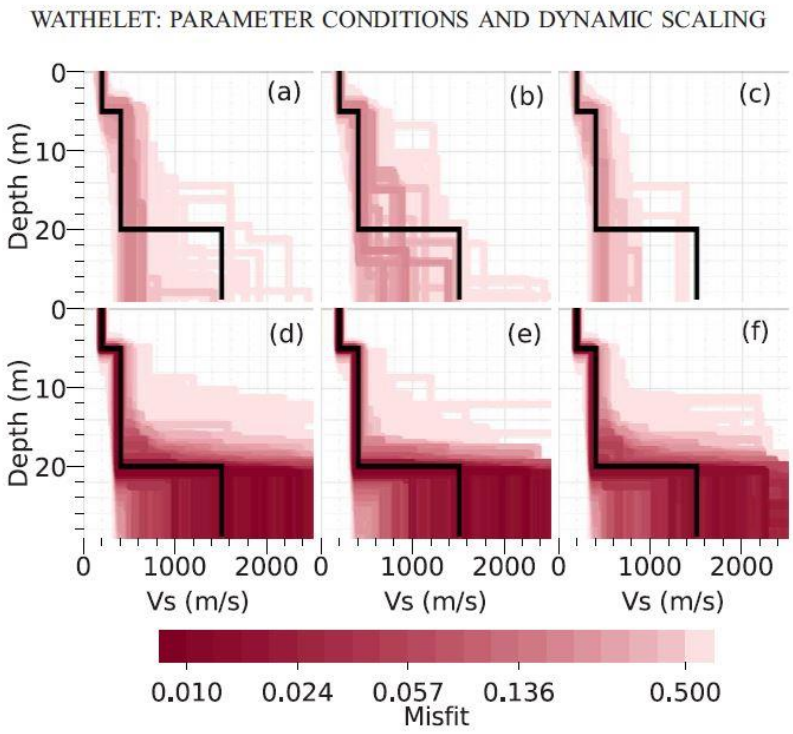

Figure 2.5. Resultant inversion flow models of Vs versus depth. Many Vs models are formed to reduce misfit as much as possible (darker reds). Subsequent iterations seek to reduce misfit from the previous model. If misfit eventually increases, the inversion will start again and repeat the same process altering initial random samples, sometimes generating thousands of models in a single run. (Wathelet, 2008)

The nearest neighbor algorithm generates initial models based on a Markov-Chain random walk process in which the first valid model with the lowest misfit becomes the seed for subsequent models (Sen and Stoffa, 1996). Voronoi sampling density cells are defined around each model (Figure 2.6). The algorithm evaluates each parameter in search of continually lower misfit. The number of models per iteration, and the total number of iterations are variable based on the number of layers in the inversion (Wathelet, 2008).

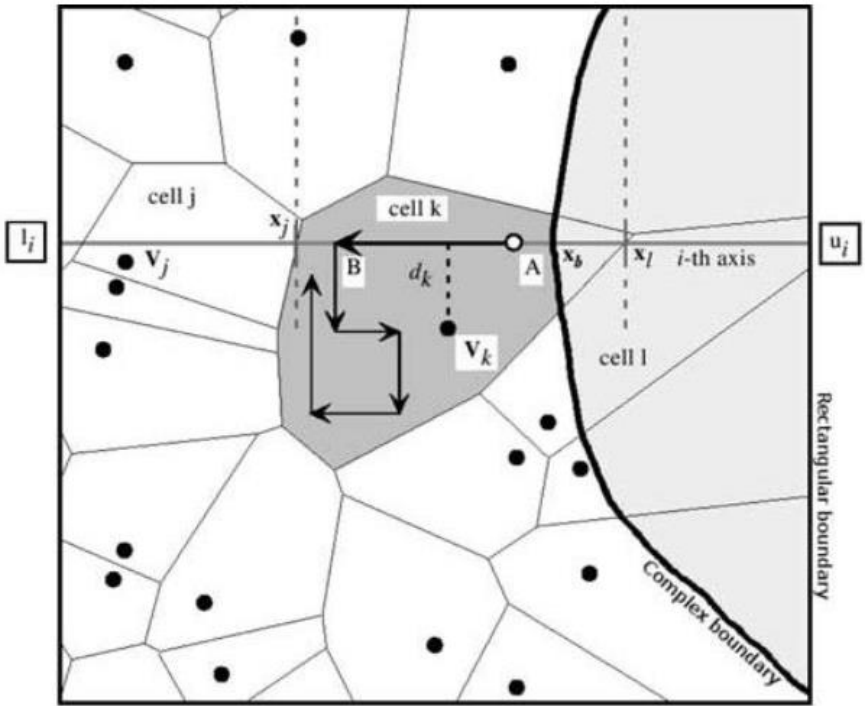

Figure 2.6. The Markov-Chain random walk used in the Nearest-Nieghbor algorithm. The exterior "rectangualr boundary" on the outside is based on user-defined parameter limits. Voronoi cells of sample density surround each valid model dot. In the example cell k, where li and ui are the limits for the i-th parameter axis, model A progresses to model B in search of lower misfit values in nearby Voronoi cells. Wathelet (2008)

CHAPTER 3. DATA ACQUISITION AND SURFACE WAVE INVERSION PROCESSING

3.1. MASW General Steps

The following chapter describes how this study acquired seismic data and processed these data using surface wave inversion to yield pseudo-two-dimensional depth-velocity profiles for the survey locations (Figure 3.1). In addition, general information is provided regarding the acquisition and interpretation of available well information such as wire line logs and cores taken in close proximity to the seismic data surveys discussed in this study.

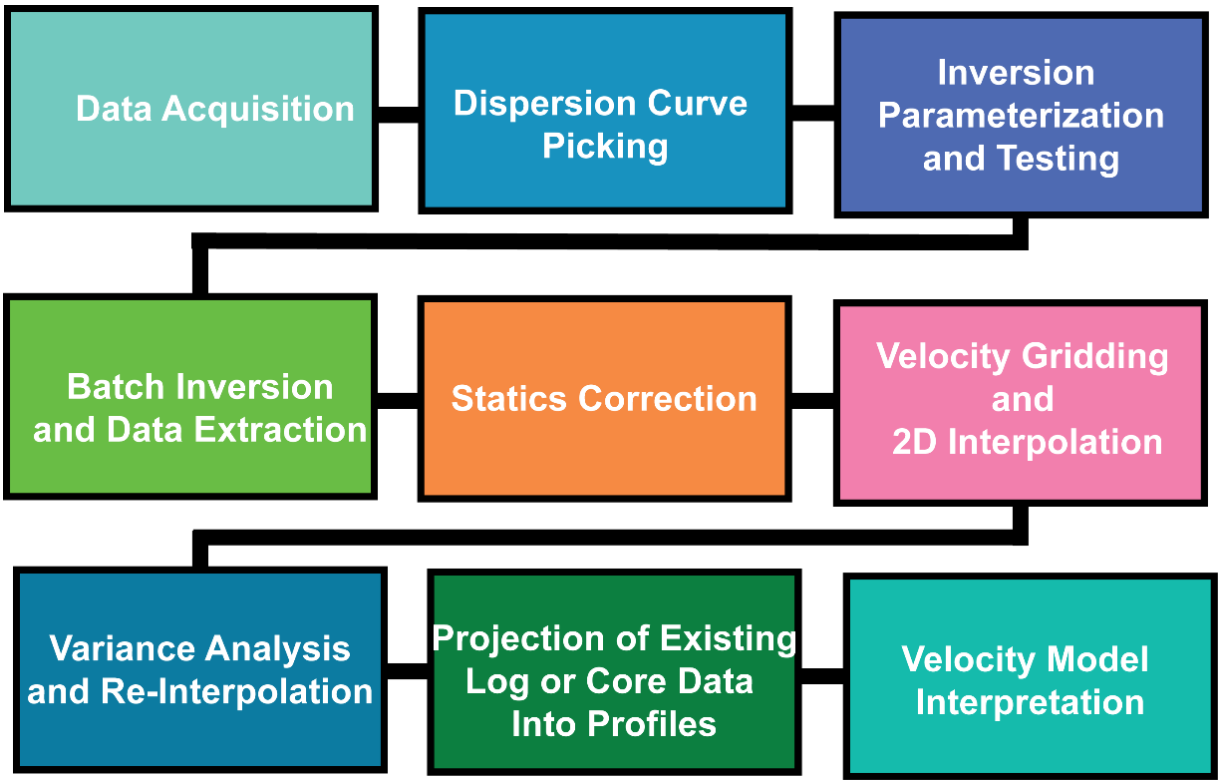

Figure 3.1. Simple flowchart of the steps taken in this study to acquire, process, invert, and interpolate seismic data.

3.2. Seismic Data Acquisition

Seismic data acquisition occurred during late 2016 and early 2017 on two survey sites selected in different locations on the False River Point bar (Figures 3.2, 3.3, 3.4). Representing different stages of the meander and depositional packages, the Bueche and Woody sites each feature a seismic line relatively perpendicular to the paleo-channel and scroll bar topography (Benton, 2018; Gostic, 2018). The Woody site also has a shorter, intersecting line or 'crossline' that runs parallel to the scroll bars to compliment the main 'inline'. At both survey sites, multiple wells were drilled yielding core data, electrical conductivity logs, and HPT logs (Olson, 2017).

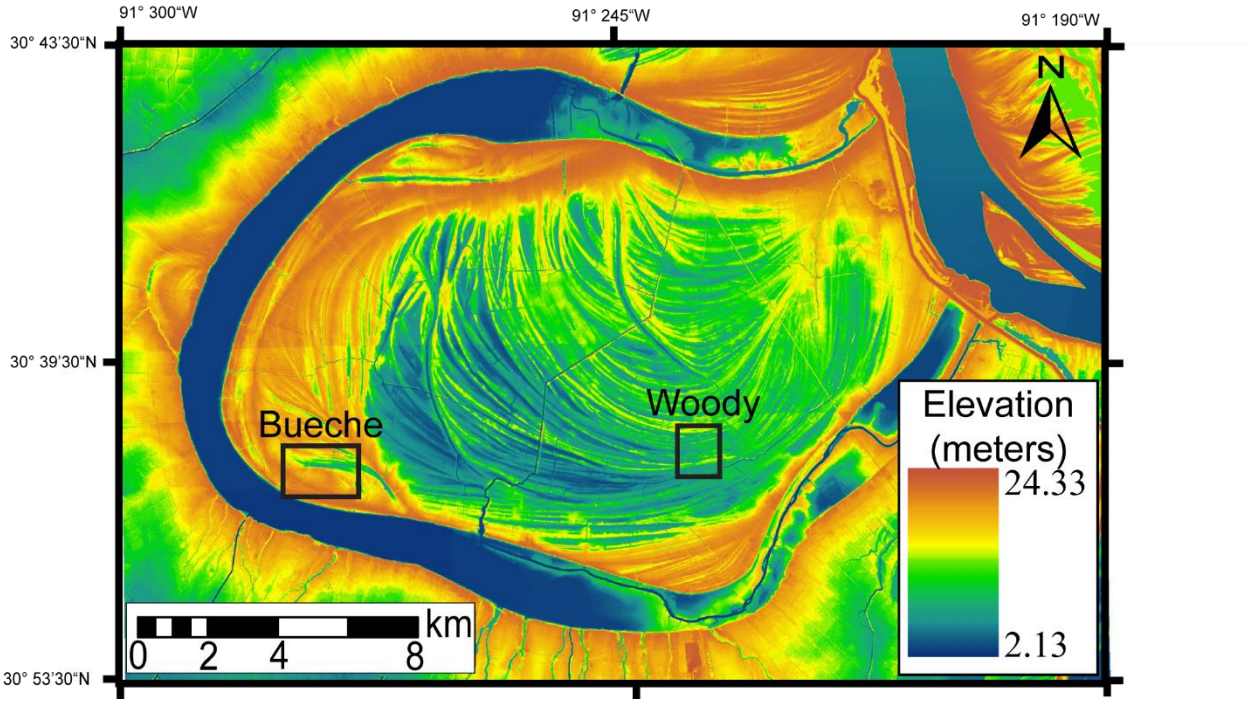

Figure 3.2. Lidar Elevation map of the False River point bar system (Cunningham et al., 2018).

Collected with the original intention of acquiring seismic reflection data, both survey sites used common shotpoint gather geometries, in which 24 horizontal-component geophones at 1 meter spacings recorded shear wave data. The Bueche survey featured alternating sources between a ‘seisgun’ and a horizontal I-beam hammer setup (Gostic, 2018). The Woody survey only utilized the hammer source (Benton, 2018). The custom built ‘seisgun’ generates horizontal shear waves by discharging a gunpowder charge perpendicular to the seismic line, and can be flipped to shoot in the other direction for an additional gather (Crane et al., 2013). The other source was a simple hammer and I beam setup, in which a person stands on an iron I-beam and swings a sledge hammer onto the side of the beam to generate the shear wave, for each side, three blows were recorded and combined to form a single source signal.

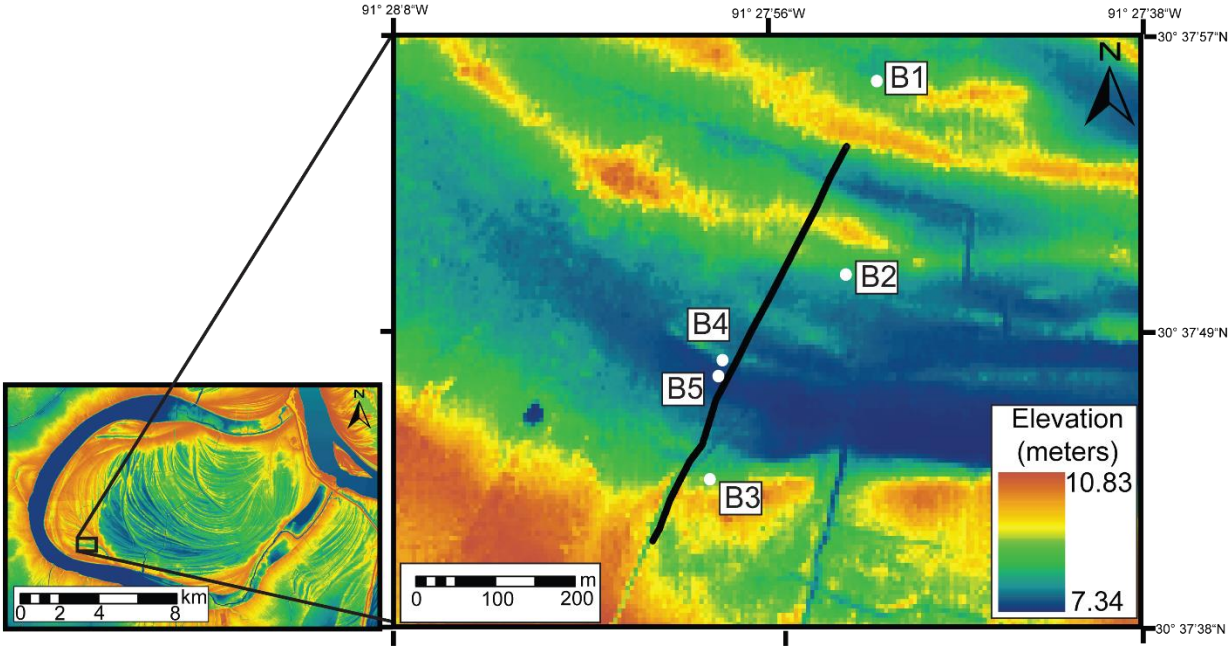

Figure 3.3. Location of Bueche seismic survey and wells on Lidar elevation image (Cunningham et al., 2018). Shotpoint numbers begin at 1 and progress to 481 in the northeastern direction. Note, in addition to the scale difference between the two maps, Lidar elevation colors on the larger map (left) is not the same as lidar elevation colors on the smaller location map (right).

Horizontal component geophones rated at 30 Hz recorded the shear wave data for both surveys (Benton, 2018; Gostic, 2018). Shear waves are less sensitive to pore-fluids as shear waves cannot propagate through liquids, making them ideal in a reflection seismic acquisition on a site such as False River, where the water table is high year-round.

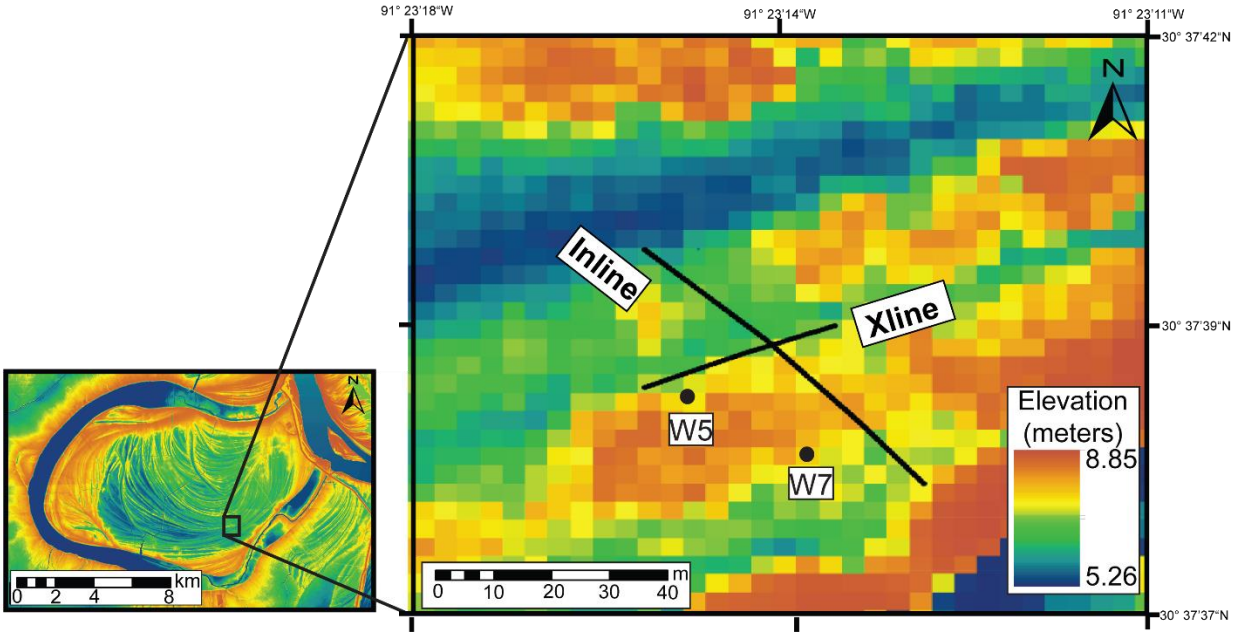

Figure 3.4. Location of Woody seismic surveys and wells on Lidar elevation image (Cunningham et al., 2018). Shotpoint numbers begin at 1 and progress to 81 in the southeastern direction for the inline and shotpoints on the crossline proceed from 1 to 41 in the eastern direction. Note, in addition to the scale difference between the two maps, Lidar elevation colors on the larger map (left) is not the same as lidar elevation colors on the smaller location map (right).

Table 3.1: Data Acquisition Specifics. Modified from (Benton, 2018; Gostic, 2018).

Survey Type	End-On
Bueche Line Length	481 meters
Woody Inline Length	81 meters
Woody Crossline Length	48 meters
Bueche Receiver Direction (Relative to Source)	NE
Woody Inline Receiver Direction (Relative to Source)	SE
Woody Crossline Receiver Direction (Relative to Source)	NE
Shots per Shot Point	2
Distance between Shots	1 meter
Traces per Shot	24
Receiver Spacing	1 meter
Minimum Receiver Offset	1 meter
Maximum Receiver Offset	24 meters
Sampling Interval	500 microseconds
Sampling Duration	4.096 seconds
Samples per Trace per Shot	8192
Sampling Delay	-10 microseconds

3.3. Available Well Data

In addition to the seismic data acquired by this study and others, well log and core data taken in close proximity to the seismic surveys are also available for analysis. Drilling performed during the spring months between 2014-2016 utilized a series of Geoprobe© machines to drill, run wireline logs, and core wells in different study areas across False River point bar (Lechnowskyj, 2015; Olson, 2017). For the Bueche study area, 5 drilled wells provide electrical conductivity (EC) data and two provide sediment cores (Olson, 2017) (Figure 3.3). For the Woody site near both the inline and crossline surveys, 2 wells provide EC log data (Figure 3.4). Electrical conductivity (EC) is a downhole lithology identifying tool that measures the sediment's ability to maintain a flow of electrical current at different depth intervals (Olson, 2017). Finer grained material such as clay tend to support more electrical flow, and thus show higher EC measurements than coarser grained sediments composed of sand or gravel (Revil and

Glover, 1998). Sediment coring in the form of spot cores for two Bueche wells (B2 and B3) provide core photos and core descriptions made using the Wentworth classification scheme (Olson, 2017). Well information is used in this study to generally inform inversion parameterization and during velocity profile interpretation.

3.4. Inversion General Information

This study utilizes an inversion algorithm and software program developed by Wathelet (2008). The program Dinver as a sub-component of the Geopsy software package, facilitates both the dispersion curve smoothing, and the actual inversion execution GUI. Dinver employs the Nearest Neighbor inversion algorithm, in which thousands of forward models generated to account for the picked dispersion curves with pre-selected parameter limits can eventually produce a model that can closely resemble the actual V_s profile.

3.5. Creating Dispersion Images

From recorded seismic data, the creation and interpretation or 'picking' of dispersion images provides the input that undergoes inversion to become a vertical V_s profile (Appendix A). In order to convert recorded time-offset domain data into frequency and phase velocity, the data are transformed into the offset-frequency domain by using a Fourier transform (Park et al., 1998) (Appendix B).

$$U(x,\omega) = \int u(x,t)e^{i\omega t}dt \tag{3.1}$$

where time-offset domain $u(x,t)$ becomes offset-frequency $U(x,\omega)$, which in turn describes phase $P(x,\omega)$ and amplitude $A(x,\omega)$ spectra:

$$U(x,\omega) = P(x,\omega)A(x,\omega) \tag{3.2}$$

Further, the offset-frequency domain $U(x,\omega)$, relates to angular frequency and phase velocity through the angular wavenumber K_ω.

$$U(x,\omega) = e^{-iK_\omega x}A(x,\omega) \tag{3.3}$$

The angular wavenumber K_ω is the ratio of phase velocity c_ω to angular frequency ω

$$K_\omega = \frac{\omega}{c_\omega} \tag{3.4}$$

Using this ratio along with an assumed phase velocity, the offset-frequency domain $U(x,\omega)$ is transformed into the wavenumber-frequency domain $V(\omega,k)$.

$$V(\omega,k) = \int e^{-i(K_\omega - k)x}[A(x,\omega)/|A(x,\omega)|]\,dx \tag{3.5}$$

For each frequency and a given velocity, the above integral can sum all the trace wavefields and provide a maximum wavenumber-frequency domain dispersion image if the case is true that angular wavenumber (K_ω) and wavenumber (k) are equal (Officer, 1974). When this is true, a wave with that frequency and phase velocity travelled over that defined spacing. Eventually,

dispersion curves for all the phase velocities and their frequencies are calculated using the function $I(\omega, c)$ that defines dispersion in frequency-phase velocity domain (Park et al., 1999).

$$I(\omega, c) = \int e^{-i\omega\left(\frac{1}{c\omega}-\frac{1}{c}\right)x} [A(x, \omega)/|A(x, \omega)|]dx \qquad (3.6)$$

The above process can be conducted for calculated common midpoint gathers (CMP's) or conducted for each single trace depending on the scope of the survey and analysis (Hayashi and Suzuki, 2004). The dispersion images produced will then undergo interpretation before the data ultimately undergoes inversion.

3.6. Picking Dispersion Curves

Before inversion, the above-generated dispersion images are interpreted for their frequency-phase velocity curves. Generation of the dispersion image is conducted by a modified program developed by Goff (2016) (Appendix B). In the case of the Bueche survey, 451 unique shotgathers each will yield a dispersion curve. The data used here have undergone the initial steps of reflection processing, such as header assignments, polarity reversal (to remove an error in the acquisition equipment), and source integration in the case of the Bueche data, all of the steps that usually come just before the surface wave is removed (Appendix A) (Goff, 2016).

Interpretation of the newly created dispersion images consists of 'picking' the dispersion curve for each individual shotgather. This picking consists of making visual selections as a digitized line or points on the dispersion image of maximum phase velocity and minimum frequency. On most dispersion images, multiple modes of phase-velocity frequency curves exist. This study only identifies and picks the fundamental mode, because it is the easiest to define in images and when inverted alone can yield velocity-depth information at the lowest relative errors

(Xia et al., 2003). By picking a dispersion curve on a dispersion image, interpretation of this fundamental mode is the usual outcome. These interpretive picks act as the ‘measured’ aspect of the inversion problem (Figure 3.5).

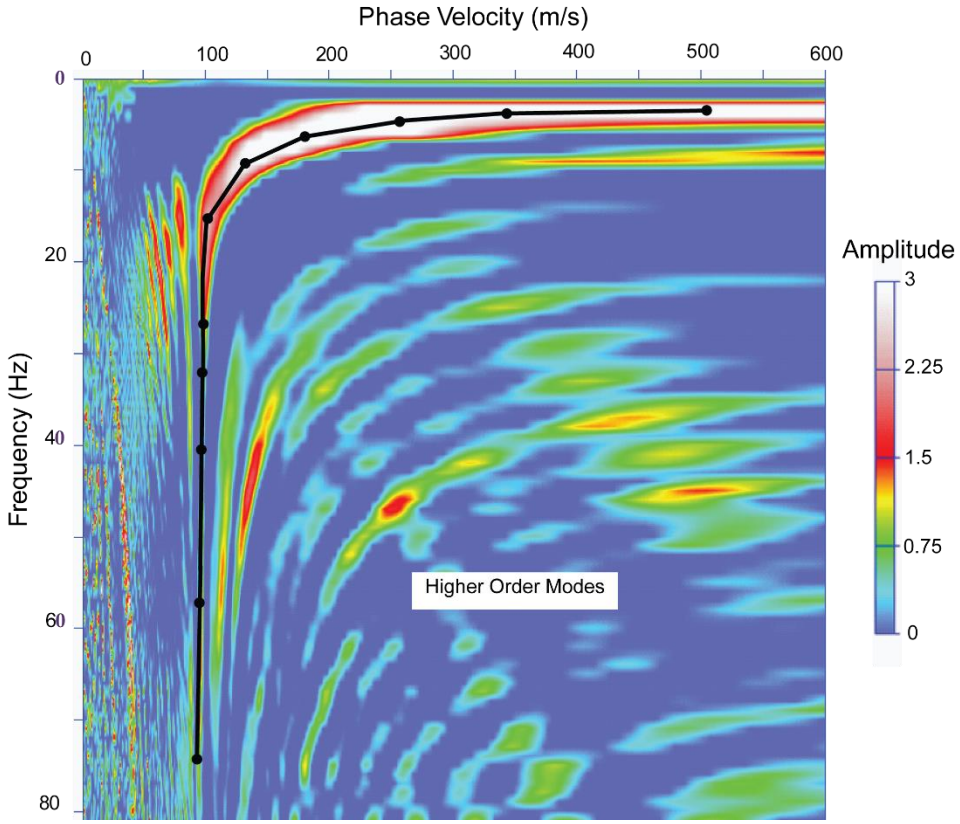

Figure 3.5. A raw dispersion image calculated and inverted from the Bueche dataset (shotgather 31) The picks are indicated by the black dots. These points and the are used in the inversion. Higher order modes include all curves in higher phase velocity regimes indicated in this image below the higher amplitude fundamental mode, these are typically not selected for inversion because they are more difficult to identify (See above section 2.1). This image was generated by the same program used for visualizing and picking the data (Appendix B.1)

3.7. Dispersion Curve Cutting and Resampling

Dispersion curve data (in the form of two column ASCII files of frequency (Hz) and phase velocity (m/s)) must undergo several modifications before inversion can occur (Appendix C.1) First, the phase velocity data must be transformed into slowness (s/m) by taking its reciprocal. Dinver inversion only inverts and displays this format of dispersion data. In order to reduce the possibility of erroneous dispersion picks, a simple frequency cut is then applied to each dispersion curve, removing any picks that lie outside the acceptable range between 2 Hz and 50 Hz. This step removes any potential dispersion picks that were made that lie outside of the accuracy of the dispersion image picking zone (Appendix C.1).

Next, the dispersion data is resampled to improve the inversion effectiveness. I employ a straightforward frequency-linear resampling of 50 samples between each curve's frequency minimum and maximum (Wathelet, 2018). Resampling is an important step in generating dispersion curve data that influences the inversion process in a way that best reflects the data (Wathelet, 2008) (Figure 3.6). Following this transformation, cutting, and resampling of the dispersion data, these ASCII files are then converted into .target files (Appendix C.1) This type of file is what the inversion software program Dinver requires for batch inversion, and the step also allows the data to be marked as Love wave data, rather than the default Rayleigh wave indication in the program. All of these steps: transformation, cutting, resampling, and target file creation are conducted by the program Xresample_Targetcreation.sh, using the Geopsy programs *gpcurve* and *gptarget* (Appendix C.1).

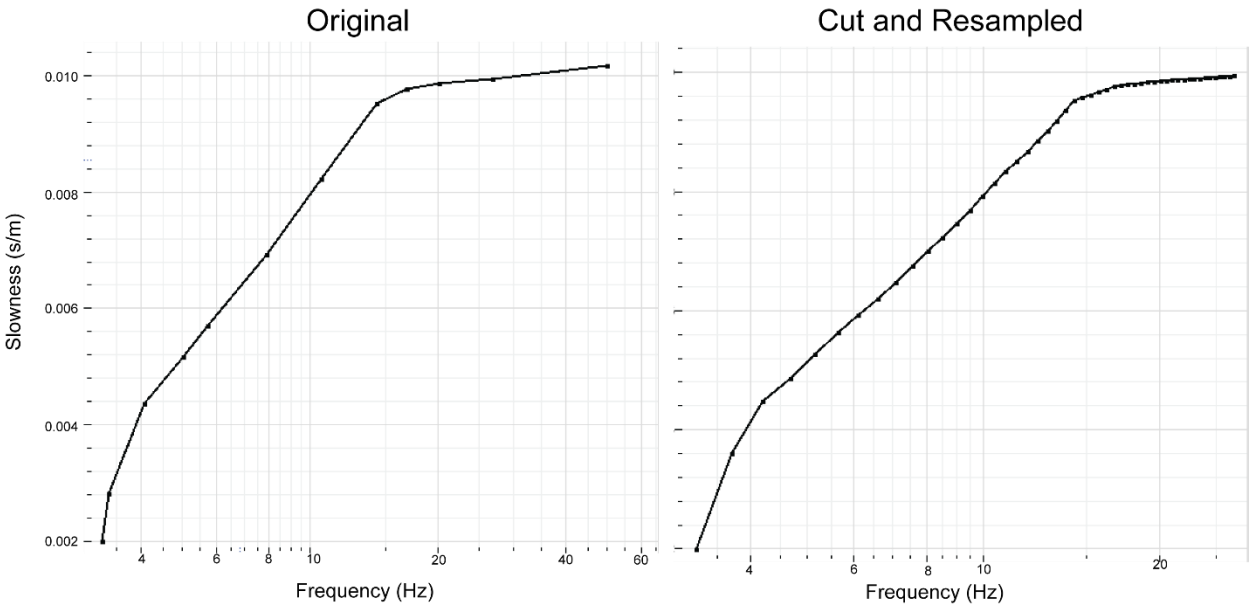

Figure 3.6. Example of dispersion curve resampling. LEFT. un-resampled dispersion curve, raw from dispersion picking, where each single dot represents a manually selected dispersion pick. RIGHT. cut and resampled dispersion curve, now 50 frequency-slowness picks are distributed linearly about the existing line, and high frequency picks above 50 Hz are removed. Note the difference in horizontal logarithmic scale between plots.

3.8. Inversion Parameterization: General

Once dispersion curves are interpreted, this 'observed' data must then undergo inversion to yield vertical 1-dimensional shear velocity profiles. The inversion of surface wave data depends greatly on sound parameterization (Appendix C.2). Limitations set by parameterization, in turn are inferred from pre-existing knowledge or assumptions of the media. The parameters V_s (Shear Velocity), layer thickness, V_p (P-wave velocity), density, and Poisson's ratio are each given specified limitations that are kept constant during the inversion process. As my Love wave inversion does not depend on V_p and Poisson's ratio, both V_p and Poisson's are required inputs for Dinver in order to run, although selections have no effect on Love wave inversion (Wathelet, 2005, 2008).

3.9. Inversion Parameterization: Minimum Resolvable Layer Thickness Determination

Surface wave amplitudes decay exponentially with depth, therefore it is conventional to use a third to a half of the wavelength to calculate a V_s profile. Using wavelength values beyond this tends to show higher variance in results (Heisey et al., 1982; Xia et al., 2012). Based on the dispersion characteristics, source types, and the 30 Hz horizontal component geophones used during acquisition, this zone is calculated to be 1.6 meters, meaning the vertical resolution of the inversion in this study is 1.6 meters, and any layers thinner than this will not be specifically denoted on a vertical velocity profile (Equation 3.7). Potential high or low velocity layers that are thinner than this 1.6 m resolution limit will still have an effect on the velocity profile. Properly parameterized inversion attempts yield more robust results requiring less computing power (Poggi, 2011).

The vertical resolution here represents the thinnest resolvable velocity layer dispersion data can reasonably yield based on dispersion characteristics, source types, and the type of geophones used during acquisition. By analyzing the highest frequency that is interpretable and its corresponding phase velocity for a stack of dispersion images from each survey location, these numbers can yield an approximation of vertical resolution (Ivanov et al., 2017) (Figure 3.7).

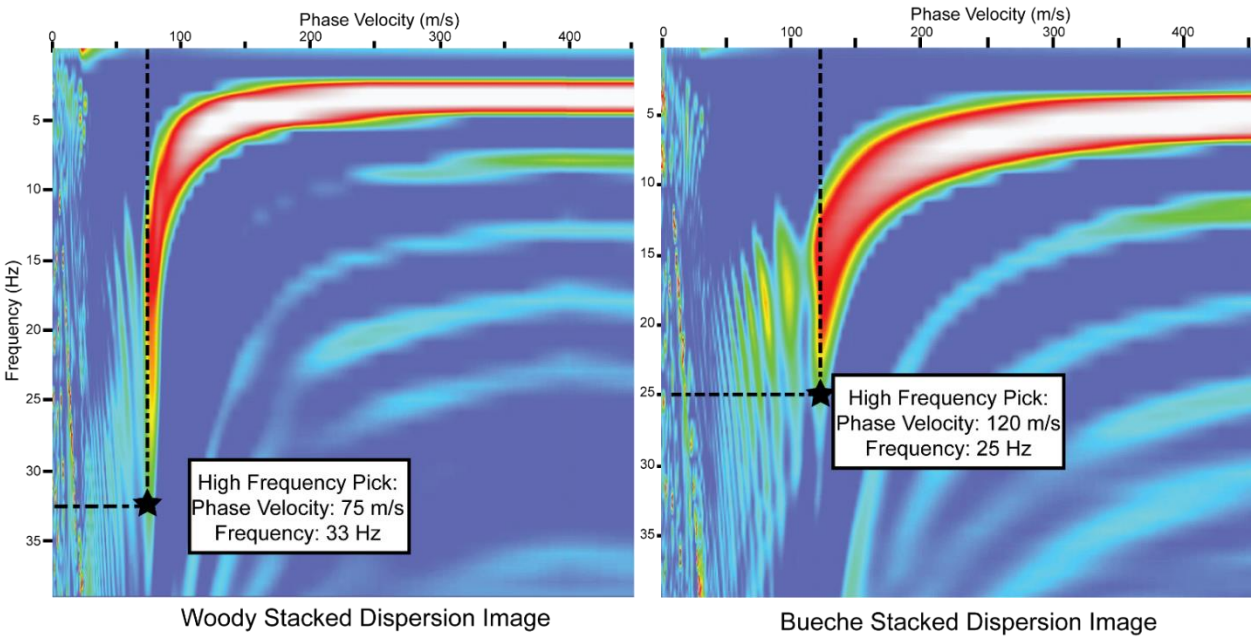

Figure 3.7. Example of how stacked dispersion images (generated from many/all shotgathers) are used to determine the maximum interpretable frequency and corresponding phase velocity for both Woody (left) and Bueche (right) to be used to calculate resolution. Images generated from Xphasevel.pl (Appendix B.1).

The vertical resolution equation:

$$\left(\frac{1}{3}\right) \times \frac{\text{Phase Velocity}}{\text{Highest Frequency}} = \text{Minimum Wavelength From Dispersion} \qquad (3.7)$$

For the Woody dispersion data:

$$\left(\frac{1}{3}\right) \times \frac{75\ \text{m/s}}{33\ \text{Hz}} = \mathbf{0.75\ m} \qquad (3.8)$$

For the Bueche dispersion data:

$$\left(\frac{1}{3}\right) \times \frac{120\ \text{m/s}}{25\ \text{Hz}} = \mathbf{1.6\ m} \qquad (3.9)$$

3.10. Inversion Parameterization: Testing Theoretical Cases

The parameters described in Table 3.2 are selected mainly for the geologic expectations of the material in the top 12 meters at False River, provided by the multiple cores and well logs (Heisey et al., 1982; Olson, 2017). Test scenarios of theoretically generated dispersion curves then helped to rest the robustness of the parameters. These scenarios featured different hypothetical potential velocity profiles and their corresponding dispersion curves calculated by *Gplivemodel*, another Geopsy program (Appendix C.2). Tested scenarios included cases where the velocity-depth relationship steadily increased, steadily decreased, changed significantly over thin layers, and behaved erratically (Figure 3.8). These theoretical curves are then inverted using the parameters to ensure that the actual velocity profiles were able to be closely recreated in the inversion results. The parameters are subsequently varied to ensure the inversion's ability to deliver as accurate a representation of the data as possible. Six layers over a half space that each range in thickness from 0.75 to 7 meters provide a decent amount of velocity space inversion method, while not creating any apparent inversion artifacts.

Table 3.2: A visual of the inversion parameters used in Geopsy's Dinver program to invert the dispersion curves. Note that for Love wave inversion, no P-wave or Possion's ratio parameters are actually used in the inversion, but Dinver requires that information be supplied in these categories in order to run without error. (Wathelet, 2008).

Layer	P-wave (m/s)	Poisson's Ratio	Shear Wave (m/s)	Bueche Layer Thickness (m)	Woody Layer Thickness (m)	Thickness Linkage
1	200- 1000	0.2-0.5	50-300	1.7-3	0.75-3	Bottom Depth
2	200- 1000	0.2-0.5	50-320	2-4	0.75-3	Thickness
3	200- 1000	0.2-0.5	50-350	2-5	1-4	Thickness
4	200- 1000	0.2-0.5	50-400	2-6	2-5	Thickness
5	200- 1000	0.2-0.5	100-450	2-7	2-7	Thickness
6	1000-2000	0.2-0.5	300-1000	HALF SPACE	HALF SPACE	HALF SPACE

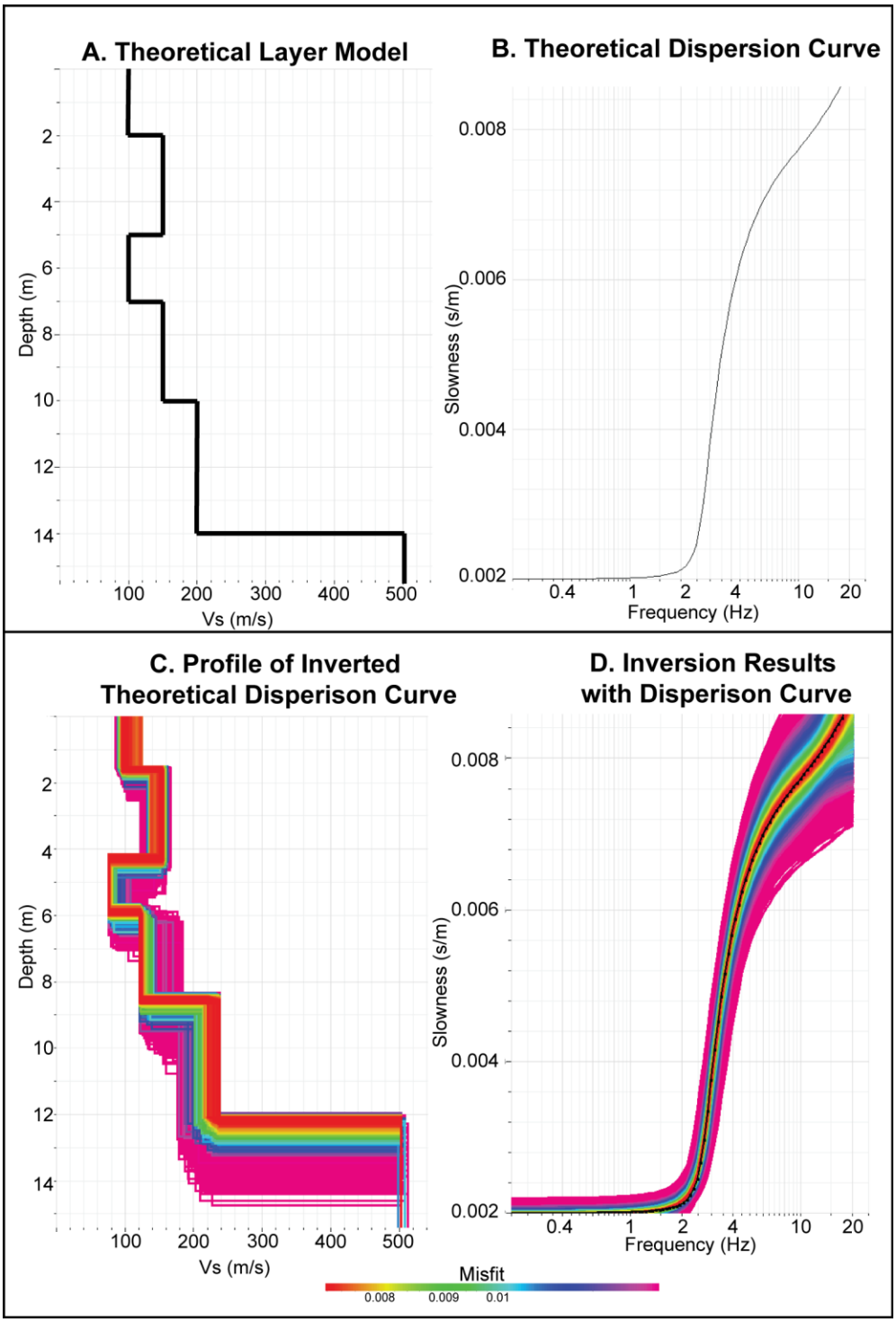

Figure 3.8. An example of how the creation and inversion of theoretical dispersion curves from theoretical layer models can aid in parameterization. First, a layer model is created (A) that represents a potential subsurface velocity scenario using the plugin Gplivemodel (Appendix C.2). The theoretical dispersion curve for this model (B) is input into Dinver's GUI and inverted using the parameterization that is being tested. The velocity-depth profile yielded by the inversion

3.11. Batch Inversion

Given the parameter limits and dispersion curves, the Nearest Neighbor inversion constructs forward models that seek to reduce misfit (see above section 2.2). For each dispersion curve associated with a shotpoint along the seismic survey, nearly 30,000 forward models are generated and tested (Figure 3.8). This number was found to produce the lowest misfit value, while not requiring an inappropriate amount of time to compute. In a case where 30,000 models produces a lowest misfit of 0.003 in 8 seconds, 100,000 models only improves the low misfit in imperceptibly small numbers, while taking nearly a minute to run (Appendix D).

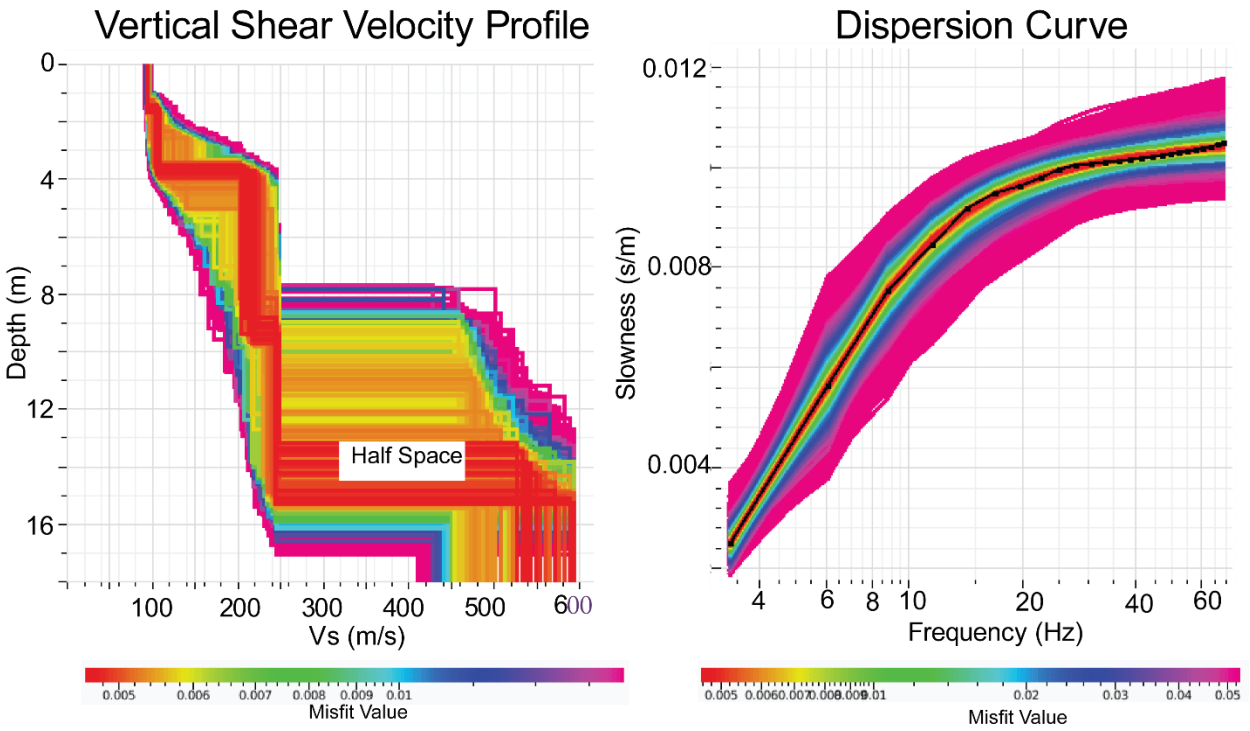

Figure 3.9. Actual displays from Dinver. The Vertical Shear Velocity Profile (left) shown with corresponding misfit values, and the dispersion curve (right) where the black dot input dispersion curve points are surrounded by those produced by the inversion and their corresponding misfit values.

In order to handle the large number of shotgathers and their associated dispersion curves for both surveys, a batch inversion program Xdinver.pl has been modified by Goff (2016). This program facilitates the inversion through Dinver bypassing the GUI (Appendix D.1). By providing the .target files for all the dispersion curves, a file containing the parameters, and the model specifications, the program efficiently performs the same task that Dinver's GUI accomplishes.

Following the batch inversion, a second program Xgrereport.pl, is implemented to extract the reports created by the inversion based on an indicated median profile of the best number of models (Appendix D.2). This process provides the output data necessary for interpolation of the velocity data, and also associated data used to identify differences between shotpoints to be implemented in error estimation during interpolation and interpretation phases (Appendix D.3).

3.12. Post-Inversion Statics Correction

Following extraction of the inversion result files, the vertical velocity profile data for each individual shotgather must be elevation corrected in order to be brought to a common elevation datum. Numerical studies of surface wave inversion have found that dispersion image generation error is very low where the topographic change slope along the survey remains less than 10 degrees, hence why this study only employs a statics correction after inversion (Zeng et al., 2012). The topographic elevation data for each shotpoint along the surveys is extracted from the Lidar elevation data (Cunningham et al., 2018). Using the lowest elevation point as the datum for each survey, all other shotgathers are are brought up by adding the difference (Figure 3.10) (Appendix E.1). These topographically corrected data can now be interpolated.

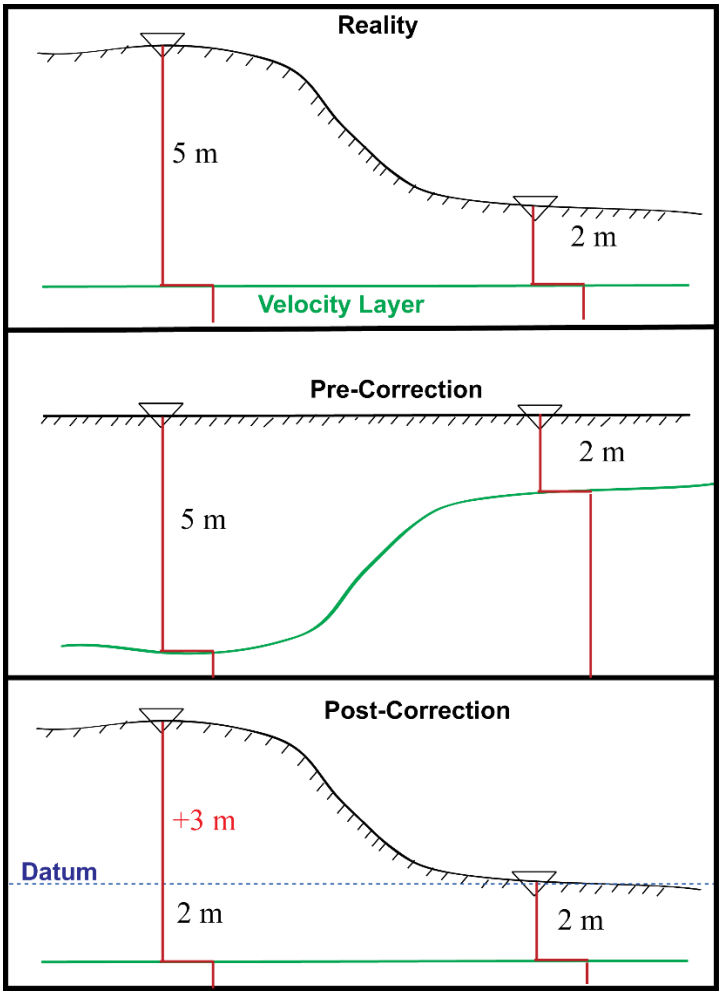

Figure 3.10. Illustration of the conceptual formulation of how statics correction was done for each individual shotpoint based on Lidar elevation data. In the top pane, a completely horizontal velocity layer is sampled at different relative depths by shotpoint locations of different elevations. Without correction, this would be interpolated to show a velocity layer of changing elevation (Middle pane). Using the low-elevation point as a datum, 3 meters are added above in order to bring the velocity layer back to its original horizontal orientation (bottom pane).

3.13. Interpolation

Data extracted from the inversion process are in the form of individual 1D shear velocity-depth profiles for each shotpoint locations along the survey. In order to best view and interpret the velocity information, a psuedo-2D velocity profile is generated using the program *Surfer* v.11. (Appendix E.2) (Golden Software, 2018). This interpolation is also useful in identifying and removing outlier 1-D profiles that vary significantly from neighboring profiles. The interpolation method of Kriging as available in the program visually produces clear and interpretable profiles, while not compromising the data of individual 1-D vertical profiles (Cressie, 1990) (Figure 3.11). When compared with another popular geological interpolation function known as inverse-distance weighting, Kriging is less likely to produce contouring "bulls-eyes", while still extrapolating into areas of little data using a basic linear variogram (Golden Software, 2018). For the Bueche velocity profile, a sampling grid of 2 meters in the horizontal and 1.7 meters in the vertical closely matches geophone spacing and calculated vertical resolution. Likewise both Woody profiles are generated from a sampling grid of 2 meters in the horizontal and 0.75 meters vertically. The same gridding spacing and algorithm used to generate the shear velocity profiles is also used to interpolate the depth-velocity variance data, providing a pseudo-2D profile of confidence in the data (Appendix E.2). These variance grids are also used to further identify and remove individual outlier 1D profiles of unusually high variance.

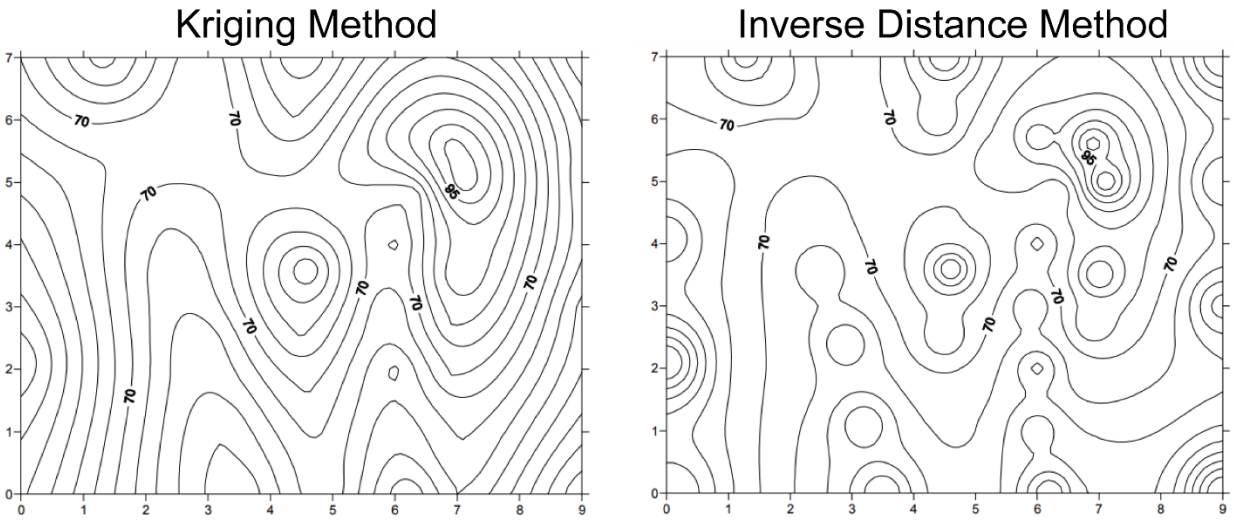

Figure 3.11. Comparison of two popular geological interpolation methods available in Surfer v.11. Kriging (left) employs a linear variogram gridding algorithim with tight spacing control while still considering each unique data point. Inverse distance weighted methods (right) are also widely used in geological interpolation, but they tend to produce bulls-eye circles around data points. (Golden Software, 2018).

3.14. Creating Velocity Variance Profiles

During the extraction of 1-D velocity vertical profiles from Dinver, the 1000 models with the lowest misfit out of all 30,000 models are used to find a mean velocity for specified depths. During this process, the range of velocities of these 1000 best models is also extracted and placed into the same array. This means that for each velocity number that is used to interpolate a 2D profile, a measurement of the velocity "variance" is also provided in the form of V_s range (Figure 5.2). These ranges of generated velocity values are gridded and profiled just like the shear velocity numbers. Initially, this variance profile is used to identify and remove abnormally high variance vertical profiles before the actual velocity data is re-gridded. By creating a visualization of velocity variance of the same extents as the actual velocity profile, it is also possible to identify low-confidence zones in the final data.

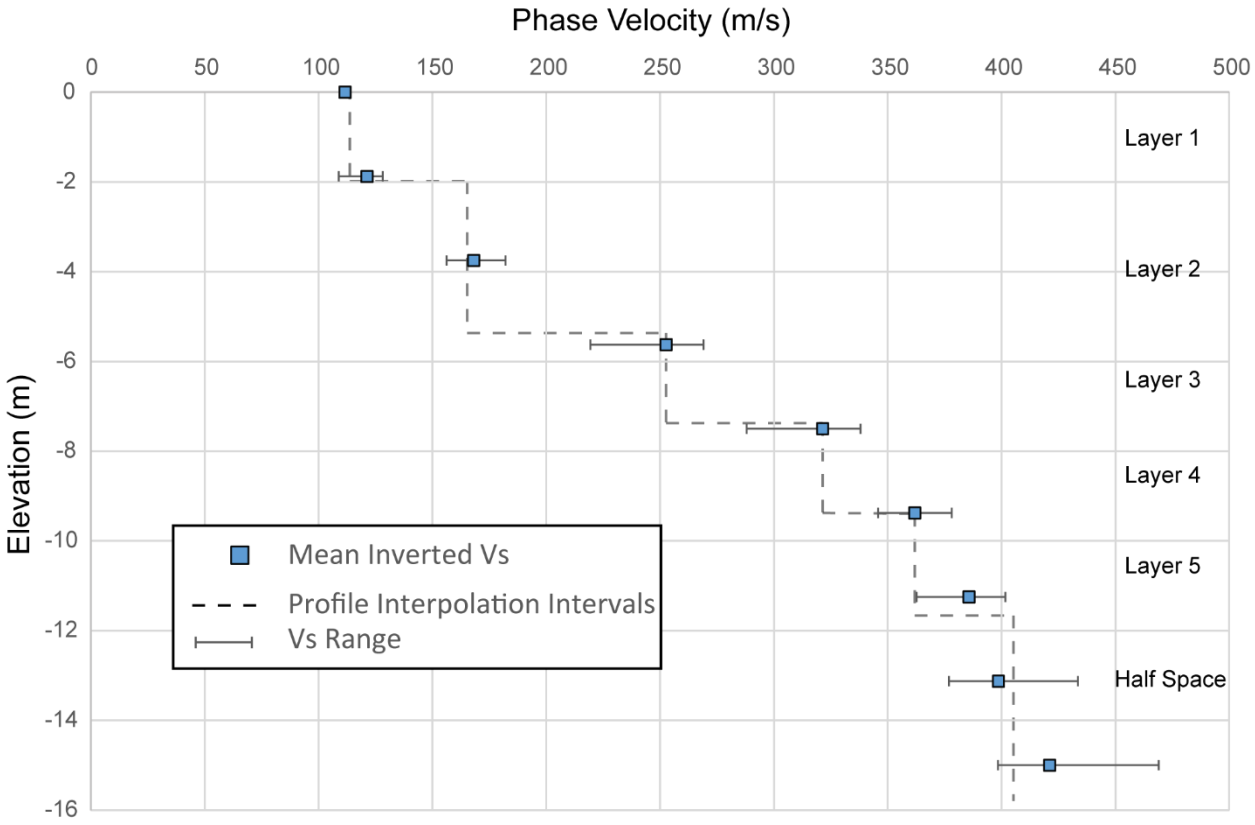

Figure 3.12. In this example using Bueche shotgather 312, mean Vs data extracted from the inversion process is shown with each data point's Vs range (variance). The dashed line represents a simplified notion of the type of velocity gradient that will be created upon gridding and interpolation. Using an extraction interval of 1.7 meters that matches the vertical resolution calculated for the profile, it is possible to see the variance expressed as discrete velocity points. This Vs range is then itself gridded and interpolated to create visual confidence profiles alongside the velocity profiles.

3.15. Dispersion Picking Error Calculation

Dispersion data points serve as the measured or observed data utilized by surface wave inversion to create velocity profiles. Because the process of selecting these dispersion curve points from calculated dispersion images requires human picking, a proper understanding of the potential error associated with this step is required. As explained above (section 3.6 Figure 3.2),

dispersion picking is essentially a visual interpretation of the location of the fundamental order mode based on the higher peaks that distinguish it from other higher order modes.

In order to quantitatively assess the error associated with human visual interpretation of these dispersion images, a small test was devised. For a select number of random shotgathers from the Bueche and Woody surveys, three different visual pickings were made. The first set of picks were drawn from the actual data that underwent inversion (A), the second picks were made by two fellow researchers given only basic instructions on how to select dispersion curve points (B), and the third were selected by myself several weeks after the actual dispersion picking was done (C). After the picks were made, they were resampled to share identical frequency numbers for easier comparison between slowness values. Five random Bueche dispersion images (shotpoints 15, 54, 160, 221, and 410) and 5 random Woody dispersion images (shotpoints 6, 21, 42, 57, and 68) were compared. For each dispersion image, all 3 cases were compared by calculating a percent difference between them, and taking the mean of all of these comparisons.

The results yielded error calculations that were lower than initially expected (Table 5.1). Most of the variance between pickings occurred in the low frequency, high phase velocity area, where it becomes visually difficult to roughly center picks within the high energy fundamental mode area. In the higher frequency areas, the fundamental mode is easier to distinguish, and thus the difference between dispersion picks was relatively low here (Figure 3.13). Dispersion data from Woody proved easier to pick, as the differences here were calculated to be less than those in Bueche dispersion cases. Also unsurprisingly, variance between the original picks (A) and those made by other researchers (B), were slightly higher than the variance between the original picks and my picks made on a later date (C).

Table 3.4: Containing percent difference calculations between picking tests: (A) original picks used in inversion, (B) picks made by other researchers given few instructions, (C) picks selected by myself several weeks after the original dispersion picks were made

	A & B % Diff	A & C % Diff	A & B % Diff	Low Freq A & C % Diff	High Freq A&C % Diff
Bueche	-10.65	-3.09	-3.60	-12.08	1.35
Woody	2.57	2.59	8.52	10.09	0.30
All	**-4.04**	**-0.25**	**2.46**	**-1.00**	**0.58**

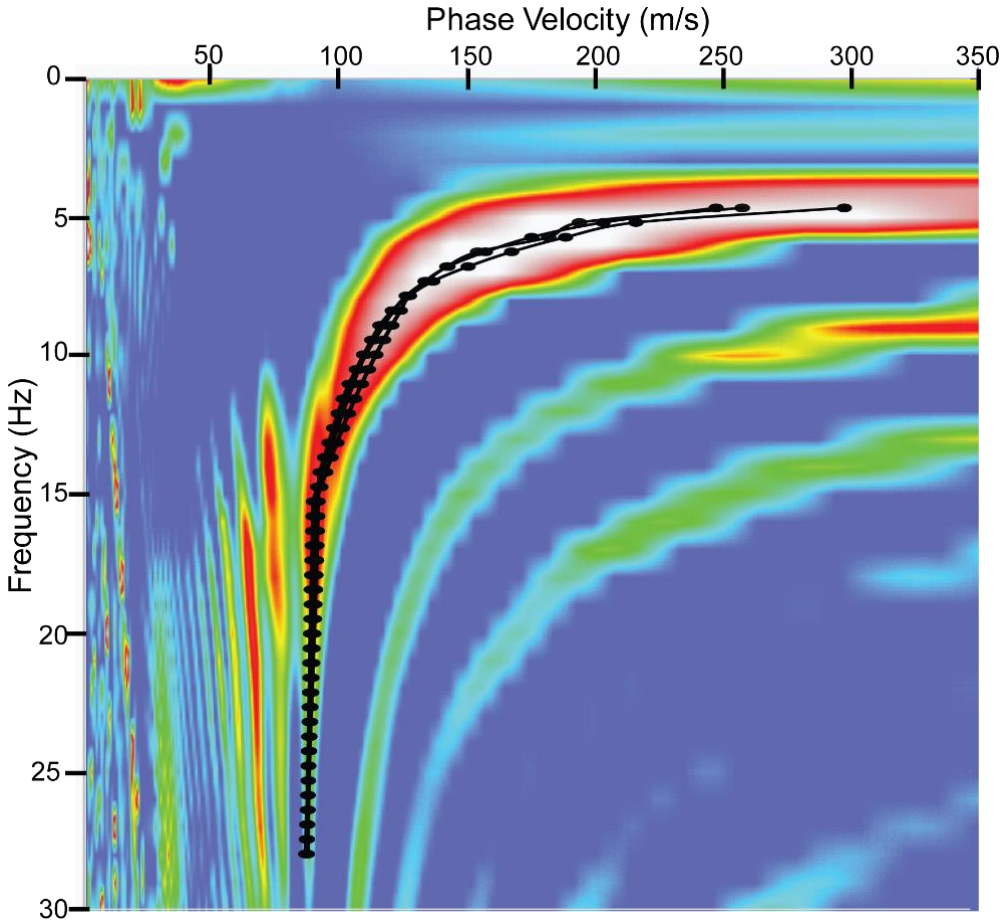

Figure 3.13. Three Picking test cases for Bueche shotpoint 54 are shown plotted on the dispersion image for the same shotpoint. The three cases are nearly indistinguishable below 12 Hz, but variance begins to increase with lower frequencies where the fundamental mode curve begins to be more difficult to visually distinguish.

CHAPTER 4. RESULTS & INTERPRETATION

4.1. Bueche Velocity Profile

At 481 meters long, the Bueche survey is the longest in this study, and also contains the most variable topography (Figure 4.1). The resultant shear wave velocity profile gridded from inversion results images up to 13 meters of the subsurface (Figure 4.2). Velocities increase with depth relatively consistently at a gradient of around 25-35 s^{-1} across the profile, but they also diminish towards the southwest (toward the paleochannel). Velocity layering also appears to be generally parallel the topog**r**aphy for most of the subsurface (Figures 4.3, 4.4). In the first 100 meters from the southwestern side of the profile, lower velocity layers thicken channel-ward in the uppermost 5-8 meters, with velocity gradients around 25 s^{-1} (Figure 4.5). In this area of the survey, the upper 1-4 meters of sediment contains velocities at and below 50 m/s. Velocities are also lower in the lowest topographic point along the survey between 170 and 210 meters with velocity gradients around 25 s^{-1} down to 7 meters depth, observed also in the Lidar map as a large swale that crosses the middle of the profile (Figure 4.1) (Cunningham et al., 2018).

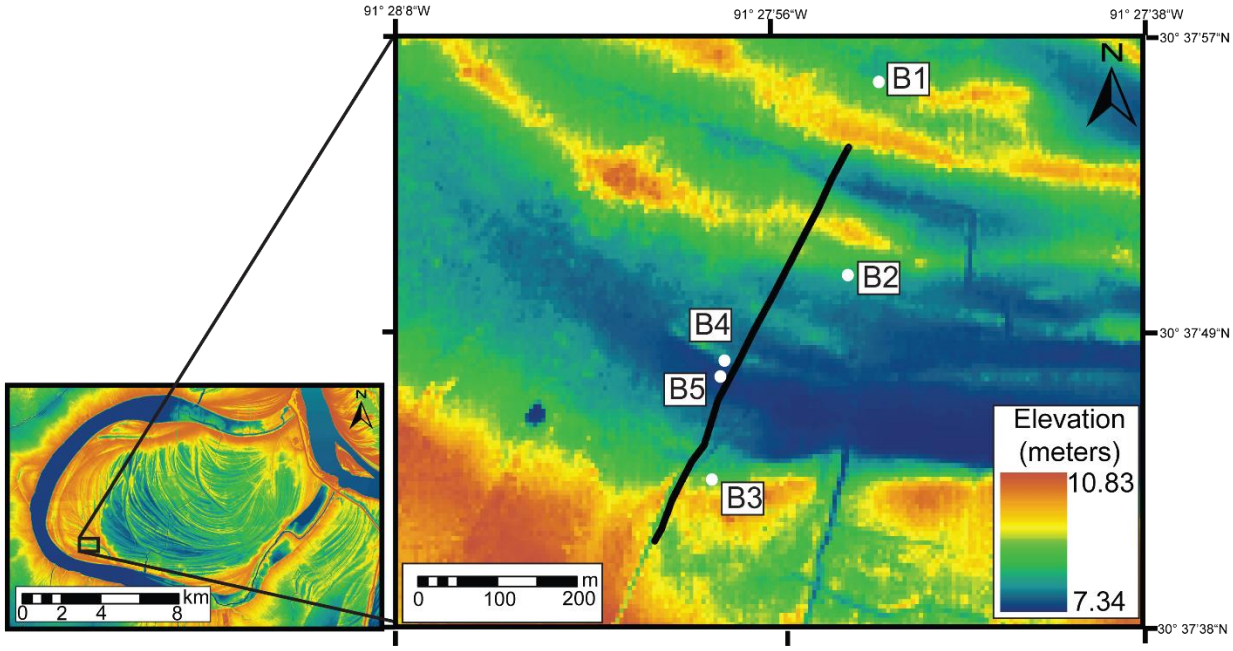

Figure 4.1. Location of Bueche seismic survey and wells on Lidar elevation image (Cunningham et al., 2018). Shotpoints begin at 1 and progress to 461 in the northeastern direction. Note, in addition to the size scale difference between the two maps, Lidar elevation colors on the smaller map (left) are not the same as Lidar elevation colors on the Bueche inset location map (right).

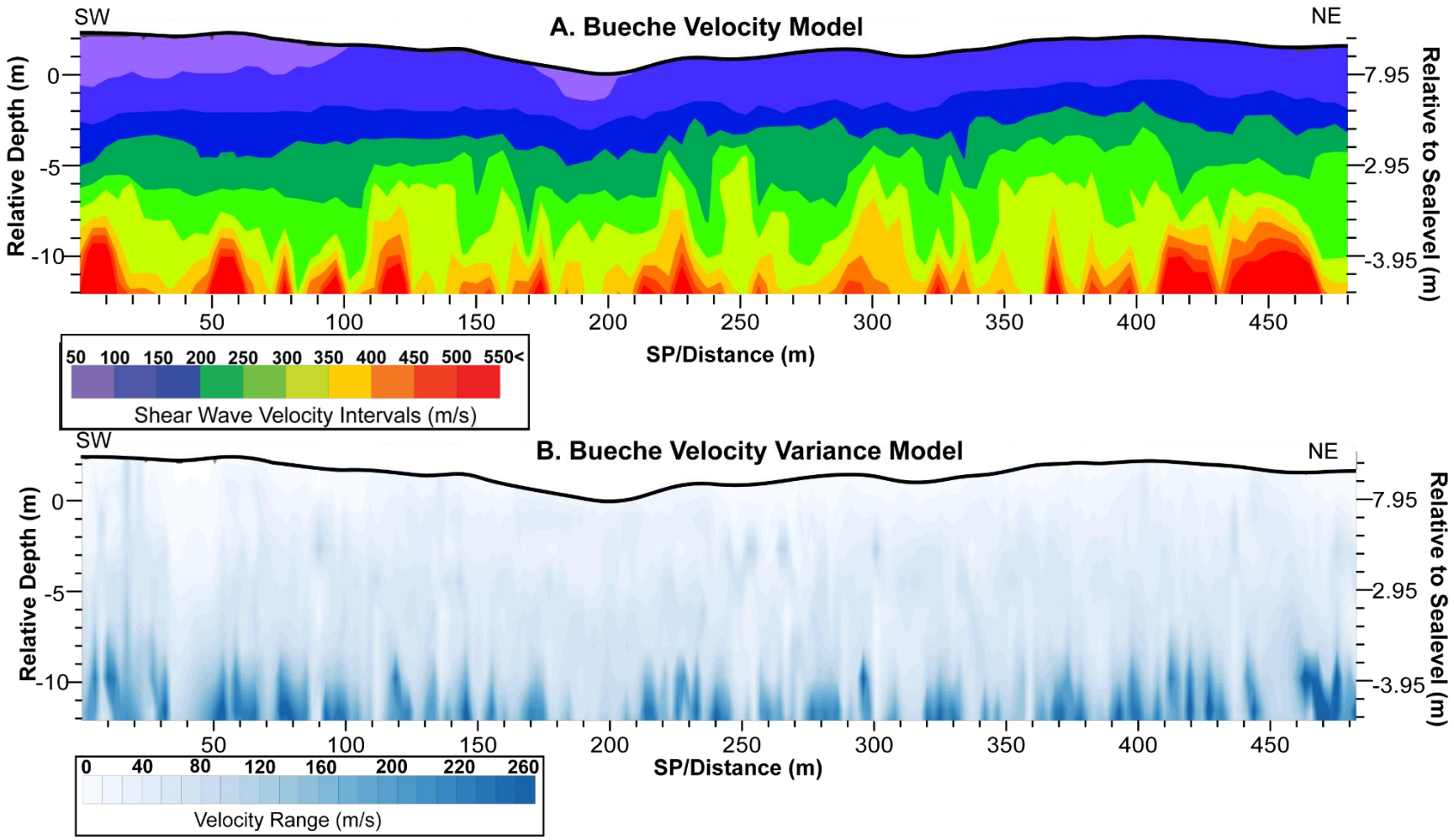

Figure 4.2. (A) Psuedo 2-D shear-wave profile of the Bueche survey. “Warmer” colors indicate increasing velocity layers values. The horizontal axis indicates shotpoint, with 1 m spacing. Depth relative to the lowest point on the survey is indicated on the right vertical Y axis, while depth relative to sea-level is indicated on the left vertical axis. (B) Bueche survey variance plot. Progressively bluer colors indicate regions of higher velocity range measured in m/s from the mean velocity values used to grid the velocity profile.

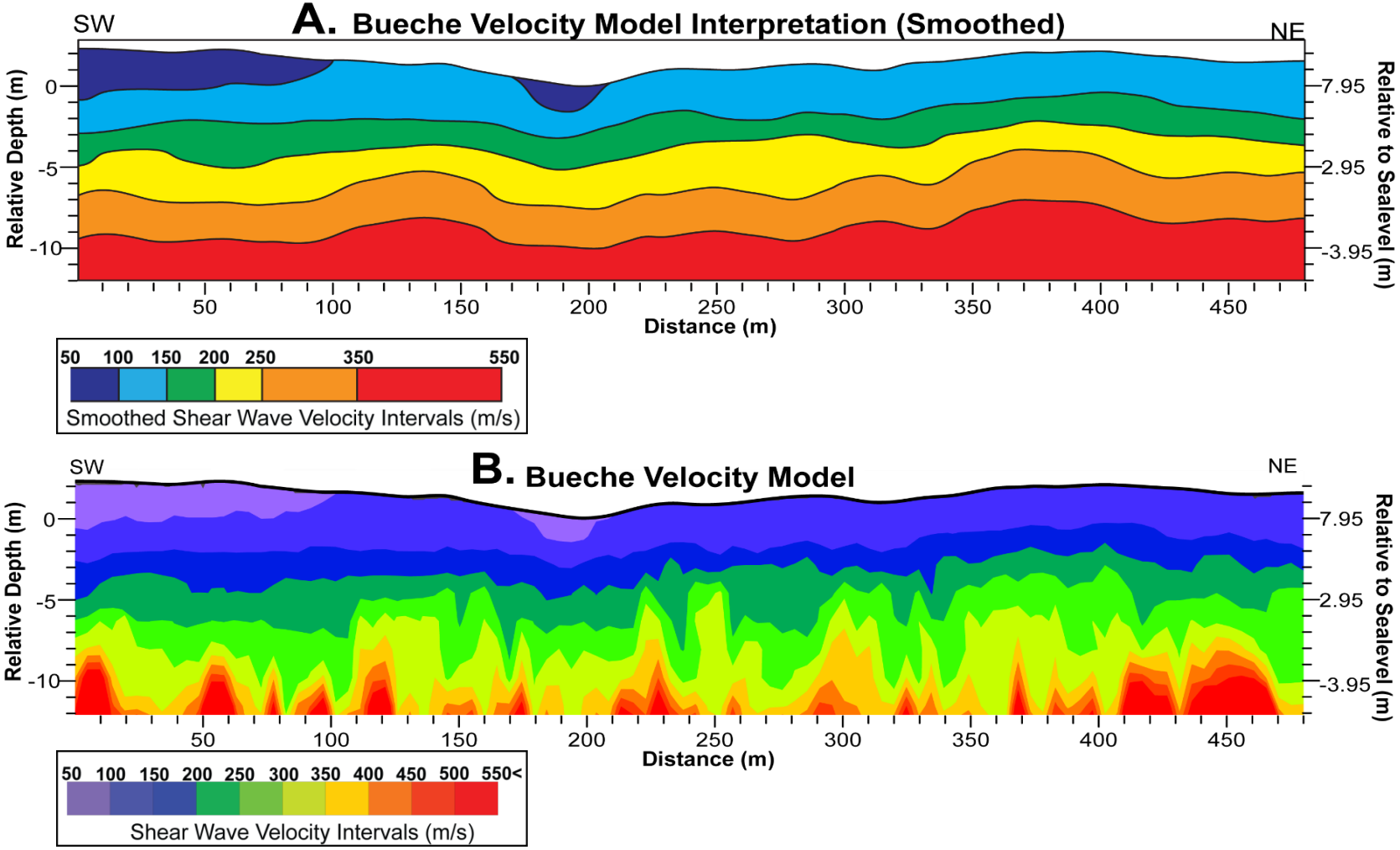

Figure 4.3. (A) A smoothed interpretation of the Bueche velocity model (B). This interpretation model aids in establishing a visual link between the topography and velocity layering, while suppressing "jaggedness" in the velocity data in zones of increasing velocity variance with depth. The colorbar for (A) features color layers that are not evenly divided between velocity values as in (B), but rather warmer colors such as orange and red feature larger interpreted velocity values as the data confidence becomes lower and velocity gradients become higher with depth.

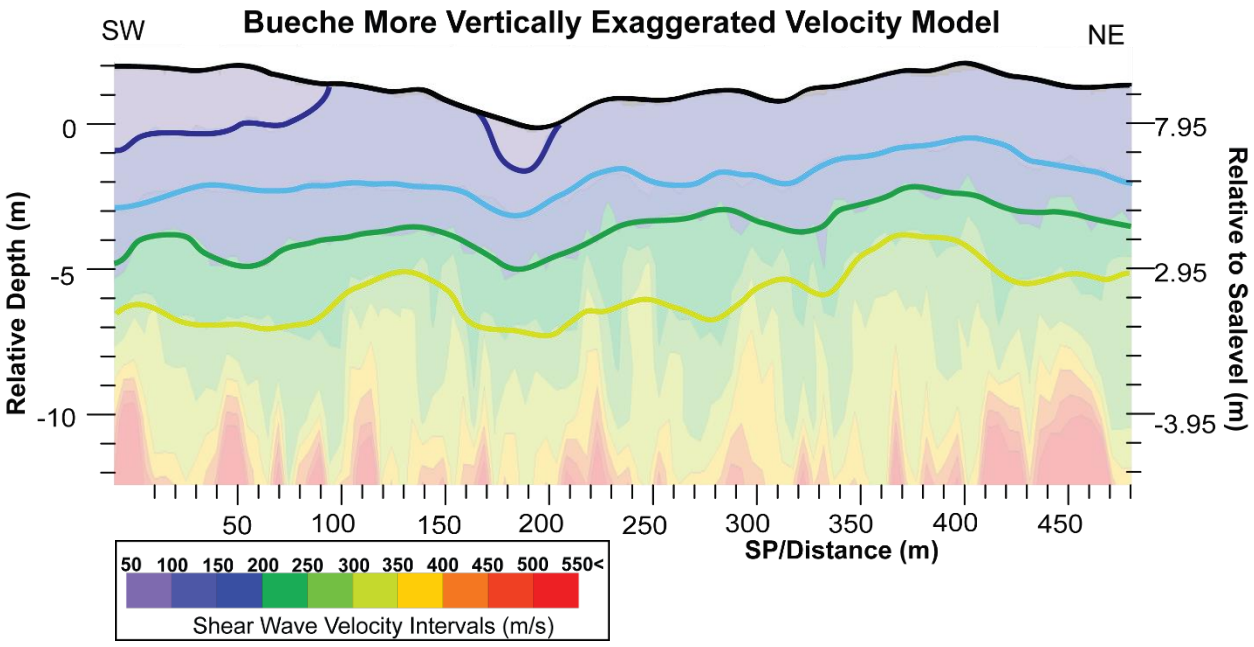

Figure 4.4. Bueche Velocity profile (VE = 1.10), and simplified interpreted velocity layer lines (Figure 4.3) showing how the layering generally follows topography (black line) for most of the profile down to 7-9 meters of depth below the surface.

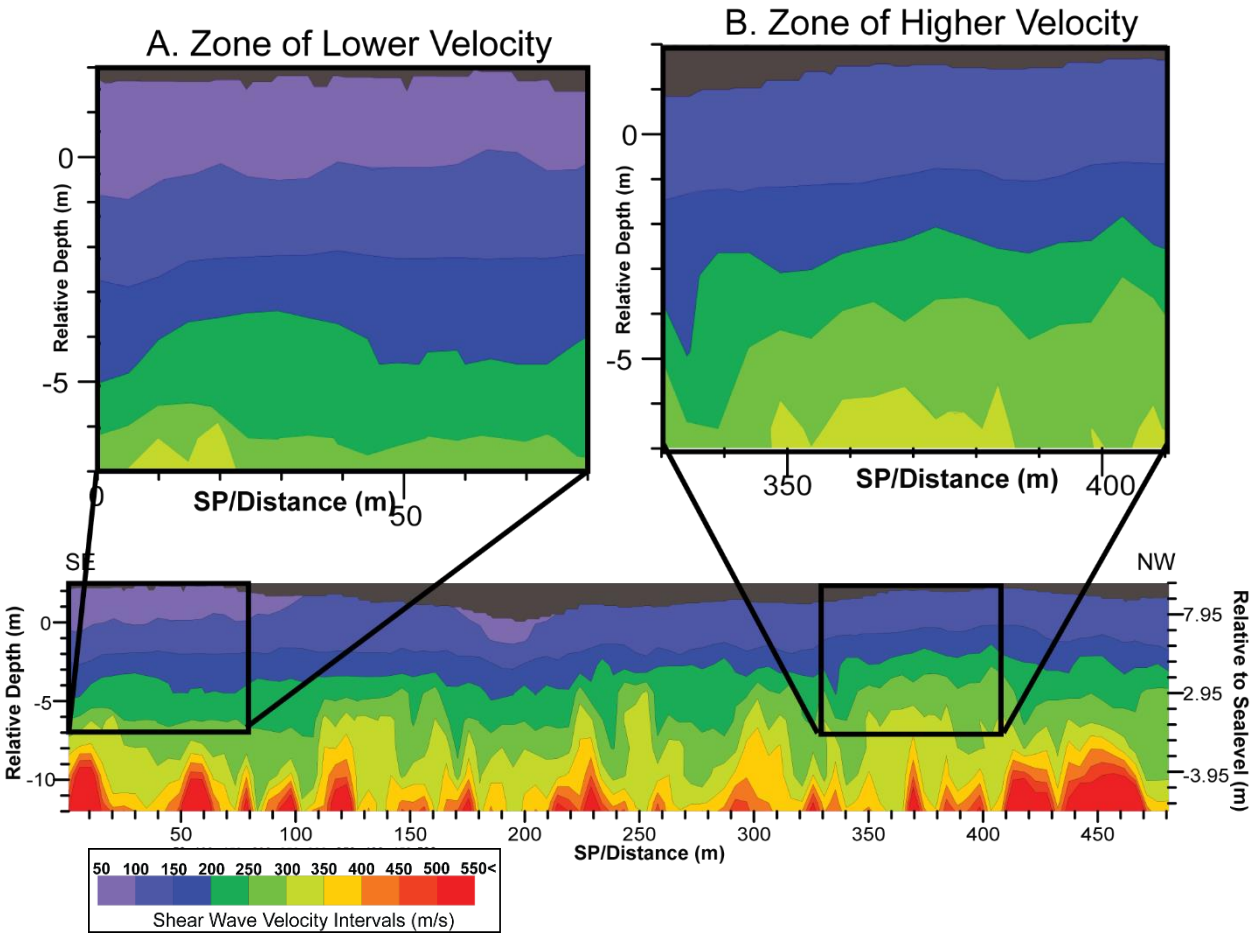

Figure 4.5. Two regions of the Bueche velocity profile identified and displayed for comparison. (A) A zone of lower velocity on the Southewestern side of the profile compared to a higher velocity zone in the Northwestern side of the profile (B). The depth of the two selections is normalized from the surface topography down to exemplify this difference in velocity layering.

4.2. Bueche Well Data Projection with Velocity Data

Projection of the electrical-conductivity (EC) logs onto the seismic velocity profile shows no clear correlation between velocity layer boundaries and log values (Figure 4.6). However the lowest conductivity log (B2) is located in a section of the velocity profile with one of the higher velocity gradients (35 s^{-1}) around shotpoint 350. The logs from wells B4 and B5 are more variable in conductivity, but appear to match B2 below 4 meters with similarly low EC values (below 25 mS/m) (Figure 4.7). The highest conductivity log in the survey, B3 shows "kicks" of high EC values below 2 meters (around 80 mS/m), where seismic velocities diminish towards the paleochannel between in the first 100 meters from the southwestern side of the profile (Figure 4.6). EC values do not appear to correlate to the velocity model, however changes in EC values between wells correlate with lateral trends in the velocity model, with both decreasing velocities and increasing EC values toward the southwest (Figures 4.8, 4.9). The EC log data from well B1 is not projected onto the profile as its location is both farther away and within another swale that the seismic profile does not sample.

The available core data for wells B2 and B3 also show this trend of decreasing grainsize toward the southwest (paleochannel-ward) (Figure 4.10) (Olson, 2017). The cores are not continuous and contain only intervals of data between 0.5 and 1 meter gaps. B3 is more clay and silt dominated than B2 in the upper 5-7 meters (Figure 4.11) (Olson, 2017). Velocities around shotpoint 100 (B3) are 50 m/s slower than velocities around shotpoint 350 (B2), despite both locations being at roughly the same elevation (Figure 4.12) (Cunningham et al., 2018).

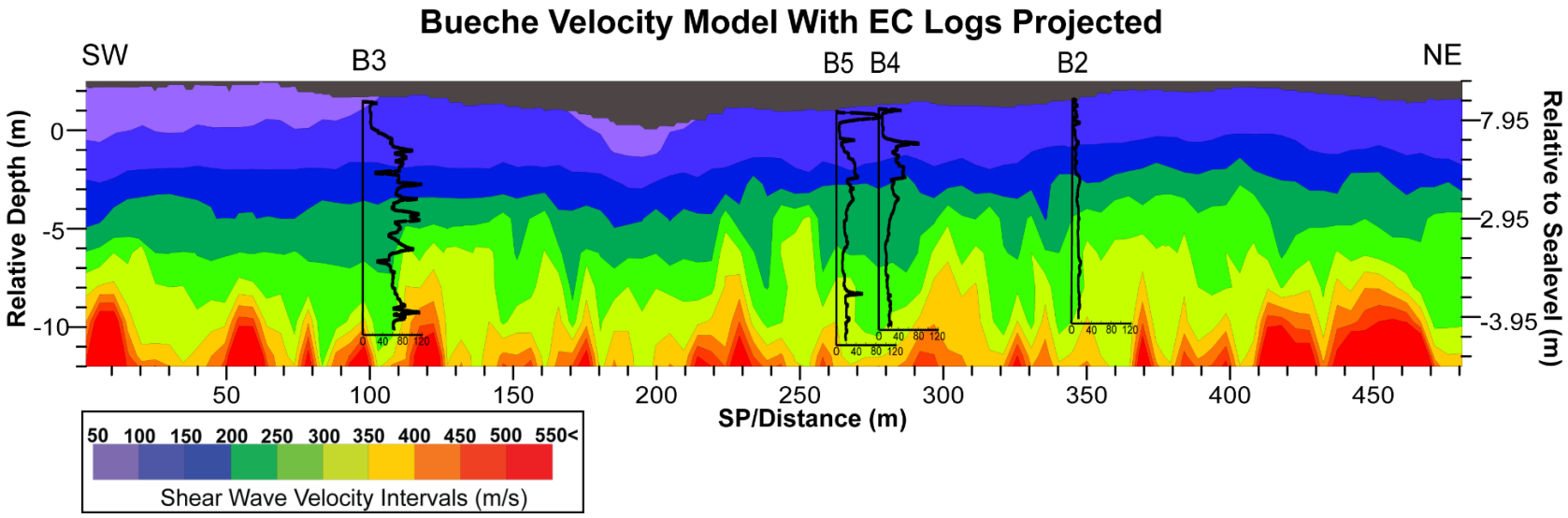

Figure 4.6. Bueche velocity model with EC logs projected onto the profile. “Warmer” colors indicate increasing velocity layers values. The horizontal axis indicates shotpoint, with 1 m spacing. Depth relative to the lowest point on the survey is indicated on the right vertical Y axis, while depth relative to sea-level is indicated on the left vertical axis. “Kicks” to the right indicate higher EC

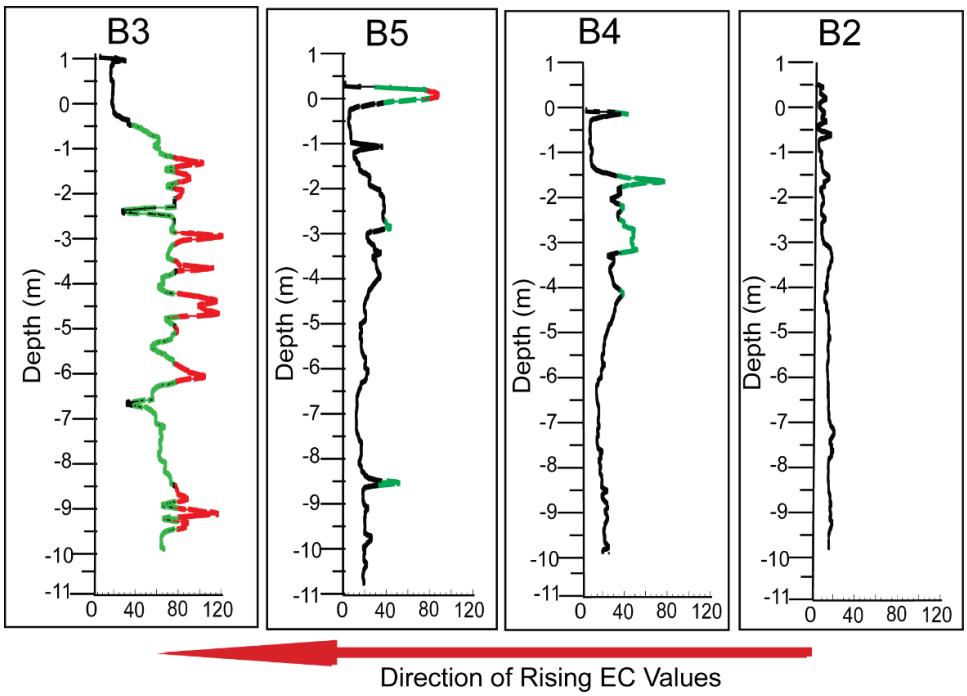

Figure 4.7. EC Log Comparison. EC data measured in milisiemens per meter (horizontal axes). EC values higher than 40 mS/m are colored green, and those higher than 80 are colored red. Example of increasing EC values in the southwestern paleochannel-ward direction (Olson, 2017).

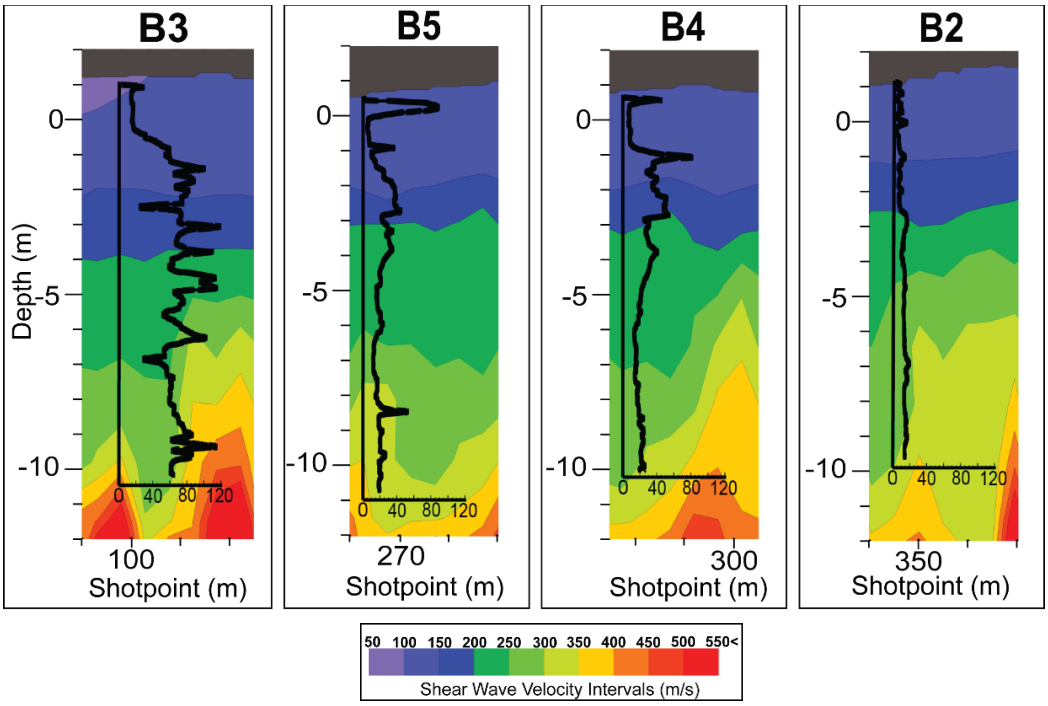

Figure 4.8. EC logs projected onto respective sections of the Bueche pseudo 2D velocity profile. It is difficult to see any correlation between EC values and velocity layering, however, EC values increase toward the southwestern (leftward) just as velocity gradients decreases from 30 s^{-1} at B2 to 20 s^{-1} at B3.

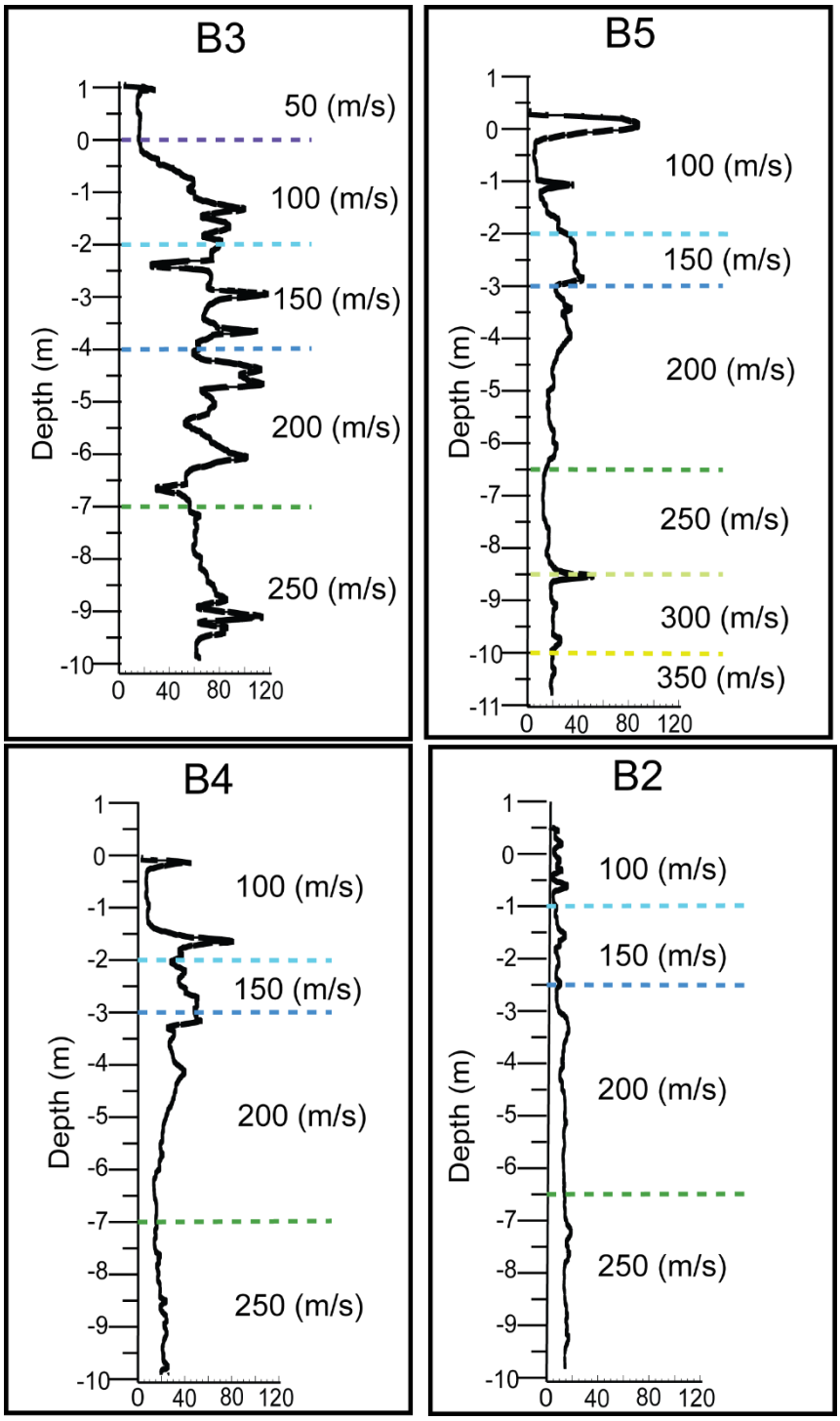

Figure 4.9. Alternate version of figure 4.8, casting EC log data (Figures 4.6 and 4.7) (Olson, 2017) with superimposed shear velocity layers derived from the pseudo 2D interpolation profile. As mentioned above, there is no discernable correlation between velocity and EC values.

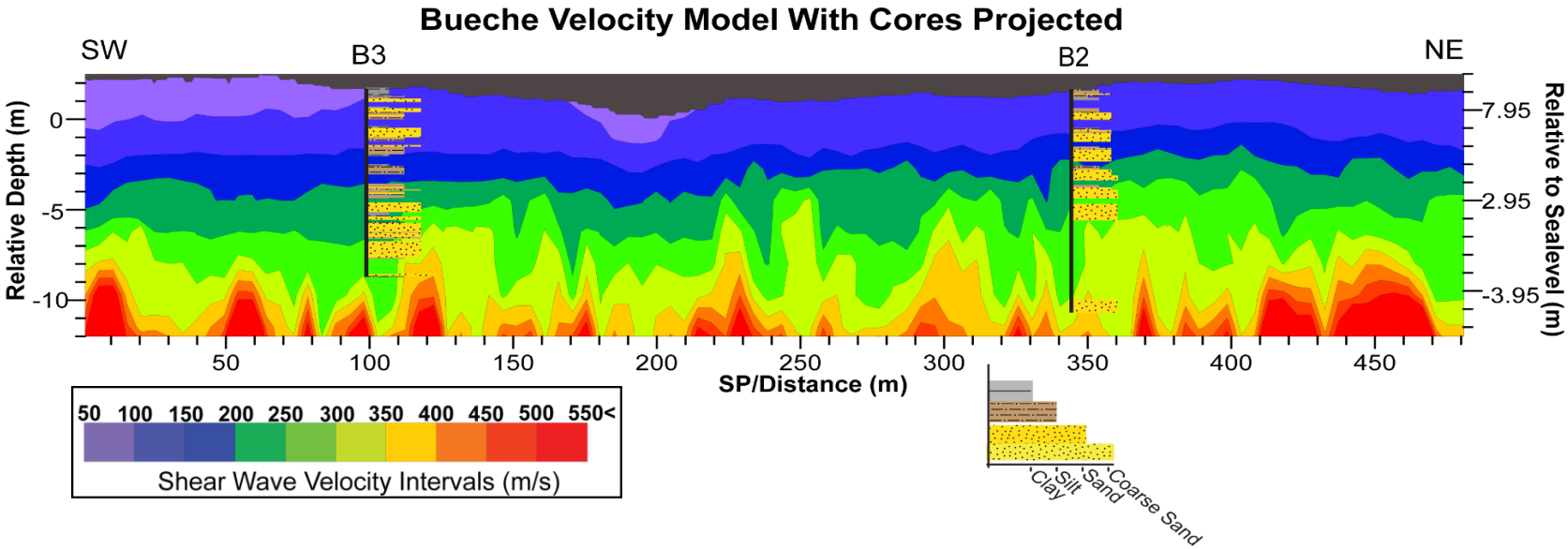

Figure 4.10. Bueche velocity model with core data interpretations projected onto the profile (Olson, 2017). "Warmer" colors indicate increasing velocity layers values. The horizontal axis indicates shotpoint, with 1 m spacing. Depth relative to the lowest point on the survey is indicated on the right vertical Y axis, while depth relative to sea-level is indicated on the left vertical axis. Sediment boxes increasing in size towards the right indicate higher grain sizes. Yellow for sand, brown for mud, and grey for clay rich sections (Olson, 2017).

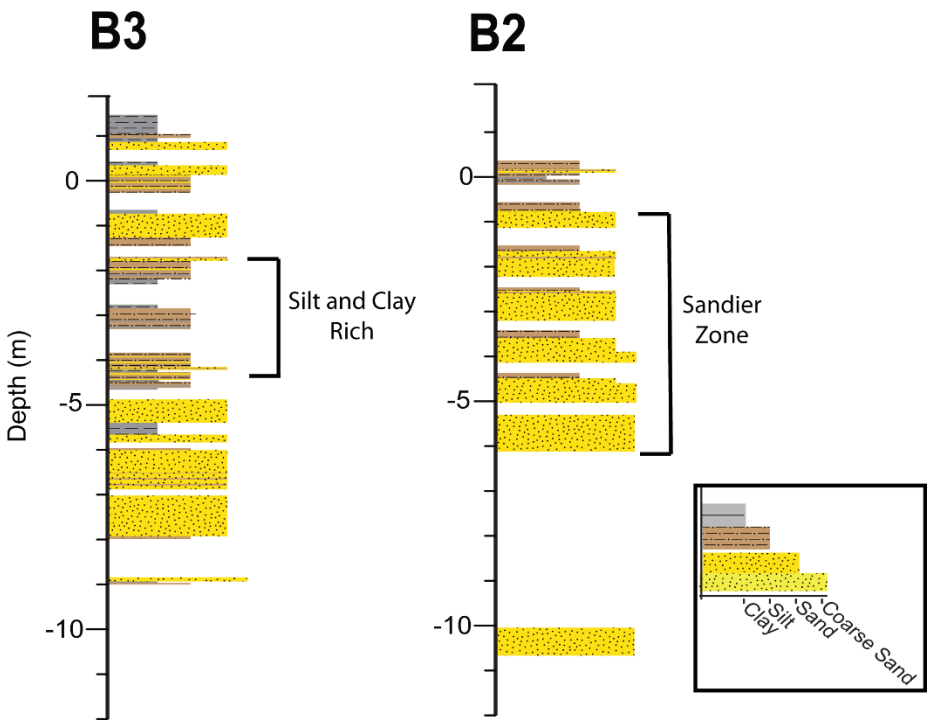

Figure 4.11. Comparison of the two existing Bueche cores B3 and B2 (Figure 4.1). B3 lies more southwestern (channel-ward) than B2, and contains more silt and clay rich zones in the top 7 meters than B2 (Olson, 2017).

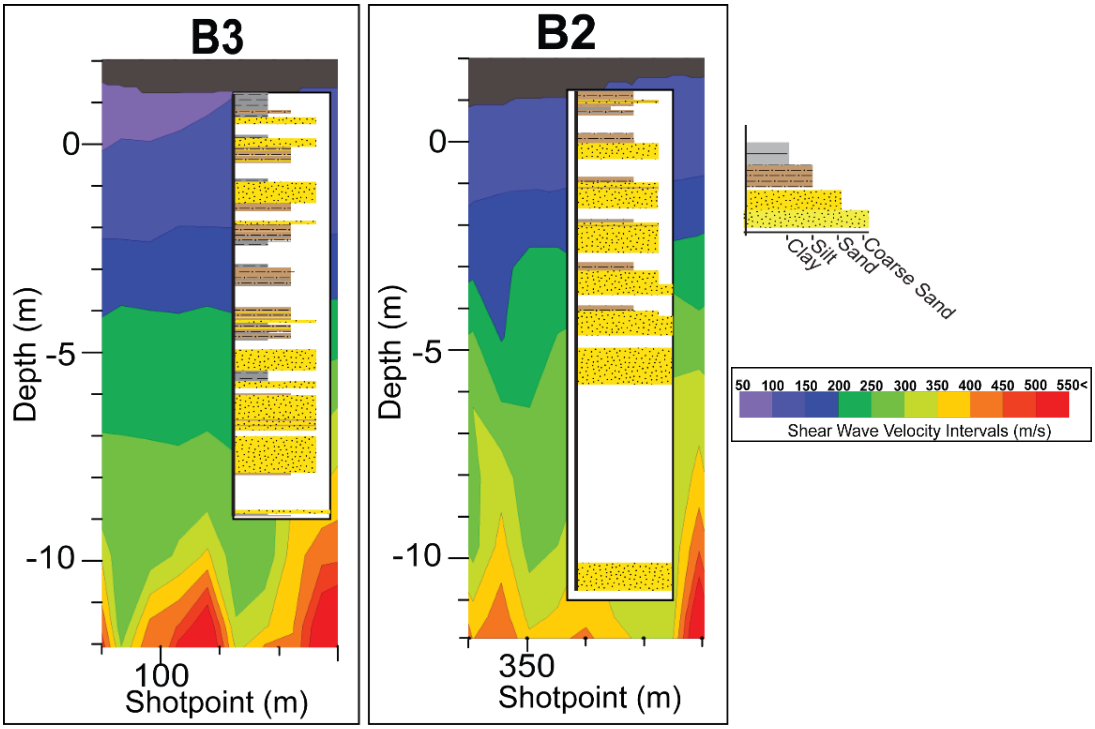

Figure 4.12. Available cores compared to respective sections of the pseudo 2-D velocity profile. It is difficult to see any correlation between the core sections and velocity layering, however the velocity data around core B3 (left) is lower than the velocity around B2 (right) by 25 m/s . Between the cores, B3 is finer grained than B2, and has EC values that are higher (see Figure 4.11) (Olson, 2017).

4.3. Woody Survey Velocity Profiles

Inline and Crossline seismic profiles from the Woody survey area are shorter in length (Inline: 81 m, crossline: 40 m) and less variable in surface topography than that of the Bueche (see section 3.2) (Figure 4.13). Woody velocity data also have higher vertical resolution (0.75 meters, see section 3.9). On average velocity data from both Woody profiles have lower values than those from Bueche by 50-100 m/s (Figures 4.14, 4.15). Both the inline and crossline profiles also contain negative velocity gradients in the uppermost 1-1.2 meters of sediment where velocity diminishes by -200 s^{-1} across the profile (Figure 4.16). Below 1.25-1.5 meters of depth, the velocity progressively increases with an average vertical velocity gradient of 25 s^{-1} down to 7 meters of depth (Figure 4.17). With the exception of the negative velocity gradient in the uppermost ~1 meter of sediment, the Woody velocity data remain slower than Bueche below than this uppermost negative velocity gradient zone (Figure 4.18). Like Bueche, velocity layers appear to parallel topography generally, but only clearly above 6-7 meters of depth (Figure 4.19). The topography varies much less than Bueche (less than a half a meter change across the inline profile and less than 0.25 m across the crossline profile).

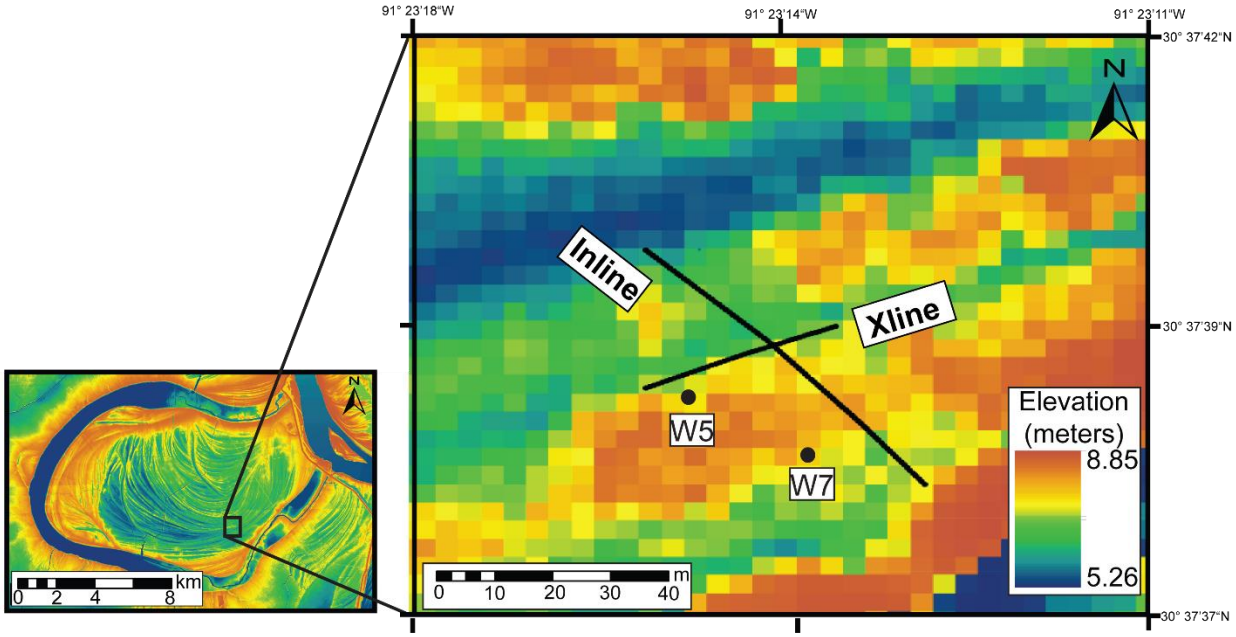

Figure 4.13. Location of Woody seismic surveys and wells on Lidar elevation image (Cunningham et al., 2018). Note, in addition to the scale difference between the two maps, Lidar elevation colors on the smaller map (left) are not the same as lidar elevation colors on the inset Woody location map (right). The crossline (abbreviated "Xline") extends E-W (L to R), while the inline extends N-S.

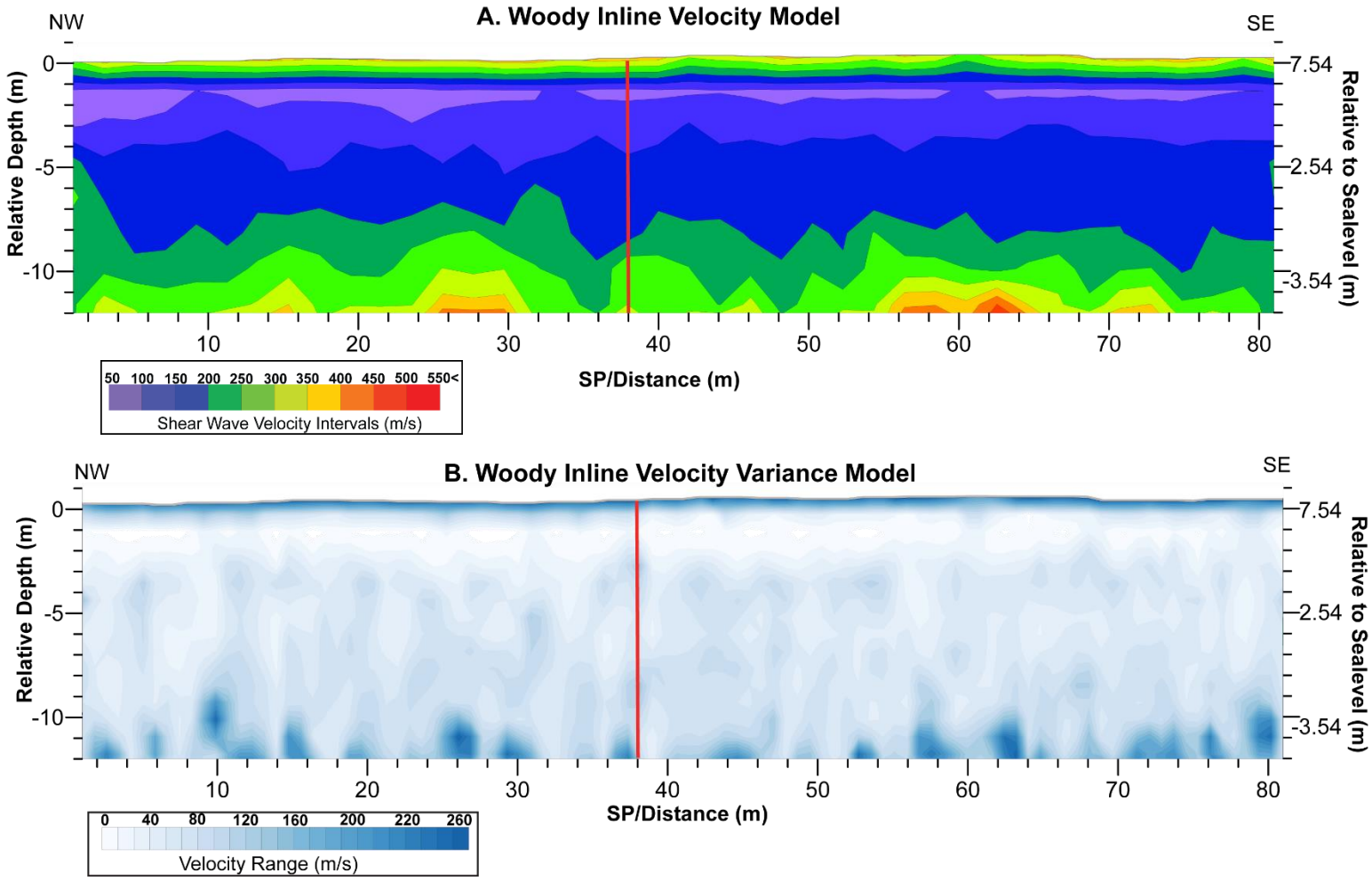

Figure 4.14. (A) Psuedo 2-D shear-wave profile of the Woody inline survey. "Warmer" colors indicate increasing velocity layers values. The horizontal axis indicates shotpoint, with 1 m spacing. Depth relative to the lowest point on the survey is indicated on the right vertical Y axis, while depth relative to sea-level is indicated on the left vertical axis. The red vertical line on the profile shows where the inline and crossline intersect eachother. (B) Woody inline survey variance plot. Progressively bluer colors indicate regions of higher velocity range measured in m/s from the mean velocity values used to grid the velocity profile

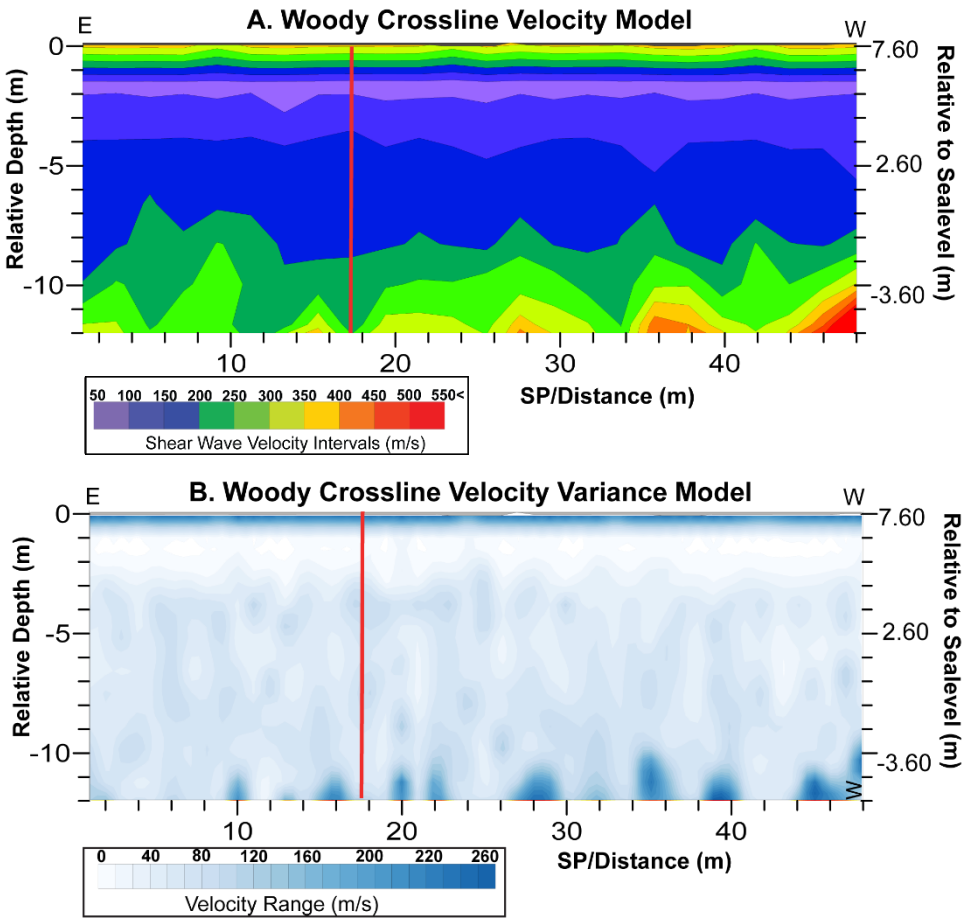

Figure 4.15. (A) Psuedo 2-D shear-wave profile of the Woody crossline survey. “Warmer” colors indicate increasing velocity layers values. The horizontal axis indicates shotpoint, with 1 m spacing. Depth relative to the lowest point on the survey is indicated on the right vertical Y axis, while depth relative to sea-level is indicated on the left vertical axis. The red vertical line on the profile shows where the inline and crossline intersect eachother. (B) Woody crossline survey variance plot. Progressively bluer colors indicate regions of higher velocity range measured in m/s from the mean velocity values used to grid the velocity profile.

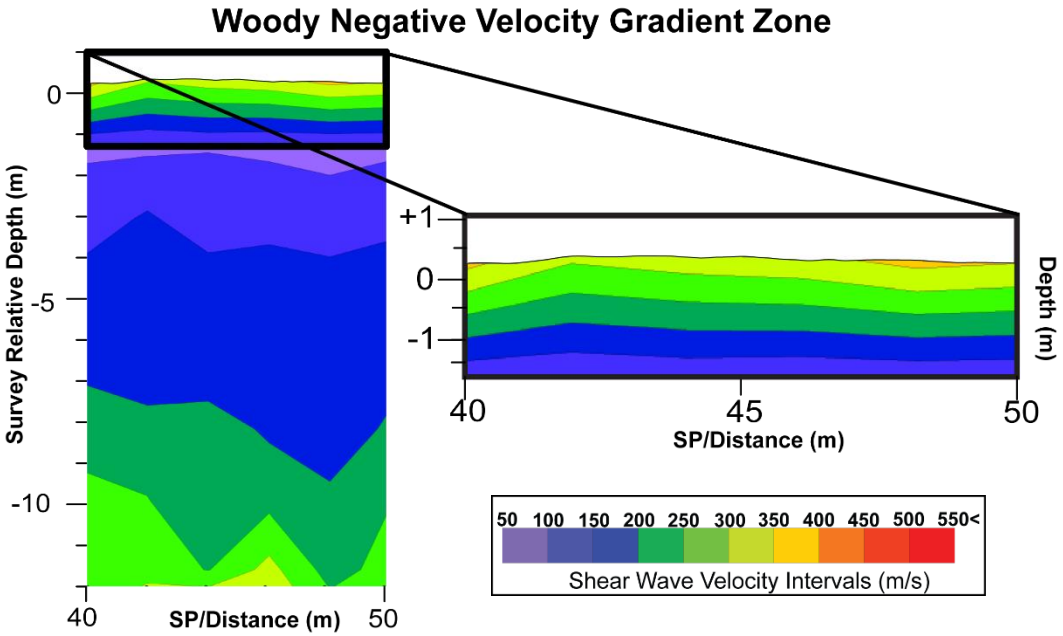

Figure 4.16. A 10 shotpoint section from the Woody Inline between 40 and 50 meters of the survey showing the high-to-low negative velocity gradient that occurs within the top 1.5 meter of Woody velocity models (Right). Here the velocity gradient is -200 s^{-1}, where velocity decreases from 350 m/s to 50m/s.

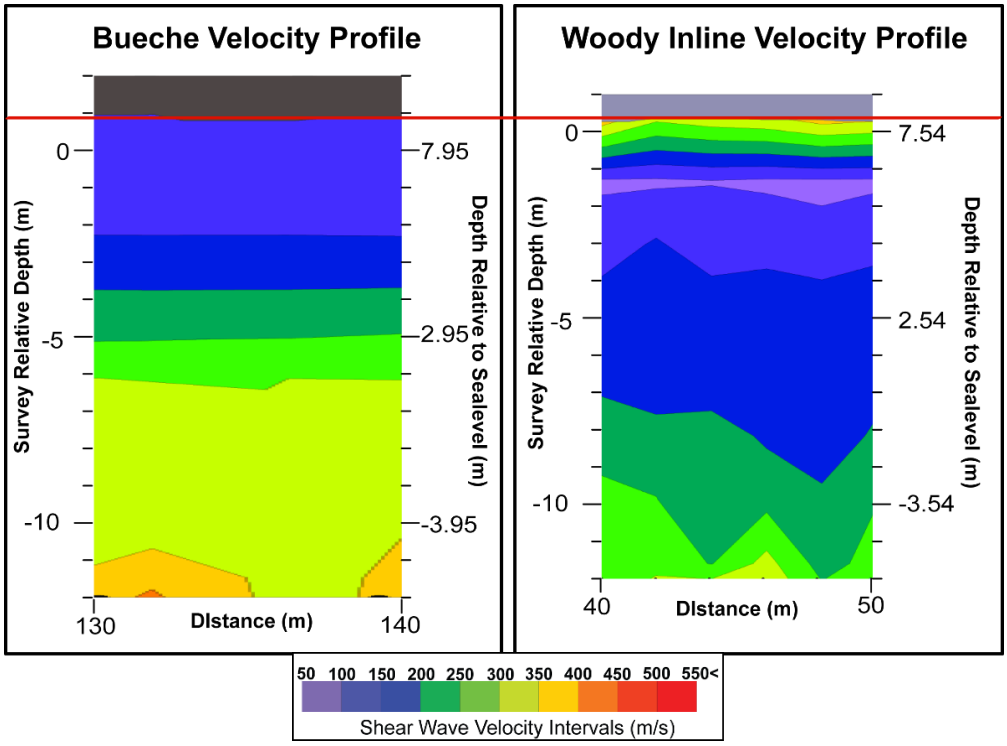

Figure 4.17. Comparison between Bueche and Woody inline velocity profile sections. The red line indicates a line of equal depth from the surface (and profiles are adjusted accordingly) for easier comparison. This shows the prevalence of faster Bueche velocities beyond the very top meter of Woody data.

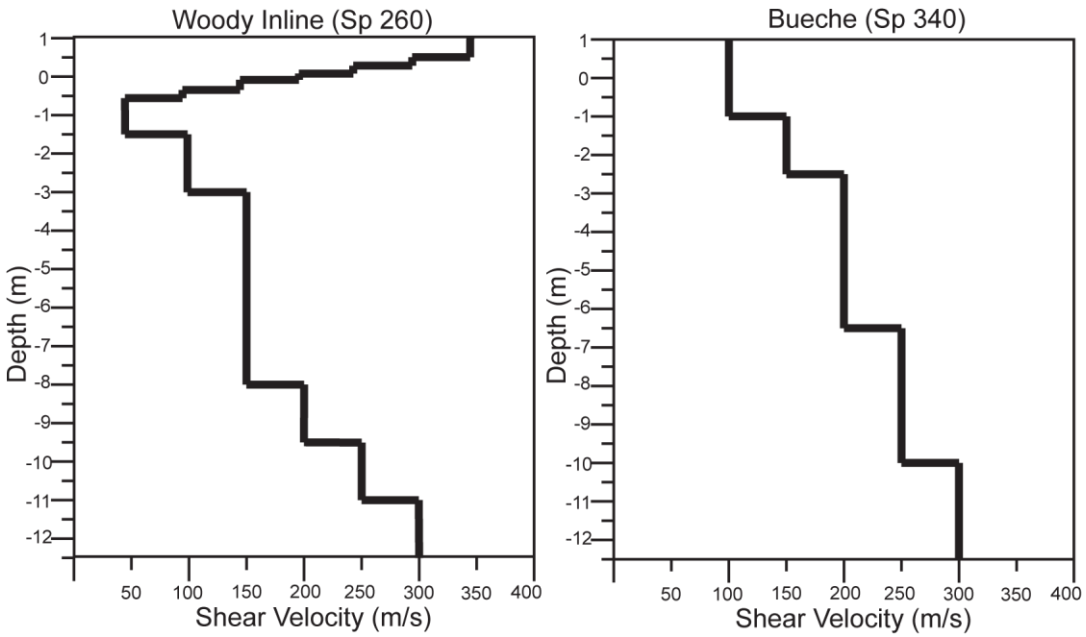

Figure 4.18. Another comparison of Woody and Bueche velocity data from different locations on the profile than the previous figure, showing velocity layering instead of profile sections. Other than the negative velocity gradient at the upper meter of the Woody data, Bueche is faster by an average of 50 m/s.

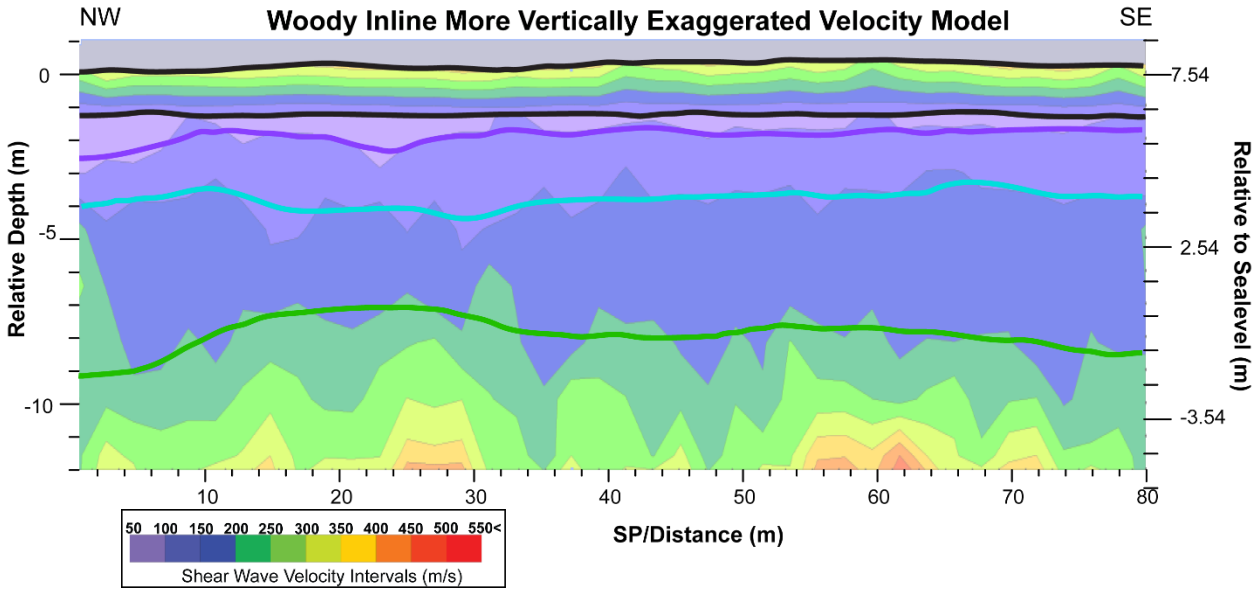

Figure 4.19. Woody Inline pseudo 2D velocity profile(VE=1.3), Colored lines are interpreted velocity layer lines in order to show how the layering generally follows topography (black line) for most of the profile, however not to the same degree as Bueche (Figure 5.3).

4.4. Woody Inline and Crossline Well Data Projection

Available EC logs are projected onto both profiles (Figures 4.20 and 4.21). EC values from wells W5 and W7 are similar to each other, each containing high EC values in the top meter (100-140 mS/m), followed by medium to lower conductivity below this with only a few small high EC zones (40-80 mS/m). The high EC "kicks" in the logs observed in the top meter appear to correlate with the observed high-to-low velocity change in the top meter of the profiles, especially at W5 when projected onto both the inline and crossline profiles (Figure 4.22). The EC data in W5 appear slightly higher in value than in W7.

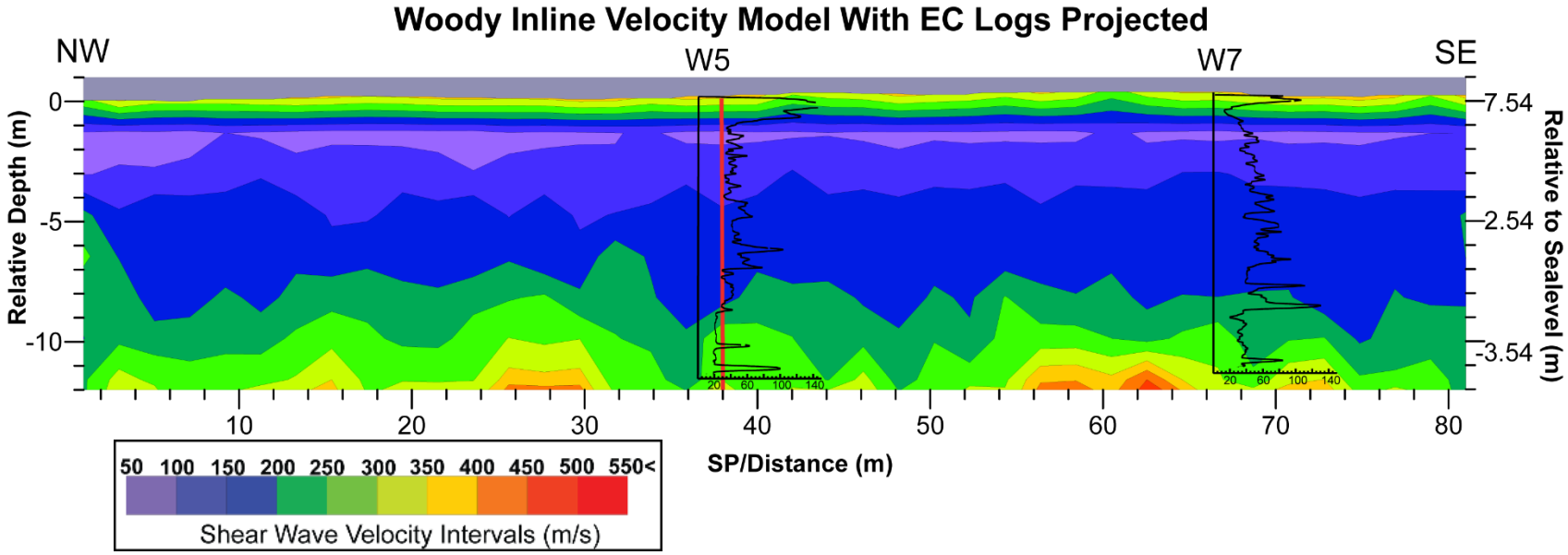

Figure 4.20. Woody inline velocity model with EC logs projected onto the profile. “Warmer” colors indicate increasing velocity layers values. The horizontal axis indicates shotpoint, with 1 m spacing. Depth relative to the lowest point on the survey is indicated on the right vertical Y axis, while depth relative to sea-level is indicated on the left vertical axis. The red vertical line on the profile shows where the inline and crossline intersect eachother “Kicks” to the right indicate higher EC measurements. EC measurements are in milliSiemens per meter (mS/m).

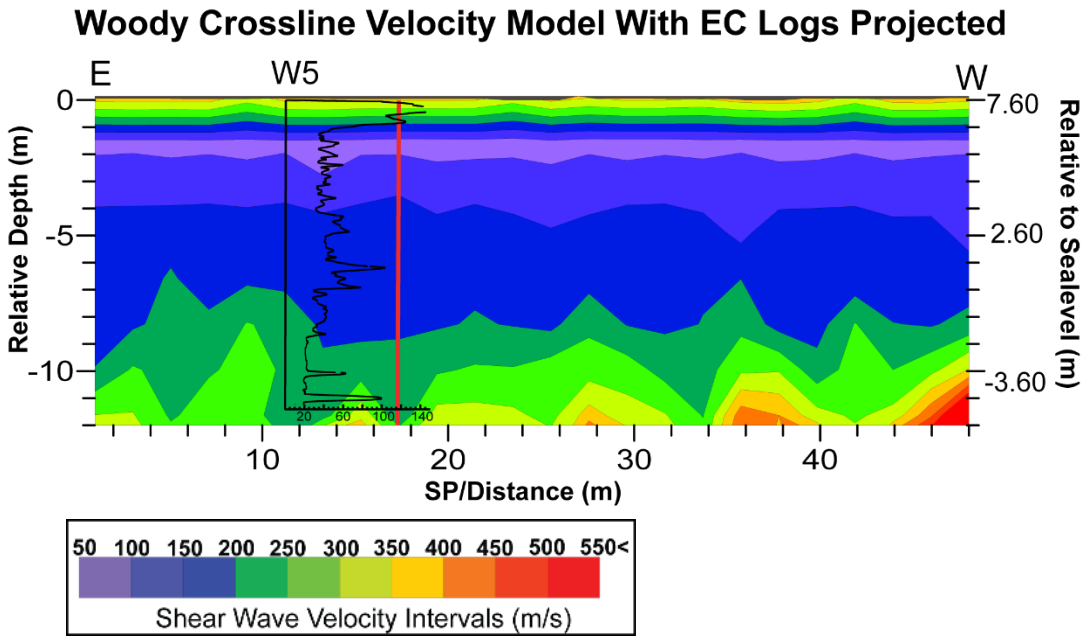

Figure 4.21. Woody crossline velocity model with EC logs projected onto the profile. “Warmer” colors indicate increasing velocity layers values. The horizontal axis indicates shotpoint, with 1 m spacing. Depth relative to the lowest point on the survey is indicated on the right vertical Y axis, while depth relative to sea-level is indicated on the left vertical axis. The red vertical line on the profile shows where the inline and crossline intersect eachother “Kicks” to the right indicate higher EC measurements. EC measurements are in milliSiemens per meter (mS/m).

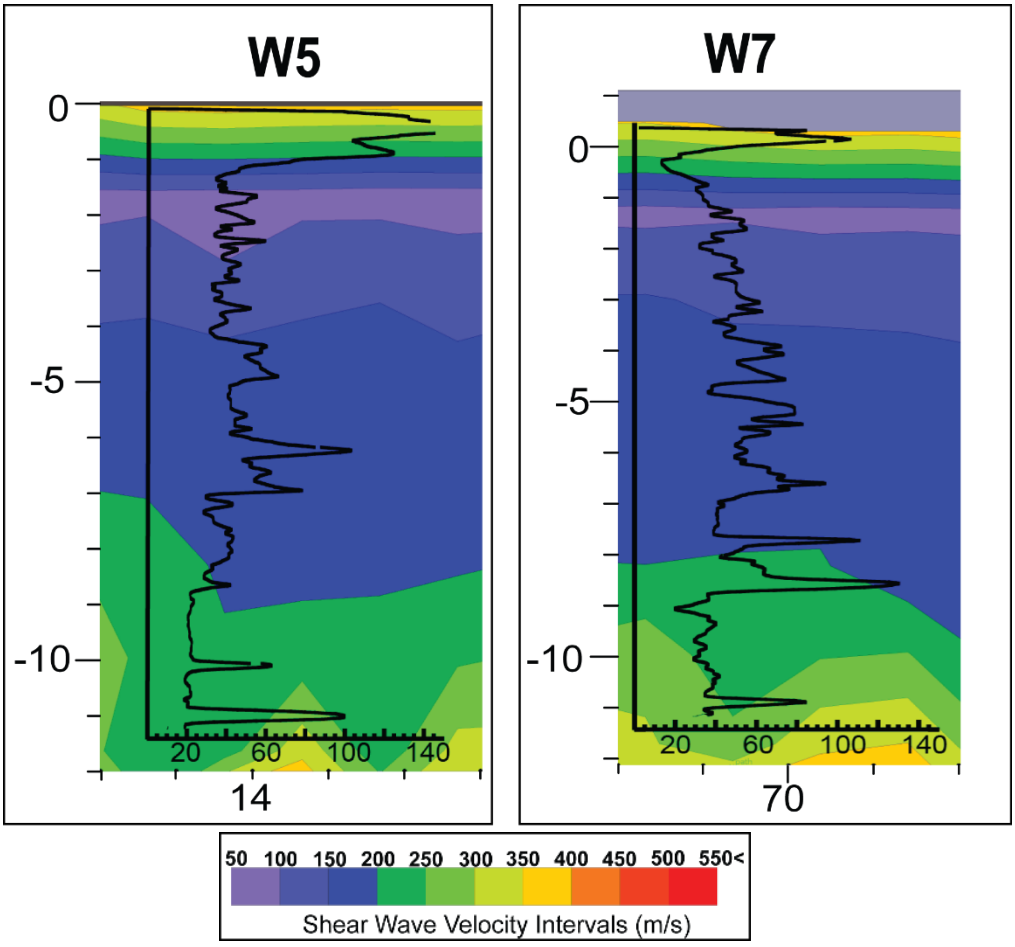

Figure 4.22. EC logs projected onto sections of the pseudo 2D velocity profile. It is difficult to see any correlation between EC values and velocity layering, with the exception of the apparent correlation between high velocities and higher EC values in the upper meter of data. The velocity profile section on the left is taken from the crossline data, while the one of the right is taken from inline data. Both the EC logs and the velocity profile sections appear similar to each other (Olson, 2017).

4.5. Velocity and Depth

As expected, velocities generally increase with depth in all 3 profiles (Figures 4.2, 4.14, 4.15). As similar surface wave inversion studies have shown in fluvial settings, increased shear wave velocities from inversion results indicate increased grainsize (Harry et al., 2005). In my results, this increase of shear velocity with depth generally correlates with decreasing electrical conductivity values, increasing grainsize, and the general expectation that points bar sediments will fine upward (Figures 4.7, 4.20, 4.23) (Sundborg, 1956).

4.6. Bueche and Woody Velocity Comparison

Velocity models for the Woody surveys are in general 50-75 m/s lower on average than the model for the Bueche survey (Figures 4.17, 4.18). This is understood as being the result of a grainsize difference between the Woody and Bueche areas observed in the EC and core data from another study (Olson, 2017), although the difference might be because of potential seasonal changes between data collection at the sites (Olson, 2017). The grainsize difference is observed in other studies in the EC logs and cores available at the different sites, and is interpreted to be due to the two locations existing at different parts of the Point bar time-stratigraphically (Figure 4.23) (Olson, 2017; Rodnight, 2005; Strick et al., 2018). The Woody survey site is located in the finer grained tail of the bar, while the Bueche survey site is located nearer to the coarser grained bar apex (Olson, 2017).

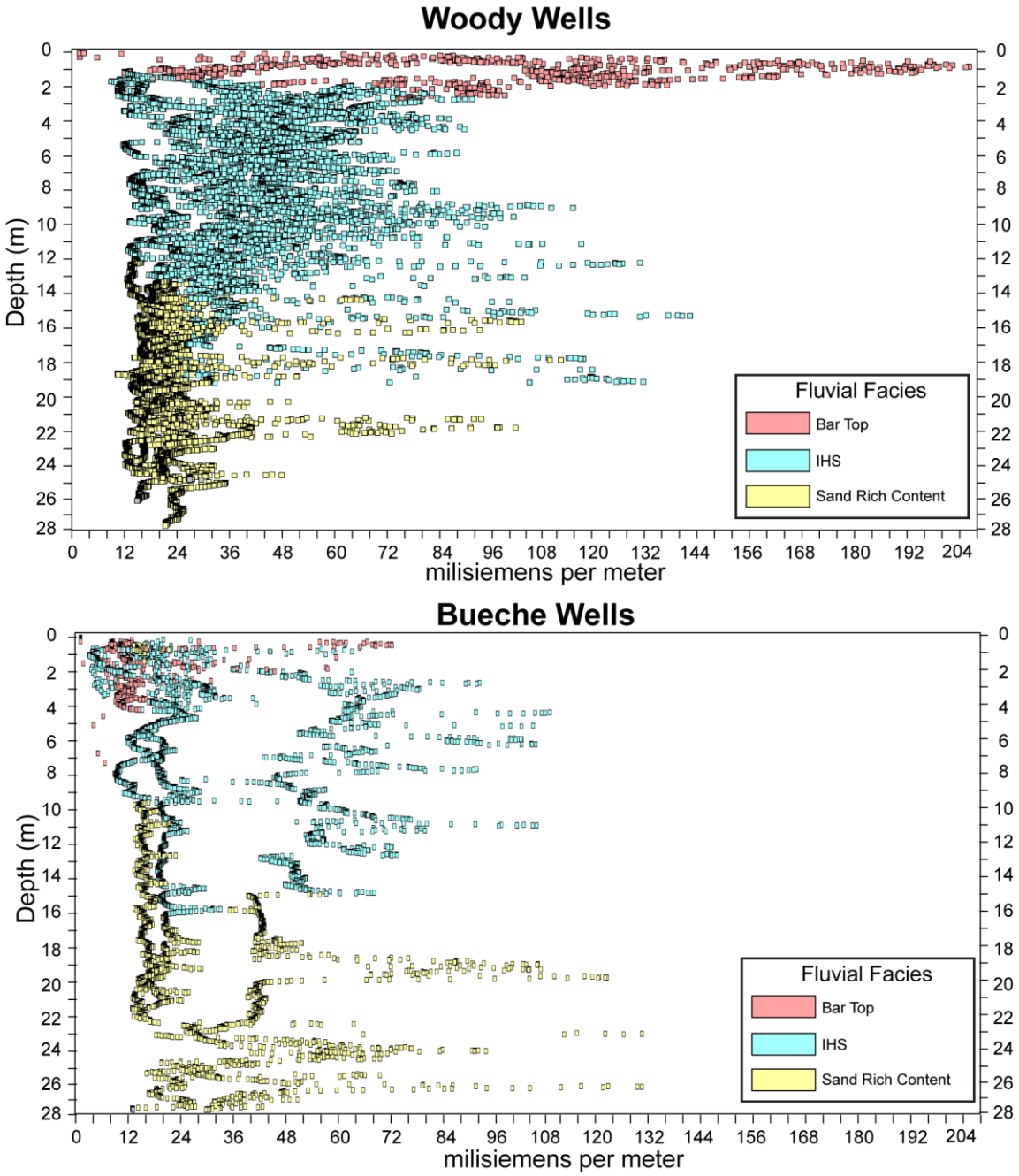

Figure 4.23. Comparison of Bueche and Woody Electrical conductivity data for all wells drilled in the areas. Woody (above) exhibits overall higher EC values down to the sand rich content (below the scope of this study) for wells W6, W7, W8, and W5. Bueche (below) EC data is much lower in the bar top facies and slightly lower in the HIS facies for wells B2, B3, B1, and B5. Note that these facies distinctions were not made by this study, nor are some of these wells mentioned in this study. These figures are modified from Olson (2017).

4.7. Woody Negative Velocity Gradient

In both the Woody Inline and Crossline velocity profiles there is a distinctive negative velocity gradient (-200 s^{-1}) in the very top meter below the surface (Figure 4.15). While this higher-velocity zone appears to correlate with a high EC zone in wells W5 and W7, this zone also correlates with a high velocity variance zone in the same area (Figures 4.22, 4.24). This high velocity/high velocity variance zone is not observed in the Bueche velocity profile or variance profile, despite having similar EC "kicks" at wells B4 and B5 in the uppermost meter of sediment (Figure 4.7). The appearance of this near-surface high velocity zone in the Woody velocity data could be the result of several factors. The zone could be an inversion artifact that results from the finer vertical resolution used for Woody data inversions (0.75 m), which might explain the high velocity variance in the zone that is similar to variance values seen at and below the half space at the bottom of the profiles (Goff, 2016; Ivanov et al., 2017). Alternatively, if the higher variance is a reasonable result of the inversion process, then the zone's correlation to the higher EC, fine-grained zone could be the result of surface compaction of finer grained materials (Bessason and Erlingsson, 2011). The compaction of finer-grained materials causing higher velocities at depth is the interpretation of a reflection study using the same data at Woody (Benton, 2018). In this regard, a similar layer is not observed in the Bueche profile could because the land surface at Woody is used primarily as agricultural land, while the Bueche land surface appears to be used more as recreational yard space and therefore presumably less trafficked by cattle and heavy machinery. Compaction from tractors, trucks, and cattle may cause finer grained sediments to actually have a higher shear velocity (Benton, 2018).

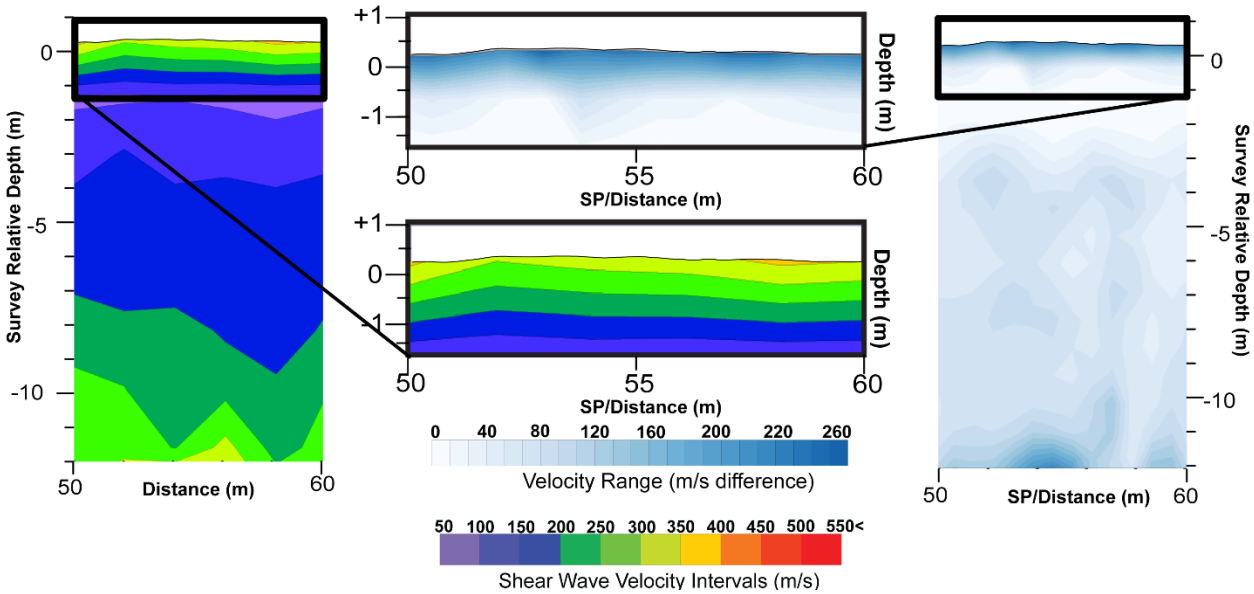

Figure 4.24. Woody negative velocity gradient zone in the uppermost ~1 meter compared to the corresponding variance data for the Woody inline. Higher variance (200 -270 m/s range) values appear along the surface of the data, along with the highest velocity values observed in the velocity profile.

4.8. Velocity Decrease Towards Paleochannel

Velocity profile data for the Bueche survey indicate a decrease in velocity gradients (from 35 s^{-1} to 20 s^{-1}) toward the southwestern section of the survey (paleochannel-ward) (Figures 4.2, 4.3, 4.5). This observation correlates with increasing EC values and decreasing grainsize in the same southwesterly direction (Figures 4.6, 4.7). It is unknown why velocities and grainsize would decrease toward the paleochannel, but it could for the same reason Woody velocities and grainsizes might be lower than Bueche, a proximity to paleochannel (Figure 1.9) (Mossop and Flach, 1983).

One potential reason for the paleochannel-ward fining observed in a longer and depositionally younger section like Bueche (Strick et al., 2018) could be related to gradual

channel abandonment. During abandonment, sand-carrying helicoidal flow in the channel is decreased and overbank-type finer deposits increase (Gostic, 2018; Mossop and Flach, 1983). Despite a lack of any well information near the large swale around shotpoint 200 in the Bueche survey, this decrease in velocity is interpreted to be caused by fine overbank sedimentation filling in this large swale (Figure 4.25) (Lewin and Ashworth, 2014).

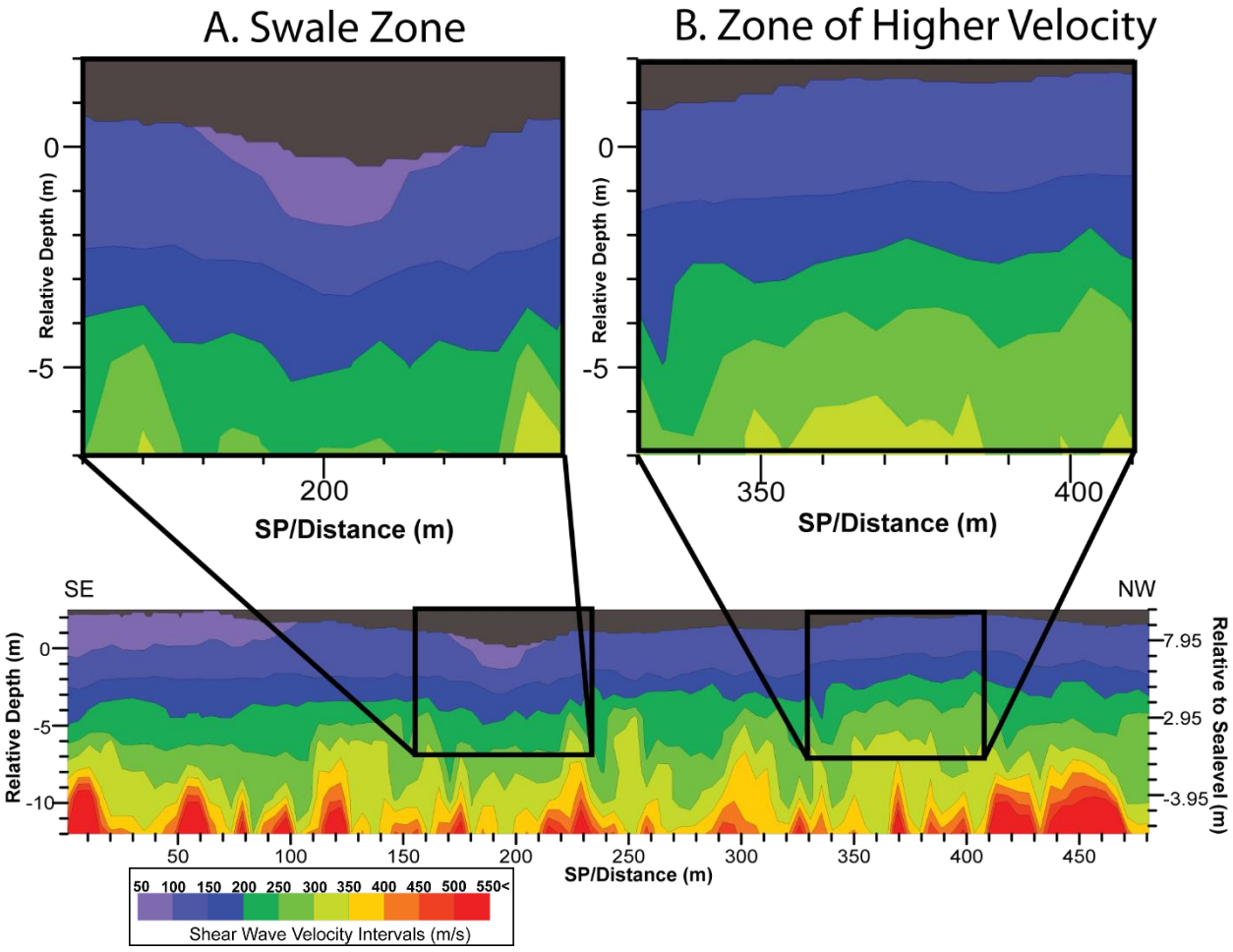

Figure 4.25. Two regions of the Bueche velocity profile identified and displayed for comparison. (A) A zone of lower velocity within the topographically low swale compared to a higher velocity zone in the Northwestern side of the profile (B). The depth of the two selections are compared from the surface topography down to exemplify this difference in velocity layering.

CHAPTER 5. DISCUSSION

5.1. Scroll Bar Development

This study interprets velocity layers as dipping away from scroll ridge crests parallel to the surface topographic expression of scroll bars within overbank sediments as well as the IHS. Because of this apparent stratigraphic linkage between IHS and overbank deposits, we find the landward migration of transverse bars scroll model to be more adequate in explaining scroll bar development at False River than the flood stage scroll model.

The transverse bar model of scroll bar development attributes scroll ridge formation to the landward migration of transverse bars (Jackson, 1976; Sundborg, 1956). In this model, the underlying IHS strata are formed by the same fluvial processes responsible for transverse bar migration and thus, should be stratigraphically linked to topography and parallel to ridge and swale undulation, dipping in both directions away from ridge crests (Gibling and Rust, 1993; van de Lageweg et al., 2014). A velocity layer model for the transverse bar scroll model is predicted to feature velocity layers of equal thickness that are parallel to the topography in both the overbank and IHS zones (Figures 5.1 and 5.2). Because the sedimentary layers dip away from the crest of the scroll ridges and towards the bottom of the swales, we expect velocity layers to dip symmetrically away from the ridges and towards the swales.

The flood-stage model of scroll bar development attributes ridges to secondary flow separation zone deposition of silty lenses from suspended sediment load during low frequency flood events (Hickin, 1974; Nanson, 1980). In this model, underlying IHS strata are deposited during regular stage lateral accretion and are predicted to dip only channel-ward and coalesce at

the base of the initial ridge deposits. Velocity layers in the IHS zone should be geometrically distinct from the ridge and swale undulation above, dipping only towards the paleochannel (Figures 5.3 and 5.4). A velocity layer model of the flood stage scroll model would potentially also reveal a velocity contrast between coarser initial ridge silts and overlying overbank clays due to the grainsize difference between the two.

This study finds that the flood stage model cannot account for the formation of scroll bars at False River, and that the transverse bar model is a more likely process for their formation. In the pseudo 2-D shear velocity profiles interpreted by this study, velocity layers are parallel to the surface topography within the IHS zone, dipping away from the scroll ridge expressed at the surface topography (Figures 5.5 and 5.6). Velocity increases with depth at a lower gradient in the upper 7 meters of sediment (20-30 s^{-1}), then at a higher gradient below that (40-60 s^{-1}). No velocity contrast is observed in the data that indicates the existence of a flood-deposited initial ridge that underlies overbank deposits, although this initial ridge might not provide enough of a grainsize contrast with surrounding overbank deposits to be identified by a velocity layer model.

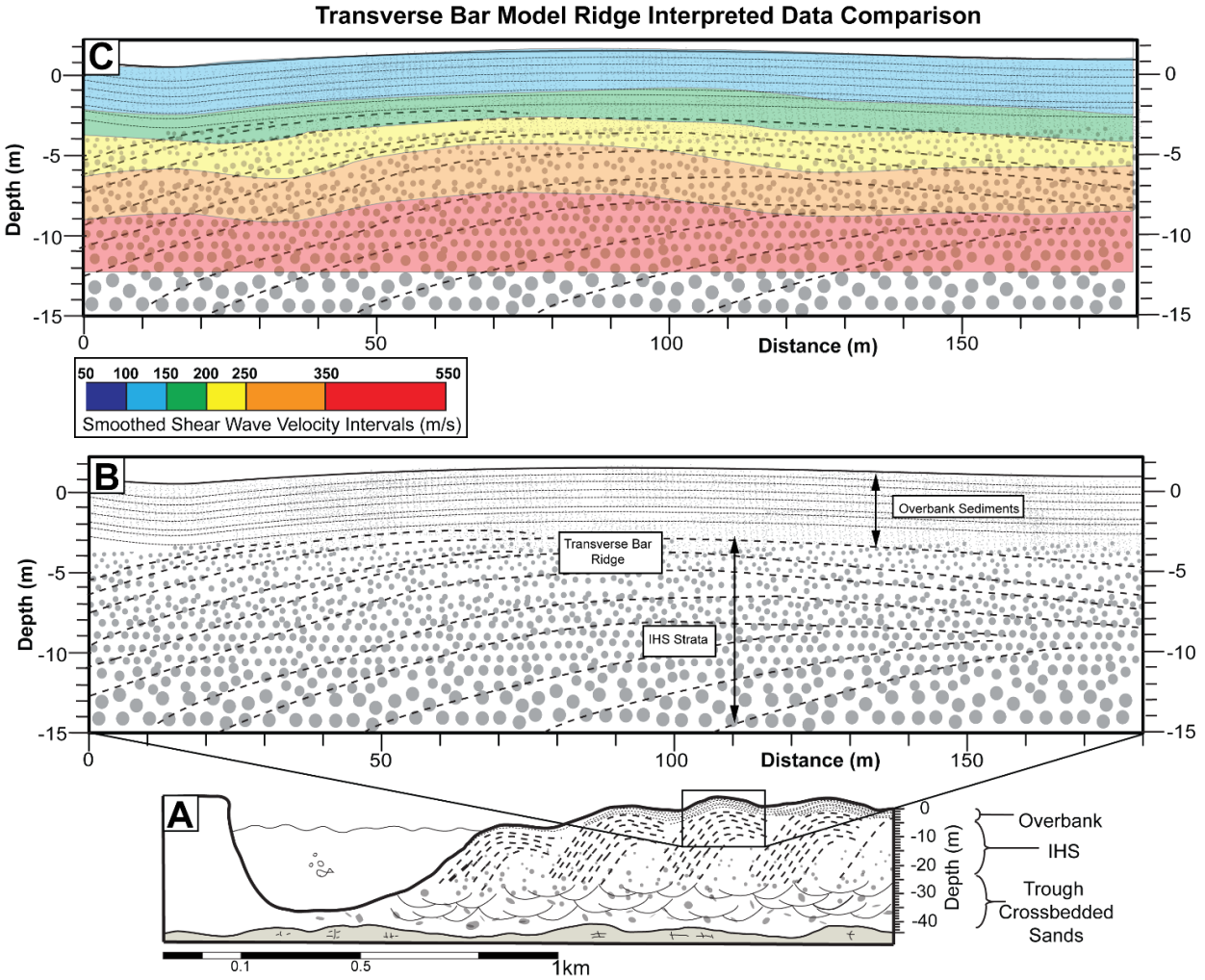

Figure 5.1. The transverse bar scroll model compared with a selection of interpreted data. (A) The transverse bar scroll model for an entire conceptualized point bar (from section 1.2). (B) The transverse bar model scaled to match the surface topographic expression of a section of the Bueche survey. In this model, IHS is parallel to the ridge expressed in the surface topography, and dip in both directions. Dots indicate grainsize. (C) A section of interpreted Bueche data (from Figure 4.3) (shotpoints 300-480) that has been superimposed on the same model depicted in (B). "Warmer" colors indicate increasing velocity layer values, increasing in range. . The velocity layers below 4 meters of depth are parallel to the surface topographic ridge, and dip similarly in two directions, indicating a potential stratigraphic link in the IHS to the scroll bar ridge.

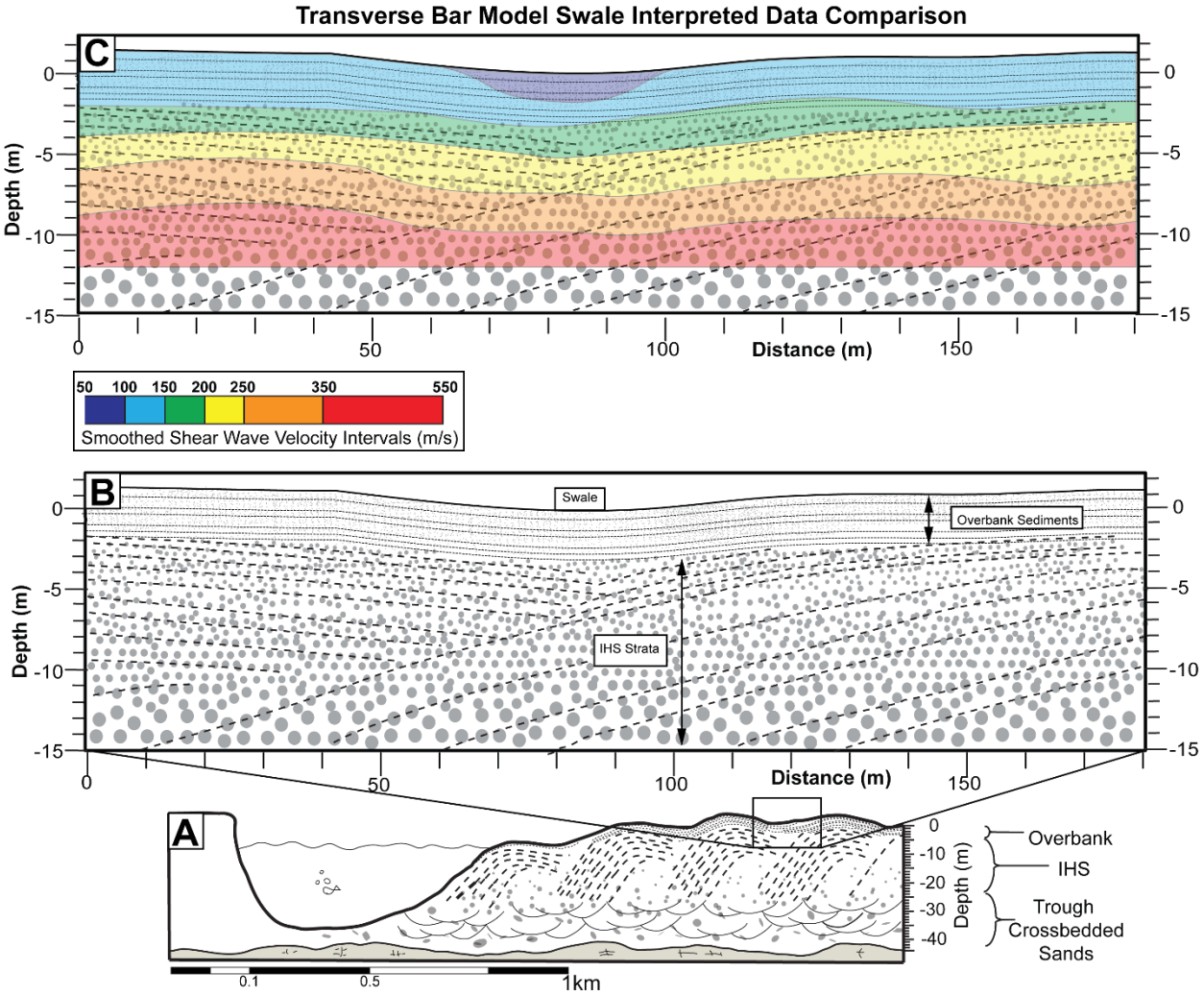

Figure 5.2. The transverse bar scroll model compared with a selection of interpreted data for a swale. (A) The transverse bar scroll model for an entire conceptualized point bar (from section 1.2). (B) The transverse bar model scaled to match the surface topographic expression of a section of the Bueche survey. In this model, IHS is parallel to the ridge expressed in the surface topography, and dip in both directions. Dots indicate grainsize. (C) A section of interpreted Bueche data (from Figure 4.3) (shotpoints 110-290) that has been superimposed on the same model depicted in (B). “Warmer” colors indicate increasing velocity layer values, increasing in range. . The velocity layers below 4 meters of depth are parallel to the surface topographic ridge, and dip similarly in two directions, indicating a potential stratigraphic link in the IHS to the scroll bar ridge and swale.

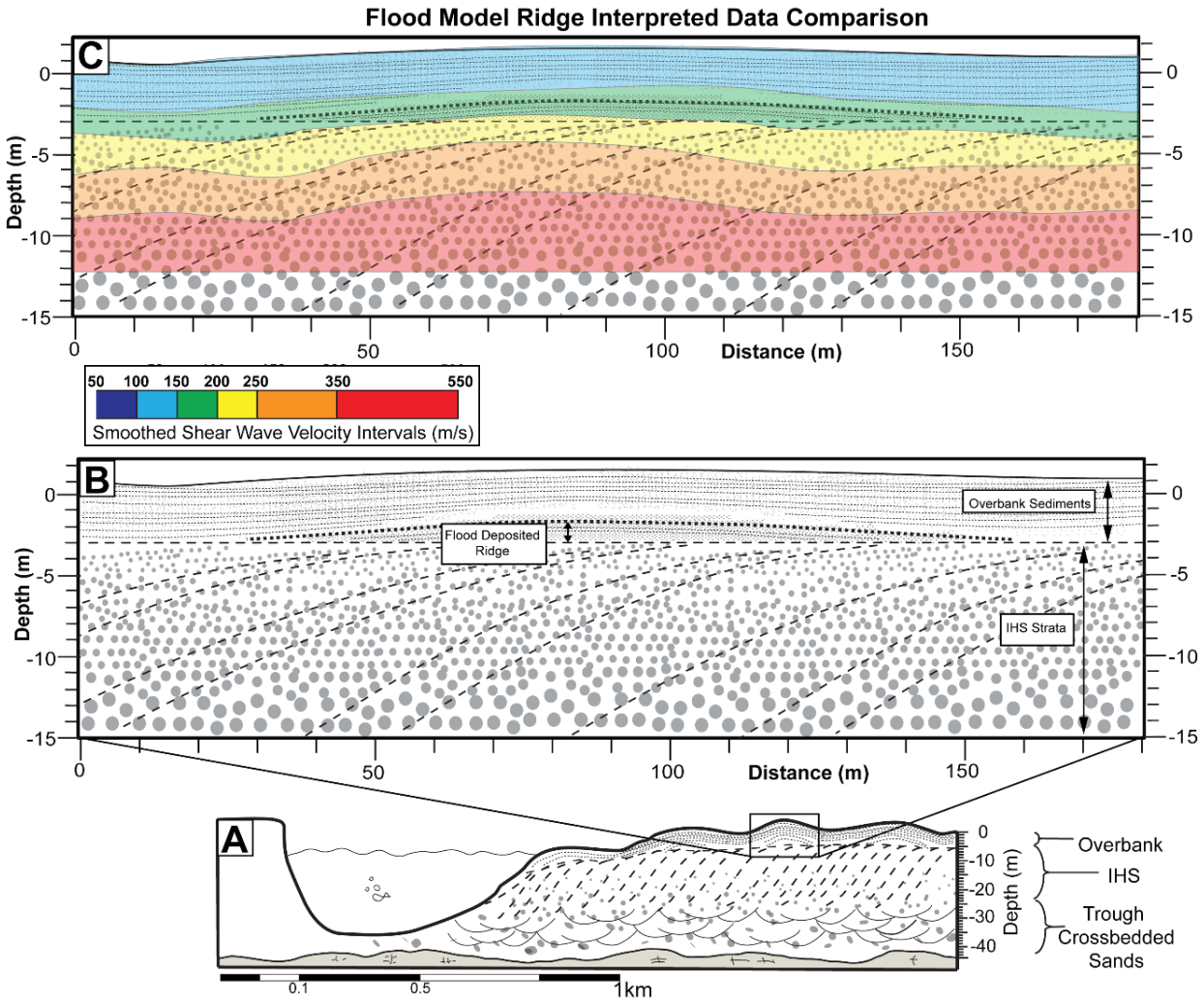

Figure 5.3. The flood stage scroll bar model compared with a selection of interpreted data. (A) The flood stage model of scroll bar development for an entire conceptualized point bar (from section 1.2). (B) The flood stage model scaled to match the topographic expression of a section of the Bueche survey. In this model, an initial ridge of flood deposited silt overlies IHS that coalesces into a non-undulating surface. IHS strata only dip toward the channel (to the left) and are not parallel to the ridge expressed at the surface and in the top 4 meters of sediment. Dots indicate grainsize. (C) A section of interpreted Bueche data (from Figure 4.3) (shotpoints 300-480) that has been superimposed on the same model depicted in (B). "Warmer" colors indicate increasing velocity layer values, increasing in range. The velocity layers below 4 meters of depth are parallel to the surface topographic ridge, and do not match the model expectations for IHS dip direction on the right side of the image, where the ridge dips inward, away from the channel. The initial flood deposited ridge described in the model is also not indicated by the velocity model interpretation.

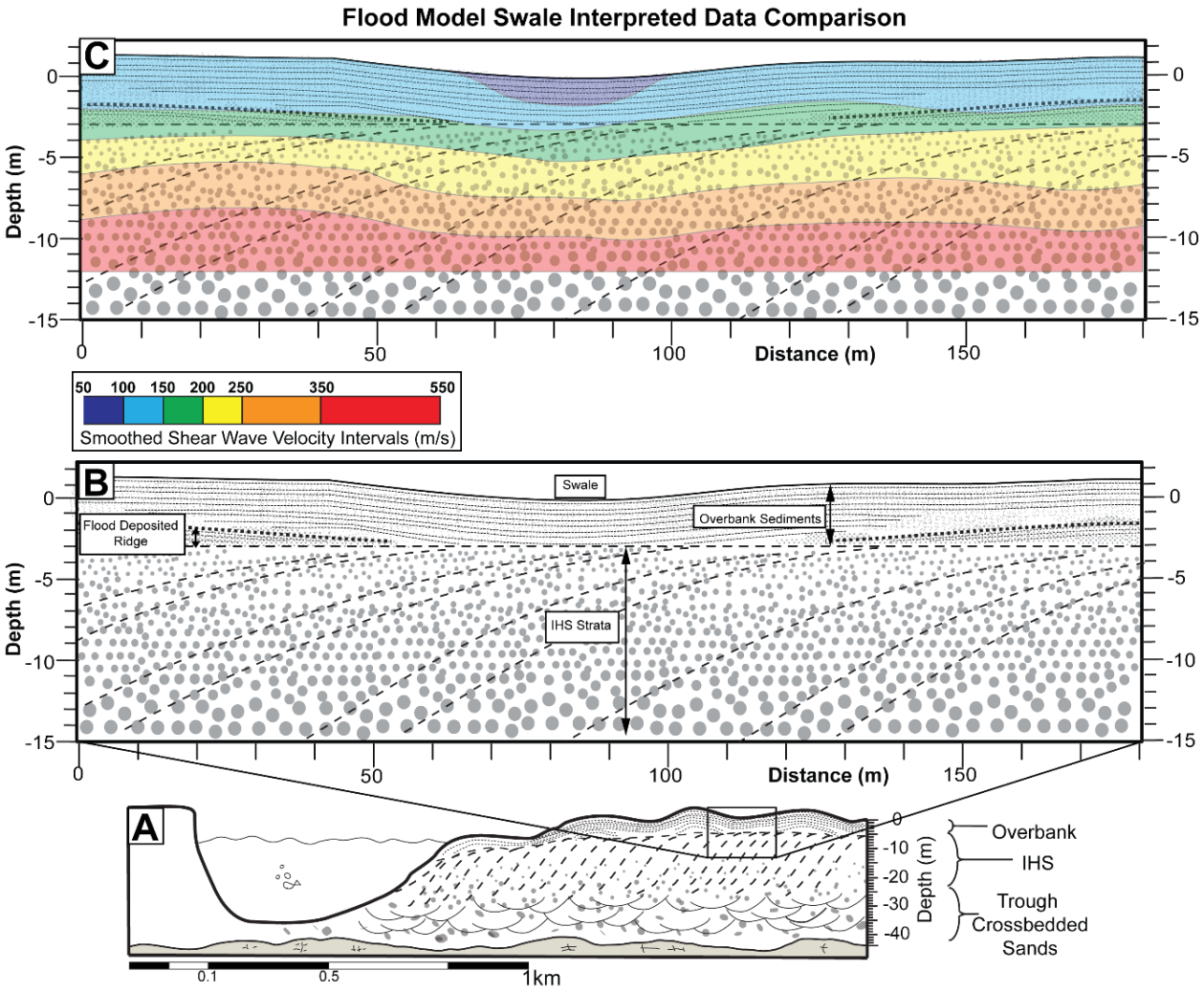

Figure 5.4. The flood stage scroll bar model compared with a selection of interpreted data for a swale. (A) The flood stage model of scroll bar development for an entire conceptualized point bar (from section 1.2). (B) The flood stage model scaled to match the topographic expression of a section of the Bueche survey. In this model, an initial ridge of flood deposited silt overlies IHS that coalesces into a non-undulating surface. IHS strata only dip toward the channel (to the left) and are not parallel to the ridge expressed at the surface and in the top 4 meters of sediment. Dots indicate grainsize. (C) A section of interpreted Bueche data (from Figure 4.3) (shotpoints 110-290) that has been superimposed on the same model depicted in (B). "Warmer" colors indicate increasing velocity layer values, increasing in range. The velocity layers below 4 meters of depth are parallel to the surface topographic ridge, and do not match the model expectations for IHS dip direction on the right side of the image, where the ridge dips inward, away from the channel. The initial flood deposited ridge described in the model is also not indicated by the velocity model interpretation.

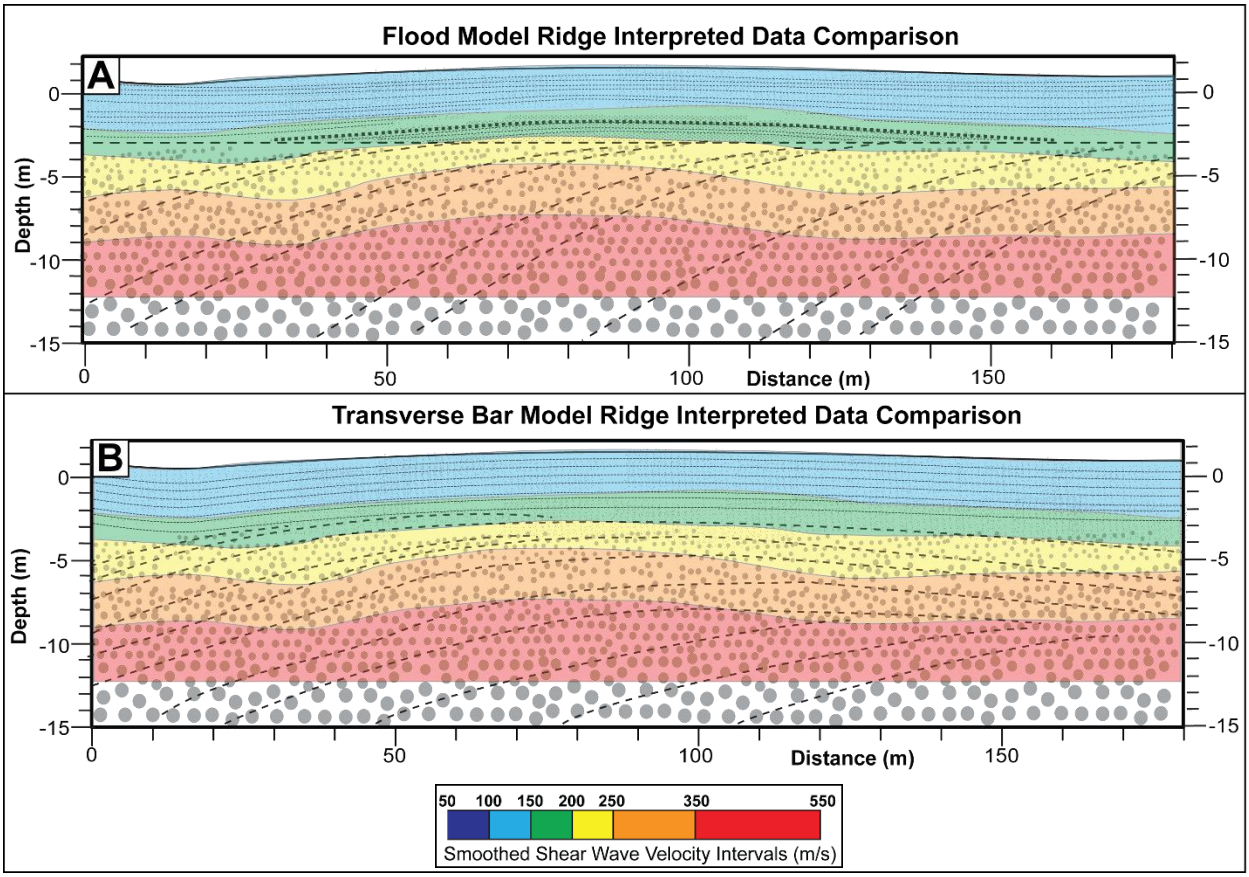

Figure 5.5. Comparison of two different models with the same velocity interpretation superimposed on both from Bueche shotpoints 300 to 480. (A) The flood model from figure 5.2, velocity layers in the IHS are parallel to topography and do not appear to correlate to model predictions of IHS strata solely dipping towards the channel. (B) the transverse bar model from figure 5.1, model predicted IHS match velocity layers in that they are parallel to surface topography and thus dip in two directions.

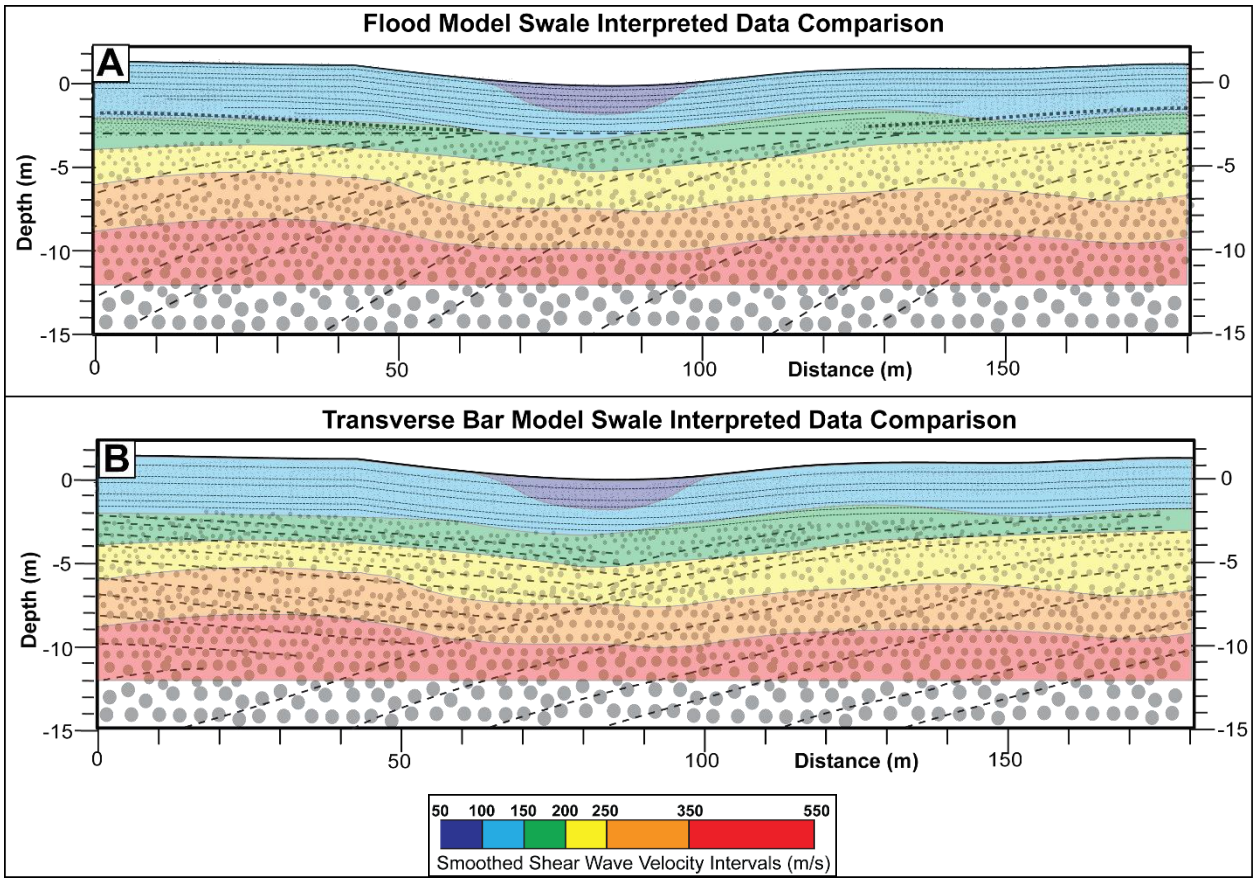

Figure 5.6. Comparison of two different models with the same velocity interpretation superimposed on both from Bueche shotpoints 110 to 290. (A) The flood model from figure 5.4, velocity layers in the IHS are parallel to topography and do not appear to correlate to model predictions of IHS strata solely dipping towards the channel. (B) the transverse bar model from

5.2. Internal Consistency in Inversion Processing

Confidence in the inversion results is higher in the shallower sections of the profiles. Dispersion data inverted by this study originates by a visual and manual picking process by which we select a series of velocity-frequency points by interpreting a dispersion image generated from a single shotgather (see section 3.6). As mentioned above (section 3.15) a simple test of the error of this process attempts to quantify the error associated with visual dispersion picking. The test finds that our consistency in making dispersion picks is less than 4 percent different for both Bueche and Woody survey datasets. Dispersion picks made for high frequency data (above 10 Hz) is much more consistent, being around 0.5 percent different, while picks made for low frequency data (below 5 Hz) is less consistent at a 10 percent average difference between the two picking sessions (Table 3.4). Similarly, velocity variance data indicates velocity ranges increase with depth, reducing confidence in the deeper sections of the profile (Figures 4.2, 4.14, 4.15). The increase in velocity range with depth (variance) could be due to this inconsistency between neighboring shotgathers originating in the raw dispersion picks, magnified by the inversion results (Goff, 2016).

Despite the potential for inconsistency during dispersion picking and inversion processing, velocity profiles for the intersecting Woody inline and crossline are extremely similar in both velocity gradient and velocity variance range where they intersect (Figure 5.7). This consistency between results is observed despite the dispersion curve picking, inversion, and profile interpolation occurring as separate processes for the two Woody surveys, only sharing the same set of inversion parameterization between them. This velocity consistency at the intersection of the two Woody surveys is taken to strengthen the quality of the dispersion picking and inversion results used in this study.

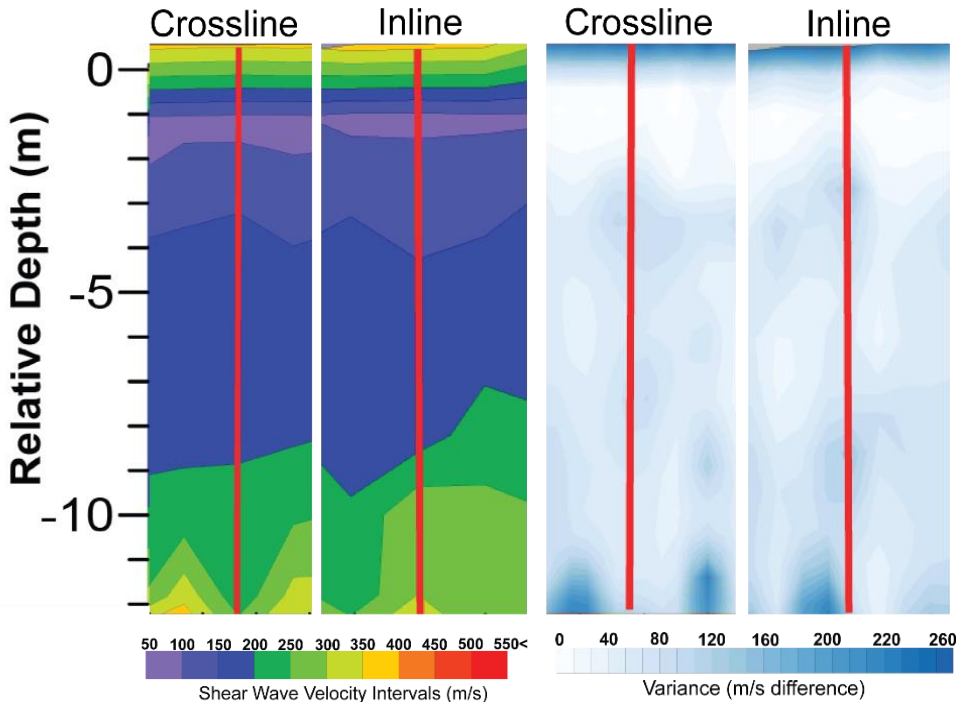

Figure 5.7. A side-by-side visual comparison of the intersection line (red lines) between the Woody inline and crossline profiles. The similarity between the two profiles is clear in both the pseudo 2D velocity and variance plot sections where they intersect. This is despite the data for each survey being separately processed.

CHAPTER 6. CONCLUSIONS AND RECOMMENDATIONS

6.1. Conclusions

Three seismic surveys on the False River point bar, a cutoff point bar of the Mississippi River, undergo surface wave inversion to develop pseudo 2D shear velocity profiles. The data inversion is conducted by a nearest-neighbor algorithm program Geopsy (Wathelet, 2008), then interpolated, interpreted, and compared to existing well data (Olson, 2017).

We interpret shear velocity layers to dip in both directions at depth within the IHS, parallel to the surface topographic expression of scroll bars. Because of this apparent stratigraphic linkage between IHS and upper bar deposits, we find the landward migration of transverse bar scroll bar development model to be more adequate in explaining scroll bar development at False River than the flood stage model which attributes scrolls to single low-frequency high-discharge events.

6.2. Recommendations for Future Work

In order to better address the question of scroll bar development using surface wave inversion, more purpose-driven data acquisition could improve velocity models and imaging capability. Acquiring a longer survey across several ridge and swale couples in the more interior sections of the False River point bar is the most important step. Both the Bueche and Woody surveys do not adequately sample enough ridge and swale topography to draw comparisons both within and between the survey sites. A longer survey that aims to acquire seismic data over as many scroll bars as possible would provide a larger sample size of subsurface data beneath scrolls. In addition, field data acquisition with the original intent of conducting surface wave

analysis could achieve higher-resolution velocity imaging by using higher frequency geophones. Although the use of higher frequency geophones comes at the price of reduced vertical penetration, sacrificing imaging depth for resolution may allow for velocity models that can resolve the thickness of individual IHS layers. Whereas the velocity inversion results presented in this study can still constrain IHS geometries as an aggregate, the ability to invert for velocity layers as thin as individual IHS layers would provide more certain estimations of the dip and dip direction of these layers in their relation to scroll bar topography. Higher vertical velocity resolution may also provide the necessary ability to image the initial ridges predicted in the flood stage model, if they in fact exist as silty lenses between overbank deposits and IHS. Along with this seismic data, wells drilled into the tops of neighboring ridges and swales would aid in velocity model analysis as it pertains to the question of scroll bar development.

REFERENCES

Aki, K., and Richards, P. G., 1980, Quantitative seismology; theory and methods A series of books in geology, United States, W.H. Freeman and Co. : San Francisco, Calif., United States.

Baar, A. W., 2013, Scroll bar formation in experimental meandering rivers [MSc PhD Dissertation Supervisor: Maarten Kleinhans]: Utrecht University.

Bagaini, C., Bunting, T., El-Emam, A., Laake, A., and Strobbia, C., 2010, Land Seismic Techniques for High-Quality Data: Oilfield Review Schlumberger, v. 22, no. 2.

Benton, N., 2018, SH-Wave Seismic Reflection Imaging and Inversion: An Analysis of Architectureal and Physical Properties of a Near Surface Point Bar [MS: Louisiana State University.

Bessason, B., and Erlingsson, S., 2011, Shear Wave Velocity in Surface Sediments: JÖKULL.

Boschi, L., 2012, The Basic Properties of Surface Waves.

Bullen, K. E., and Bolt, B. A., 1985, An introduction to theory of seismology,, Cambridge, Cambridge University Press,.

Crane, J. M., Lorenzo, J. M., and Harris, J. B., 2013, A new electrical and mechanically detonatable shear wave source for near surface (0-30m) seismic acquisiton: Journal of Applied Geophysics, v. 91, p. 1-8.

Cressie, N., 1990, The Origins of Kriging: Mathematical Geology, v. 22, no. 3, p. 239-252.

Cunningham, R., Gisclair, D., and Craig, J., 2018, THE LOUISIANA STATEWIDE LIDAR PROJECT, Volume 2018, Louisiana State University , Louisiana Oil Spill Coordinators Office, The Spatial Data Company, p. https://atlas.ga.lsu.edu/datasets/lidar2000/.

Fisk, H. N., 1947, Fine-grained alluvial deposits and their effects on Mississippi River activity, Volume 1.

Fowler, C. M. R., 2005, The Solid Earth, An Introduction to Global Geophysics, New York, Cambridge University Press.

Gibling, M. R., and Rust, B. R., 1993, Alluvial ride-and-swale topography: a case study from the Morien Group of Atlantic Canada: Alluvial Sedimentation.

Goff, D., 2016, Study of Resistivity and Shear Wave Velocity as a Predictive Tool of Sediment Type in Levee Foundation Soils, Louisiana Gulf Coast Levee System [M.S.: Louisiana State University.

Golden Software, I., 2018, Surfer 11 User's Manual Online.

Gostic, A., 2018, The Relationship Between Grain Size and Seismic Dip on the Mississippi River in False River Point Bar, False River Louisiana [MS: Louisiana State University.

Harry, D. L., Koster, J. W., Bowling, J. C., and Rodriguez, A. B., 2005, Multichannel analysis of surface waves generated during high-resolution seismic reflection profiling of a fluvial aquifer: Journal of Environmental & Engineering Geophysics, v. 10, no. 2, p. 123-133.

Hayashi, K., and Suzuki, H., 2004, CMP Cross-correlation analysis of multi-channel surface wave data: Exploration Geophysics, v. 35, no. 1, p. 7-13.

Heisey, J. S., Stockoe, K., Hudson, R., and Meyer, A. H., 1982, Determination of In-Situ Shear Wave Velocities From spectral analysis of surface waves: University of Texas at Austin.

Hickin, E. J., 1974, The development of meanders in natural river-channels: American Journal of Science, v. 274, no. 4, p. 414-442.

Ivanov, J., Miller, R. D., Feigenbaum, D., Morton, S. L. C., Peterie, S. L., and Dunbar, J. B., 2017, Revisiting levees in southern Texas using Love-wave multichannel analysis of surface waves with the high-resolution linear Radon transform: Interpretation [Tulsa], v. 5, no. 3, p. T287-t298.

Jackson, R. G., II, 1976, Largescale ripples of the lower Wabash River: Sedimentology, v. 23, no. 5, p. 593-623.

Kleinhans, M. G., 2010, Sorting out river channel patterns.: Progress in Physical Geography, p. 287-326.

Kleinhans, M. G., and van den Berg, J. H., 2011, River channel and bar patterns explained and predicted by an empirical and a physics-based method: Earth Surface Processes and Landforms, v. 36, no. 6, p. 721-738.

Lay, T., and Wallace, T. C., 1995, Modern global seismology, United States, Academic Press : San Diego, CA, United States.

Lechnowskyj, A., 2015, The Stratal Architecture of The False River Point Bar (Lower Mississippi River, LA) [MS: Louisiana State University.

Leclerc, R. F., and Hickin, E. J., 1997, The internal structure of scrolled floodplain deposits based on ground-penetrating radar, North Thompson River, British Columbia: Geomorphology, v. 21, no. 1, p. 17-38.

Lewin, J., and Ashworth, P. J., 2014, The negative relief of large river floodplains: Earth-Science Reviews, v. 129, p. 1-23.

Lomax, A. J., and Snieder, R., 1994, Finding sets of acceptable solutions with a genetic algorithm with application to surface wave group dispersion in Europe: Geophysics, v. 21 (24), p. 2617– 2620.

Morrison, M., 2017, Shallow Shear-Wave Seismic Analysis of Point Bar Deposits of False River, Louisiana [MS: Louisiana State University.

Mossop, G. D., and Flach, P. D., 1983, Deep channel sedimentation in the Lower Cretaceous McMurray Formation, Athabasca oil sands, Alberta: Sedimentology, v. 30, no. 4, p. 493-509.

Nanson, G. C., 1980, Point bar and floodplain formation of the meandering Beatton River, northeastern British Columbia, Canada: Sedimentology, v. 27, no. 1, p. 3-29.

Nanson, G. C., and Croke, J. C., 1992, A genetic classification of floodplains: Geomorphology, v. 4, no. 6, p. 459-486.

Officer, C. B., 1974, Introduction to Theoretical Geophysics, Germany, Springer-Verlag.

Olson, E., 2017, COmbining Downhole And Sediment Logging to Understand Spatial Variability in Grain Size, Facies, and Reservoir Quality of a Large-Scale Mississippi River Point Bar, False River, Louisiana [MS: Louisiana State Univiersity.

Park, C. B., Miller, R. D., and Xia, J., 1998, Imaging dispersion curves of surface waves on multi-channel record: SEG Annual Meeting Expanded Technical Program Abstracts with Biographies, v. 68.

Park, C. B., Miller, R. D., and Xia, J., 1999, Multichannel analysis of surface waves: Geophysics, v. 64, no. 3, p. 800-808.

Poggi, V., 2011, The Use of Surface Waves for Site Characterization and Seismic Hazard Analysis [PhD: ETH Zurich.

Pyrce, R. S., and Ashmore, P. E., 2005, Bedload path length and point bar development in gravel-bed river models: Sedimentology, v. 52, no. 4, p. 839-857.

Revil, A., and Glover, P. W. J., 1998, Nautre of Surface Electrical Conductivity in Natural Sands, sandstones, and clays: Geophysical Research Letters, v. 25, no. 5, p. 691-994.

Rodnight, H., 2005, Optical dating of South African fluvial sediments and comparison with radiocarbon dating of overlying sediments: Quaternary Newsletter, v. 106, p. 45-48.

Safani, J., O'Neill, A., Matsuoka, T., and Sanada, Y., 2005, Applications of Love wave dispersion for improved shear-wave velocity imaging: Journal of Environmental & Engineering Geophysics, v. 10, no. 2, p. 135-150.

Sambridge, M., 1999, Geophysical inversion with a neighboring algorithim: I. Searching a parameter Space: Geophysical Journal International, v. 138, p. 479-494.

Sen, M. K., and Stoffa, P. L., 1991, Nonlinear one-dimensional seismic waveform inversion using simulated annealing: Geophysics, v. 56, p. 1624-1638.

Sen, M. K., and Stoffa, P. L., 1996, Bayesian inference, Gibbs' sampler and uncertainty estimation in geophysical inversion: Geophysical Prospecting, v. 44, no. 2, p. 313-350.

Socco, L. V., Foti, S., and Boiero, D., 2010, Surface-wave analysis for building near-surface velocity models; established approaches and new perspectives: Geophysics, v. 75, no. 5, p. 75A83-75a102.

Song, X., Gu, H., Liu, J., and Zhang, X., 2007, Estimation of shallow subsurface shear-wave velocity by inverting fundamental and higher-mode Rayleigh waves: Soil Dynamics and Earthquake Engineering [1984], v. 27, no. 7, p. 599-607.

Sternberg, H., 1956, A Contribution to the Geomorphology of the False River Area, Louisiana [PhD: Louisiana State University and Agricultural & Mechanical College.

Stokoe, K. H., 1994, Characterization of geotechnical sites by SASW method, in Geophysical characterization of sites: ISSMFE Technical Committee #10.

Strick, R., Ashworth, P., Graeme, A., and Lewin, J., 2018, Morphology and spacing of river meander scrolls: Geomorphology.

Strick, R. J. P., 2016, Floodplain Geomorphology and Topography in Large Rivers: University of Brighton.

Sundborg, A., 1956, The river Klaraelven; a study of fluvial processes: Geografiska Annaler, v. 2-3, p. 125-316.

van de Lageweg, W. I., van Dijk, W. M., Baar, A. W., Rutten, J., and Kleinhans, M. G., 2014, Bank pull or bar push; what drives scroll-bar formation in meandering rivers?: Geology [Boulder], v. 42, no. 4, p. 319-322.

Wathelet, M., 2005, Array recordings of ambient vibrations: surface-wave inversion [PhD: Universite de Liege.

-, 2008, An improved neighborhood algorithm; parameter conditions and dynamic scaling: Geophysical Research Letters, v. 35, no. 9, p. @L09301-@L09301.

-, 2018, Geopsy Project, Volume 2018.

Xia, J., Miller, R. D., Park, C. B., and Tian, G., 2003, Inversion of high frequency surface waves with fundamental and higher modes: Journal of Applied Geophysics, v. 52, no. 1, p. 45-57.

Xia, J., Xu, Y., Luo, Y., Miller, R. D., and Cakir, R., 2012, Advantages of using multichannel analysis of Love waves (MALW) in determining near-surface shear-wave velocity: Survey Geophysics, v. 33.

Zeng, C., Xia, J., Miller, R. D., Tsoflias, G. P., and Wang, Z., 2012, Numerical investigation of MASW applications in presence of surface topography: Journal of Applied Geophysics, v. 84, p. 52-60.

APPENDICES. PROCESSING FLOWCHART

The following appendices provide a general flowchart containing all of the steps and appendices associated with surface wave inversion used in this study. Each appendix may contain several scripts, each preceded by instructions that outline their uses and specifications.

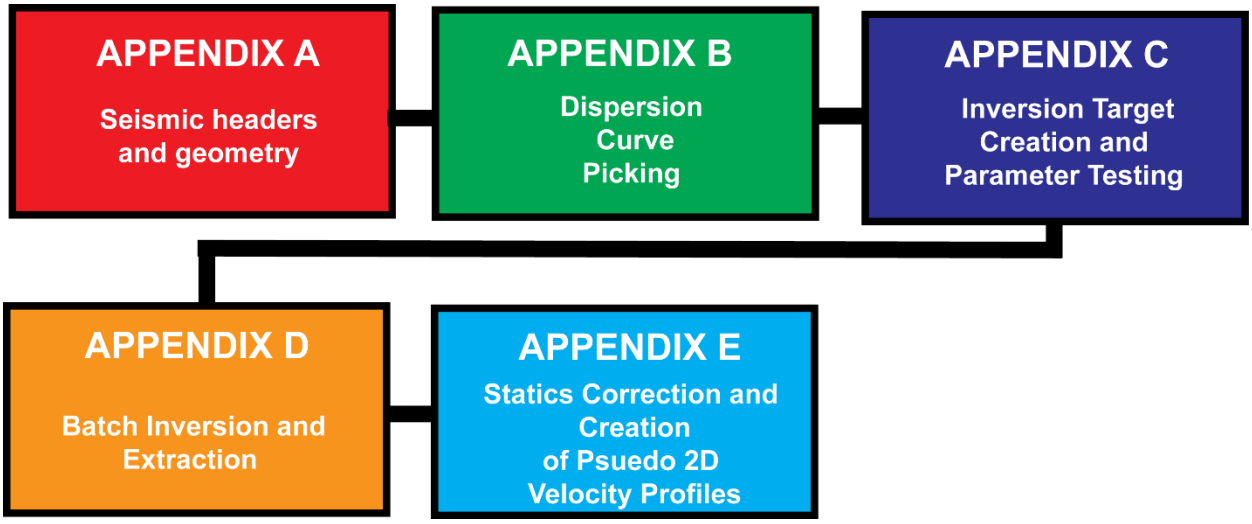

Figure A.1. Basic flowchart of Appendix sections and the processes they detail.

APPENDIX A. SEISMIC HEADERS AND GEOMETRY

The following appendix includes a perl script that can be used to add spatial headers to segy files in Seismic Unix. For dispersion image interpretation, concatenated files that contain multiple shotgathers with shotpoint headers is required. For more information on this process and the general processing steps conducted early in reflection processing for both Woody and Bueche surveys, see (Benton, 2018; Gostic, 2018; Morrison, 2017).

A.1. Program: Suclean_geom.pl

Program location: Zamin/home/bodom5/FalseRiver/seismics/pl/Bueche/All/H/1/bodom5

```
#! /usr/bin/perl
use Moose;

=head1 DOCUMENTATION

=head2 SYNOPSIS

 PROGRAM NAME: Suclean_geom.pl
 AUTHOR: Juan Lorenzo
 DESCRIPTION: script to clean and add geomtery to headers
 DATE Version 1 June 3, 2012
 DATE Dec 31 2014 converting to Moose
 DATE Feb. 18, 2015 adapt for False River case
 DATE June 1, 2016 adapt for Bueche property at False River case

=head2 Import

 perl classes container and system variables

=cut

  use SU;
  my ($DATA_SEISMIC_SU)                         =
System_Variables::DATA_SEISMIC_SU();
  my ($DATA_SEISMIC_SEGY)             = System_Variables::DATA_SEISMIC_SEGY();
  use SeismicUnix qw ($suffix_segy $suffix_su $suffix_ascii $suffix_bin $suffix_geom
$suffix_hyphen $suffix_lsu $go $in $to $out);

=head2 Instantiate classes

  message,flow,suchw,sushw

=cut

 my $log                = new message();
 my $run                = new flow();
 my $suchw           = new suchw();
 my $sushw           = new sushw();

=head2 Declare variables

  Make them local
```

```
=cut

 my ($endian,$num_files,$i);
 my (@segyfile,@segyfile_in,@segyfile_out);
 my (@segyread,@segyread_inbound,@segyread_outbound);
 my (@file,@sufile);
 my (@sufile_inbound,@sufile_outbound);
 my (@sufile_in,@sufile_out);
 my (@flow,@suchw,@sushw);
 my (@sushw_outbound,@sushw_headers_to_wipe,@sushw_replace_w_);
 my (@sushw_inbound);
 my (@items);

=head2 Establish

 file names and directories
 inbound and outbound refer to complete paths

=cut

  $file[1]                  = 'All_IR_1';

  $sufile_in[1] = $file[1].$suffix_su;
  $sufile_inbound[1]   = $DATA_SEISMIC_SU.'/'.$sufile_in[1];
  $sufile_outbound[1] = $DATA_SEISMIC_SU.'/'.$file[1].$suffix_geom.$suffix_su;

=head2 sushw information

 clean the unused header values
 but keep field traces fldr

=cut

  $sushw_inbound[1]   = $sufile_inbound[1];
  $sushw_outbound[1]     = $sufile_outbound[1];

 $sushw_headers_to_wipe[1]           =
'tracl,tracr,tracf,cdp,cdpt,trid,nvs,nhs,duse,swdep,scalel,scalco,counit,sx,sy,ep,fldr,year,day,minu
te,hour,sec';
 $sushw_replace_w_[1]                          =  '0,0,0,0,0,0,0,0,0,0,0,0,0,0,0,0,0,0,0,0,0,0,0,0,0,0,0';

=head2 Information about data files

sushw for I-beam
```

```
    $sushw->clear();
    $sushw->key($sushw_headers_to_wipe[1]);
    $sushw->first_val($sushw_replace_w_[1]);
    $sushw[1] = $sushw->Step();

    $sushw->clear();
    $sushw->key('fldr,tracl,tracf,tracr');
    $sushw->first_val('1,1,1,1');
    $sushw->intra_gather_inc('0,1,1,1');
    $sushw->inter_gather_inc('1,0,0,0');
    $sushw->gather_size('24,840,24,48');
    $sushw[2] = $sushw->Step();

    $sushw->clear();
    $sushw->key('offset,ep');
    $sushw->first_val('1,1');
    $sushw->intra_gather_inc('1,0');
    $sushw->inter_gather_inc('0,1');
    $sushw->gather_size('24,24');
    $sushw[3] = $sushw->Step();

    $sushw->clear();
    $sushw->key('sx');
    $sushw->first_val('1');
    $sushw->intra_gather_inc(0);
    $sushw->inter_gather_inc('1');
    $sushw->gather_size('24');
    $sushw[4] = $sushw->Step();

    $sushw->clear();
    $sushw->key('gx');
    $sushw->first_val('2');
    $sushw->intra_gather_inc(1);
    $sushw->inter_gather_inc('1');
    $sushw->gather_size('24');
    $sushw[5] = $sushw->Step();

=cut

    $sushw->clear();
    $sushw->key($sushw_headers_to_wipe[1]);
    $sushw->first_val($sushw_replace_w_[1]);
    $sushw[1] = $sushw->Step();

    $sushw->clear();
    $sushw->key('fldr,tracl,tracf,tracr');
```

```
    $sushw->first_val('1,1,1,1');
    $sushw->intra_gather_inc('0,1,1,1');
    $sushw->inter_gather_inc('1,0,0,0');
    $sushw->gather_size('24,1944,24,48'); #change the last value on this line to 48 after testing
(tracr) - if it doesn't work
    $sushw[2] = $sushw->Step();

    $sushw->clear();
    $sushw->key('offset,ep');
    $sushw->first_val('1,1');
    $sushw->intra_gather_inc('1,0');
    $sushw->inter_gather_inc('0,1');
    $sushw->gather_size('24,24');
    $sushw[3] = $sushw->Step();

    $sushw->clear();
    $sushw->key('sx');
    $sushw->first_val('1');
    $sushw->intra_gather_inc(0);
    $sushw->inter_gather_inc('1');
    $sushw->gather_size('24');
    $sushw[4] = $sushw->Step();

    $sushw->clear();
    $sushw->key('gx');
    $sushw->first_val('2');
    $sushw->intra_gather_inc(1);
    $sushw->inter_gather_inc('1');
    $sushw->gather_size('24');
    $sushw[5] = $sushw->Step();

=pod

  DEFINE FLOW(S)

=cut

 @items = ($sushw[1],$in,$sushw_inbound[1],$to,
          $sushw[2],$to,$sushw[3],$to,$sushw[4],
          $to,$sushw[5],$out,$sushw_outbound[1],$go);

 $flow[1] = $run->modules(\@items);

# RUN FLOW (s)
  $run->flow(\$flow[1]);
```

```
# LOG FLOW
  print $flow[1]."\n\n";
# $log->file($flow[1]);
```

APPENDIX B. DISPERSION CURVE PICKING

The following appendix describes how dispersion images and created and interpreted to yield dispersion curve data. The perl program Xphasevel.pl generates dispersion images created from a concatenated file of shotgathers when given a specific ep (shotpoint) from the seismic header information. The program prompts the user to input this concatenated shotgather file, followed by a prompt to input the ep (shotpoint) that will be used to make a dispersion image. Within Xphasevel.pl, it is important to note that a user can combine multiple shotpoints surrounding the indicated shotpoint if desired. In order to view the dispersion data picks after they have been made, a second image is generated with the picks after a set amount of time indicated at the bottom of the script.

B.1 Program: Xphasevel.pl

Program location: Zamin/home/bodom5/FalseRiver/seismics/pl/Bueche/All/H/1/bodom5

```
#!/usr/bin/perl

=head1 Documentation

=head2 Synopsis

        Program:        Xphasevel.pl
        Purpose:        Creation of a Dispersion Curve
        Author:         Derek S. Goff, modified by Nathan Benton and Blake Odom
        Date:           November 17 2013 V1.1
                Nov 28 2016, add perldoc (Juan M. Lorenzo)
                        Sep 15 2017, add disp image feedback display
        Description:    Implements  suphasevel.pm
                        Creates phase velocity dispersions

=head2 Uses
```

```
    Subroutines:
        manage_files_by
        System_Variables (for subroutines)

    Varibale Definitions:
        SeismicUnix (Seismic Unix modules)

=cut

 use Moose;
 use SeismicUnix qw ($in $out $on $go $to $suffix_ascii $off $suffix_su);
 use System_Variables;
 use message();
 use flow();
 use suximage();
 use suxwigb();
 use suamp();
 use suphasevel();
 use suifft();
 use sufilter();
 use sugain();
 use suflip();
 use suwind();
 use suop();
 use sufilter();
 use sushw();


=head2  Instanitiate Classes

        Create a new version of a package6
        Give it a new name if desired
   Use classes:
        flow
        log
        message
        sufilter
        suximage
      suop

=cut

 my $log                        = new message();
 my $run                        = new flow();
 my $suximage                           = new suximage();
```

```
 my $suxwigb                = new suxwigb();
 my $suamp                  = new suamp();
 my $suphasevel                     = new suphasevel();
 my $suifft                 = new suifft();
 my $sufilter               = new sufilter();
 my $sugain                 = new sugain();
 my $suflip                 = new suflip();
 my $suwind                 = new suwind();
 my $suop                   = new suop();
 my $smooth                 = new sufilter();
 my $sushw                  = new sushw();


=head2 Use directory navigation system

=cut

 my ($DATA_SEISMIC_SU) = System_Variables::DATA_SEISMIC_SU();
 my ($PL_SEISMIC)      = System_Variables::PL_SEISMIC();


=head2 Declare local variables


=cut

 my (@flow, @items);
 my (@suamp, @suximage, @suxwigb, @suphasevel, @sufilter, @sugain, @suflip);
 my (@suwind,@suop,@smooth,@sushw);
 my (@file_in, @sufile_in, @inbound, @file_out, @outbound);
 my (@outpicks);


=head2 Define the file name

   of the shot record to be used to
    compute a multi-mode phase velocity dispersion map

   IMPORTANT
  ->Please note that output files will be amped
  ->They will not be complex frequency data!!

=cut


#file input
```

```
print("Input File Name: \n");
my $inFile_name=<STDIN>;
chomp($inFile_name);
print("Input EP Number: \n");
my $ep=<STDIN>;
chomp($ep);

 $file_in[1]                    = $inFile_name;
 #$file_in[1]                   = $inFile;

 $sufile_in[1]                  = $file_in[1].$suffix_su;
 $sufile_in[1]                  = $file_in[1];

 $inbound[1]                    = $DATA_SEISMIC_SU.'/'.$sufile_in[1];

 $file_out[1]                   = $file_in[1]."_ep$ep".'_phvel';
 $outbound[1]                   = $DATA_SEISMIC_SU.'/'.$file_out[1].'.su';
 $outpicks[1]                   = $PL_SEISMIC.'/'.$file_out[1].'_picks';

 $file_out[1]                   = $file_in[1]."_ep$ep".'_phvel';

=head2 suphasevel

        fv = The starting phase velocity (pv) to process
            -> Not always in (m/s)
            -> Depends on units in geometry (header)
        nv = How many steps to take
            -> Number of velocities to test
        dv = Step Size0
            -> How large a gap between
                -> test velocities
        fmax = Maximum frequency to process

        fv+nv*dv = largest velocity tested

      scalel is needed to rescale the plotting and
      phasevel parameters

      my $default_scalel  = -1; # does nothing

=cut

 my $scalel        = -1;           #BTO
 my $dv           = 1;  #m
 my $new_dv        = $dv * (-$scalel);
```

```
 $suphasevel   -> clear();
 $suphasevel   -> fv("1");
 $suphasevel   -> nv("500");  #BTO
 $suphasevel   -> dv($new_dv);
 $suphasevel   -> fmax("40");#BTO
 $suphasevel   -> norm($off);
 $suphasevel   -> norm($on);
 $suphasevel   -> verb($on);
 $suphasevel[1]          = $suphasevel->Step();

#my $name_it="$file_out[1]"._picks';
#my $move_it="mv $name_it PhasevelPicks";
#system($move_it);
#print("\n\n\n $move_it \n\n\n");

=head2 Set suximage parameters

 These default settings will generate an image of
 the dispersion curve for viewing
 For actual data output

 $suximage-> style('normal'); # y axis is phase velocity
 $suximage-> style('seismic'); # y axis is phase velocity
 my $new_d2 = $dv;
 $suximage ->d2($new_d2);

=cut

 $suximage-> clear();
 $suximage-> title($file_out[1]);
 $suximage-> xlabel("Phase_Velocity");
 $suximage-> ylabel("Frequency");
 $suximage-> box_width(1100);        #BTO changed this
 $suximage-> box_height(900);
 $suximage-> cmap("hsv6"); #hsv0 for black and white
 $suximage-> legend($on); #hsv0 for black and white
 $suximage-> box_X0(1700);#nathan changed this (today?)
 $suximage-> picks(\$outpicks[1]);
 $suximage-> box_Y0(100);
 $suximage-> hiclip(3);
 $suximage-> loclip(0);
 $suximage-> legend($on);
 $suximage-> windowtitle("Dispersion Image");
 $suximage[1]  = $suximage->Step();

=head2 Create Input Image
```

```
 #$suxwigb-> clear();
 ##$suxwigb -> key('tracf');
 #$suxwigb-> title($file_in[1]);
##$suxwigb-> xlabel("Offset");
 #$suxwigb-> xlabel("Trace");
 #$suxwigb-> ylabel("TWTT_s");
 #$suxwigb-> box_width(800);
 #$suxwigb-> box_height(700);
 #$suxwigb-> box_X0(50);
 #$suxwigb-> box_Y0(50);
 #$suxwigb-> clip(10);
 #$suxwigb-> windowtitle("Original_Data");
 #$suxwigb[1]  = $suxwigb->Step();

=cut

=head2 Set amplitudes

 make output absolute

=cut

 $suop-> clear();
 $suop-> abs();
 $suop[1] = $suop->Step();


=head2 Smooth phase vel plot

 freq resolution sufiltered out
 needs to know in advance the dimension
 of the fft and the number of
 phase-velocity traces

=cut

 $sushw-> clear();
 $sushw-> key('trid');
 $sushw-> key('trid');
 $sushw-> first_value('1');
 $sushw-> inter_gather_inc('0');
 $sushw-> intra_gather_inc('0');
 $sushw[1] = $sushw->Step();
```

```
=head2 Smooth phase vel plot

 freq resolution sufiltered out
 needs to know in advance the dimension
 of the fft and the number of
 phase-velocity traces

=cut

 $smooth-> clear();
 $smooth-> freq('0,0,40,100');
 $smooth-> amps('1,1,1,0');
 $smooth[1] = $smooth->Step();


=head2 Set type of traces to output

          amp gives amplitude traces
          phase gives phase traces...
          see suamp.pm for further instruction
    -> None are really neccessary
    -> amp is default

=cut

 $suamp-> clear();
 $suamp-> mode('real');
 $suamp[1] = $suamp->Step();


=head2 Set Filtering Parameters

=cut

 $sufilter-> clear();
 $sufilter-> freq("0,0,80,100");          #BTO
 $sufilter[2]  =  $sufilter->Step();

=head2 Add Gain to traces

=cut

 $sugain         -> clear();
 $sugain         -> agc($on);
 $sugain         -> width(.1);
```

```
 $sugain[1]   =    $sugain->Step();

=head2 Add Gain to output of suamps

=cut

 $sugain         -> clear();
 $sugain         -> pbal($on);
 $sugain[1]   =    $sugain->Step();

=head2 Window time value of traces

=cut

 $suwind         -> clear();
 $suwind         -> key('ep');
 $suwind         -> min(($ep-2));#Need double parenthetical to stack disp images from
neighboridng ep
 $suwind         -> max(($ep+2));#
 $suwind[1] = $suwind->Step();

=head2  Window by offset traces

  in meters
=cut

 my $min_offset         = 1 ;
 #my $max_offset       = 96 ;
 my $max_offset         = 24 ;
 my $new_min_offset           = $min_offset * (-$scalel);
 my $new_max_offset           = $max_offset * (-$scalel);


 $suwind         -> clear();
 $suwind         -> key('offset');
 $suwind         -> min($new_min_offset);
 $suwind         -> max($new_max_offset);
 $suwind[3] = $suwind->Step();

=head2 Window by time

  Window by time

=cut

 $suwind         -> clear();
```

```
$suwind         -> tmin(0);
$suwind         -> tmax(1);
$suwind[2] = $suwind->Step();


=head2

 Create Window for picking

=cut

=head2 Define Flows

=cut

=head2  Create outbound file

=cut

 @items = ($suwind[1],$in,$inbound[1],
          $to,$suwind[2],
          $to,$suwind[3],
          $to,$sufilter[2],
          $to,$suphasevel[1],
          $to,$suamp[1],
          $out,$outbound[1],
          $go);

 $flow[1]        = $run -> modules(\@items);

=head2 Produce image of input shot record



Produce image of input shot record

=cut

 @items = ($suwind[1],$in,$inbound[1],
          $to,$suwind[2],$to,$suwind[3],
             $to,$sufilter[2],
             $to,$sugain[1],
             $to,$suxwigb[1],
             $go);
 $flow[2]        = $run -> modules(\@items);
```

=head2 Phasevel dispersion image w filter or gain, Windowed

Phasevel dispersion image w filter or gain, Windowed

=cut

```
 @items       = ($suwind[1],$in,$inbound[1],
                ,$to,$suwind[2],
                $to,$suwind[3],
                $to,$sufilter[2],
                $to,$suphasevel[1],
                $to,$suamp[1],
                $to,$sugain[1],
                $to,$suximage[1],$go);
 $flow[3]     = $run -> modules(\@items);
```

=head2 Run Flows

=cut

```
 $run->flow(\$flow[1]);
# print $flow[3]."\n";

 $run->flow(\$flow[2]);
 #print $flow[2]."\n";  #nathan did this

 $run->flow(\$flow[3]);
 #print $flow[3]."\n"; #anathan did this
 #print $flow[6]."\n";


#Danger Zone---------------------------------------------------

sleep 0.005;

my $ar1="$suwind[1] $in $inbound[1] $to $suwind[2] $to $suwind[3] $to $sufilter[2] $to
$suphasevel[1] $to $suamp[1] $to $sugain[1] > inFile_1.su";
my $blah="cat $outpicks[1] > A1.txt";
my $commando2='suximage npair=$(wc -l < A1.txt) curve=A1.txt < inFile_1.su &';

system($ar1);
system($blah);
#system($commando1);
system($commando2);
```

APPENDIX C. INVERSION TARGET CREATION AND PARAMETERIZATION

This appendix details major treatments and processes that raw dispersion pick files must undergo before batch inversion is conducted. The flowchart and table below summarize these steps.

Figure C.1. Basic Steps in converting dispersion picks into properly processed target files for use in batch inversion.

Table C.1: Table explaining the steps shown in above Figure C.1.

Step	Details
1. Parsing	• Converts 2 column files (Freq|Phase velocity) to 4 column file needed for target conversion (Freq|Slowness|Stdev|Weight)
2. Frequency Cutting and Resampling	• Frequency resampling for 50 samples on a frequency (linear) scale • Frequency cutting based on desired data limitations
3. Target File Creation	• Converts 4 column text file into .target file required for batch inversion in dinver • Also indicates that dispersion data is Love wave based

C.1. Program: Xresample_TargetMaker.sh

Program Location:
Zamin/home/bodom5/FalseRiver/seismics/geopsy/Bueche/All/H/1/bodom5/PicksPreparation

This shell script performs all of the steps indicated in the above table. The File-in section of the script must be given the specific text pick files. The final output file .target are needed for Xdinver.pl batch inversion.

```
#!/usr/bin/perl

#=pod
#
#=head1 Documentation
#
#=head2 Synopsis
#
#       Program:        Xresample.pl
#       Purpose:        To do frequency cutting, resampling of dispersion curves, and creation of target files
#       Author:         Blake Odom and Nathan Benton
#       Date:           January 24 2018
#       Description:    Implements gpcurve to cut and resample ASCII files of disperison data by frequency for higher quality inversion results
#                       Also changes the structure of the ASCII file format so they may act as target files for the Dinver inversion used in Xdinver.pl
#                       More information at http://www.geopsy.org
#                       This program uses geopsy modules gpcurve and gptarget
#
#=head2 Uses
#
#       Subroutines:
#
#       Variable Definitions:
#
#
#
#=cut

#Single Text File That Contains all of the Raw Dispersion Pick Files' Names
##This is done because of the existing data gaps in the Bueche
###For New set of dispersion pick files, just copy and past all of the file names directly into this script

for inFile_1 in as.su_ep100_phvel_picks
```

; do

#Part 1: Parse

#This formats the original ASCII pick file (Frequency|Velocity) into the target file format accepted by Dinver inversion (Frequency|Slowness|Stdev|Weight). Stdev and Weight are always 0 and 1 respectively. This is done in the sed
#Velocity is turned into slowness simply by taking the reciprocal in the awk
awk '{ rec = 1 / $2; print $1,rec }' ${inFile_1} > ${inFile_1}_out.txt
sed 's/$/&\t0\t1/' ${inFile_1}_out.txt > ${inFile_1}_rec_par.txt

#Part 2: Frequency Cut

#This uses gpcurve to apply a cut to the frequencies. Anything below 2 Hz or anything above 50 Hz is cut.

gpcurve ${inFile_1}_rec_par.txt -cut -min 2 -max 50 > ${inFile_1}_cut_out.txt

#Part 3: Resampling

#gpcurve does the resampling of 50 samples between the frequency min and max for the particualr disperision curve. The resampling is done on a frequency-scaling (linear scaling), which is the default.
#This final step outputs a .target file that can be easily fed into the inversion program Dinver

gpcurve ${inFile_1}_cut_out.txt -resample 50 > ${inFile_1}.resampled

#Part 4: Creating a Target File Using gptarget

#awk prints the columns of each txt trgt file, then pipes it into gptarget which creates a love wave target that contains the relevant disperison image

awk '{ print $1,$2,$3,$4 }' ${inFile_1}.resampled | gptarget A -L 0 ${inFile_1}.target

#THis exec command closes the stdin that is piped into the gptarget. It functions like Ctrl-D on the command line, marking the completion of the input stdint

exec <&-

#0<&-

done

echo Done;

C.2. Synthetic Dispersion Curve Creation with Gplivemodel and Gptarget

The *Geopsy* programs Gplivemodel and Gptarget allow the user to create and view layer models using a GUI, then creates a synthetic dispersion curve for the model that allows for inversion testing for different scenarios possible in the actual dispersion data.

The GUI Gplivemodel allows the user to enter in P and S wave velocities along with thickness and density to form a visual layer model. This program is used to tweak and select layer models to be turned into synthetic theoretical dispersion curves. To enter the GUI, the user most only type gplivemodel into the command line. Once in the program's GUI. A box in the lower right hand corner will prompt the user to enter in the velocity model in the format:

6 (number of layers including the half space)

(thickness)	(P velocity)	(S velocity)	(Density)
2	500	100	1700
-	-	-	-
-	-	-	-

If the number of layers (rows) do not equal the number indicated on the first line of the data, then the layer model will not be visible. Once the user is satisfied with the visual of their layer model, copy the rows and columns (including the first line number of layers) and save the data in an ASCII file as [name].model.

Once this file is created, then gpartget can be used from the command line to create a dispersion curve file form this layer model. Into the command line the user must type:

gptarget [Name].model –L 1 –R 0 > [Name].disp

If using Rayleigh wave data instead of love wave data, the command would read –L 0 –R 1 instead. Once this .disp file has been created, it is ready to be brought into the Dinver GUI just like any other dispersion curve to be tested for inversion parameterization.

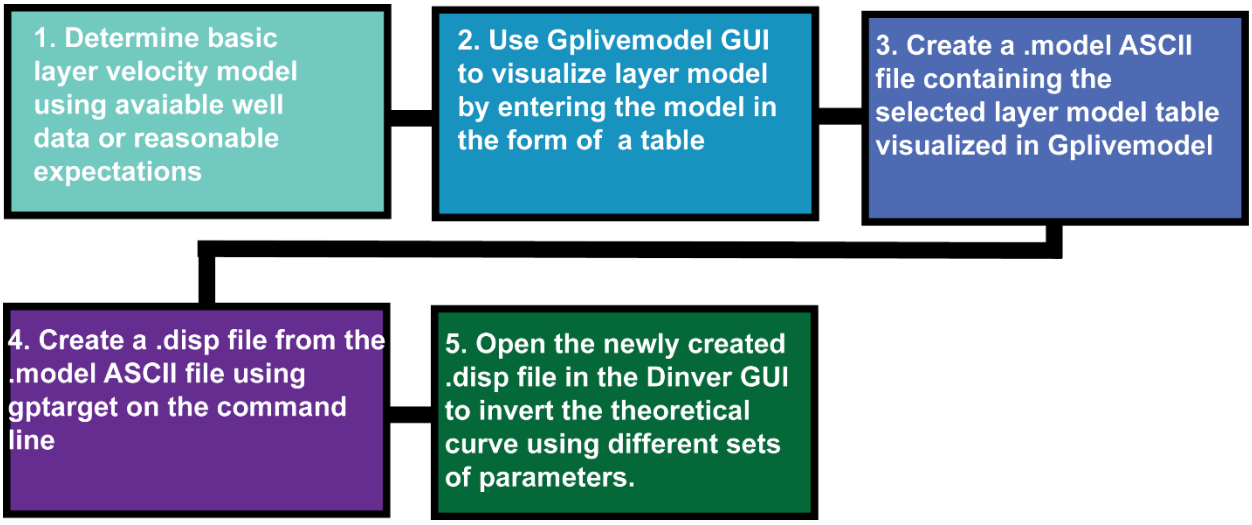

Figure C.2. Steps needed to create, view, and convert theoretical velocity models into dispersion curves that can be inverted to test parameterization against different potential subsurface velocity scenarios.

APPENDIX D. INVERSION AND EXTRACTION

The following appendix discusses the process of batch inversion, including the scripts required to actually undertake the inversion itself, as well as extract information from the inversion results that can be used to interpolate a 2D profile of velocity data.

Before batch inversion and Xdinver.pl can be run, .target files must be placed in a specific target directory, and user-designated .param parameterization files must first be created in Geopsy's dinver GUI program, then placed into a Param folder. Before attempting batch inversion, the user should first become familiar with dinver. Proper use of modeling specifications and parameterization will save computing time, and ensure data-specific decisions are made or understood before applying the process to every single dispersion file in a batch-sense.

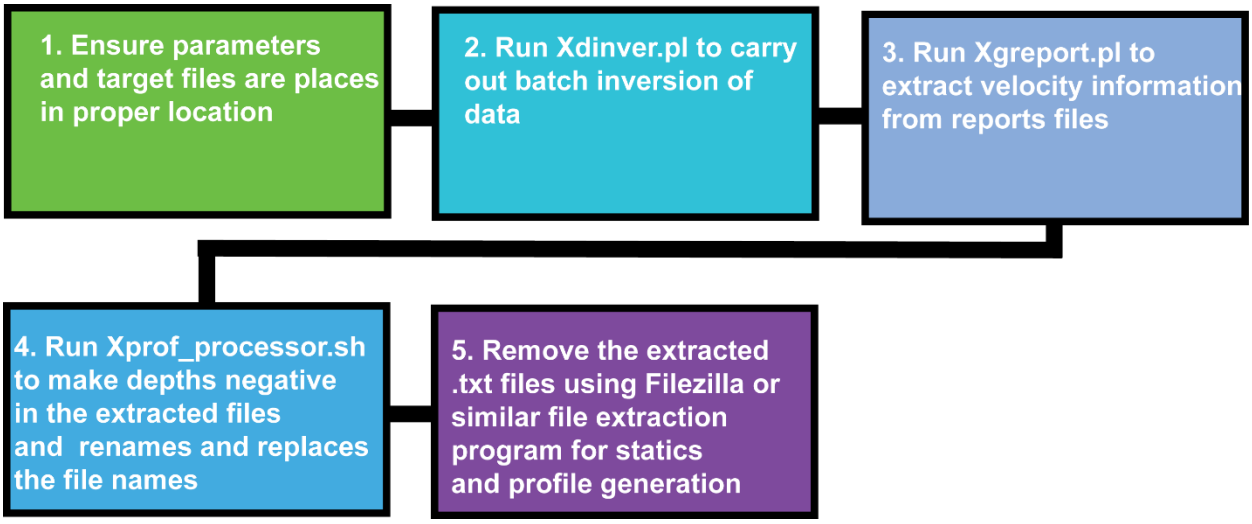

Figure D.1. Steps in batch inversion, reports file extraction to a ASCII file, and converting the depth in that file to be negative.

D.1. Program: Xdinver.pl

This perl script undertakes the actual inversion. Zones below commented with multiple asterix indicate an area of major user input.

Program Location: Zamin/home/bodom5/FalseRiver/seismics/geopsy/Bueche/All/H/1/bodom5

```
#!/usr/bin/perl

=pod

=head1 Documentation

=head2 Synopsis

        Program:        Xdinver.pl
        Purpose:        Inversion of Dispersion Curve
        Author:         Derek S. Goff
        Date:           May 1 2015
        Modifications:  Blake Odom Jan 30 2018
        Description:    Implements  suphasevel.pm
                        Inverts Dispersion Curve using
                        Geopsy's dinver program
                More information at http://www.geopsy.org
        Changes by Blake:      Changed inversion inputs and Filein (to change by ep) for Woody and Bueche Falseriver seismic data
=head2 Uses

    Subroutines:
        manage_files_by
        System_Variables (for subroutines)
cd /usr/local
    Varibale Definitions:
        SeismicUnix (Seismic Unix modules)

=cut

 use Moose;
 use SeismicUnix qw ($in $out $on $go $to $suffix_ascii $off $suffix_su);
 use System_Variables;
 use message();
 use flow();
 #use SU;
 #use lib '/home/usr/local/geopsy';
```

```
use Dinver;
use File::Path qw(make_path remove_tree);

my $log                         = new message();
my $run                         = new flow();
my $dinver                      = new Dinver();


=pod

 2. Utilize zamin.lsu.edu directory navigation syste

=cut

 my ($DATA_SEISMIC_SU) = System_Variables::DATA_SEISMIC_SU();
 my ($GEOPSY) = System_Variables::GEOPSY();


=pod

 Set Geopsy Directory File System (NEED TO FIX BECAUSE IT IS NOT GOING TO
BODOM5 Sub-geopsy folder!!)

=cut

 my ($GEOPSY_PARAM)    = $GEOPSY.'param/';
 my ($GEOPSY_TARGET)   = $GEOPSY.'target/';
 my ($GEOPSY_ENV)      = $GEOPSY.'env/';
 my ($GEOPSY_REPORTS) = $GEOPSY.'reports/';

=pod

 Create Geopsy Directory system if it doesnt exist

=cut

if (-e $GEOPSY_PARAM) {#do nothing
}
else { make_path("$GEOPSY_PARAM", "$GEOPSY_TARGET", "$GEOPSY_ENV",
"$GEOPSY_REPORTS",
                { verbose => 1, mode => 0771 });
}

my (@flow, @items);
my (@dinver,@parameters);
my (@file_in, @target_in, @inbound, @file_out, @outbound);
```

```
my $t_suffix = '.target';
my $p_suffix = '.param';
my $r_suffix = '.report';
my $start_ep = 1;   #Indicate Here which ep should start this run


for ( my $ep=$start_ep; $ep <=481; $ep+=1) {                    #Indicate Here which ep to stop at
for a given run. Also can change increment if needed.

        $file_in[1] = $GEOPSY_TARGET.$ep.'_phvel_picks';
        $target_in[1] = $file_in[1].$t_suffix;
        $inbound[1] = $target_in[1];
        $parameters[1] = $GEOPSY_PARAM."Buche_New_faster".$p_suffix;
        $file_out[1] = $GEOPSY_REPORTS."Bueche_New_".$ep;
        $outbound[1] = $file_out[1].$r_suffix;
=pod

 Set Dispersion Curve Inversion options
 See Dinver.pm for more information

=cut

 $dinver         -> clear();
 $dinver         -> plug("DispersionCurve");
 $dinver         -> target($inbound[1]);
 $dinver         -> param($parameters[1]);
 $dinver         -> itmax("100"); # 0 iterations = Pure Monte Carlo
 $dinver         -> ns0("50"); # Initial Models to create
 $dinver         -> ns("300"); # Models per iteration
 $dinver         -> nr("50"); # Best Models to consider
 $dinver         -> output($outbound[1]);
# $dinver        -> force();
# $dinver        -> resume();
 $dinver[1] = $dinver->Step();

 print ($dinver[1]."\n");
 system ($dinver[1]);
 print ("\n\nMoving to next target\n");

}

#close for loop
```

D.2. Program: Xgreport.pl

This perl script extracts data from the .reports file created for each given shotpoint by Xdinver.pl. From these .reports file Xgreport.pl looks for a mean or median velocity value for incremental depths indicated by the user. It outputs a multi-column .txt file that can be used for interpolation and 2D profile creation.

Program Location: Zamin/home/bodom5/FalseRiver/seismics/geopsy/Bueche/All/H/1/bodom5

```
#!/usr/bin/perl

=pod

=head1 Documentation

=head2 Synopsis

        Program:        Xgreport.pl
        Purpose:        Extract Vs Profiles from inversion
        Author:         Derek S. Goff
        Date:           May 1 2015
        Description:    Implements  Gpdcreport.pm
                        Extracts information from geopsy .report files
                        using Geopsy's gpdcreport program
                    More information at http://www.geopsy.org

        Fully implement the following bash code into a perl program:
        gpdcreport /home/dereg/LondonAvenueCanal/seismics/geopsy/060112/Z/reports/5lay_-
495_-480.report -gm -best 10 | gpprofile -vs -resample -d 25 -n 25 | grep -v "#" | awk '{print
$2,$1}'|gphistogram -x-count 25 -mean

        Version 0.2 to use | gphistogram -x-count -x-min...

=head2 Uses

    Subroutines:
        manage_files_by
        System_Variables (for subroutines)

    Varibale Definitions:
        SeismicUnix (Seismic Unix modules)
```

```
=head2 Output Data

        col1: depth (m)
        col2: Vs (m/s)
        col3: Standard deviation (m/s)
        col4: ? Probably number of samples in bin (like fold)
        col5: cmp

=cut

 use Moose;
 use SeismicUnix qw ($in $out $on $go $to $suffix_ascii $off $suffix_su);
 #use SU;
 use message();
 use FileHandle;
 use flow();
 use Gpdcreport; # requires .pm file. Can be found in gom/archive and must be copied into
/usr/local/pl
 use Gpprofile; # requires .pm file. Can be found in gom/archive and must be copied into
/usr/local/pl
 use Gphistogram; # requires .pm file. Can be found in gom/archive and must be copied into
/usr/local/pl
 use Gpviewdcreport; # requires .pm file. Can be found in gom/archive and must be copied into
/usr/local/pl
 use File::Path qw(make_path remove_tree);
 use Data::Dumper;

 my $log                    = new message();
 my $run                    = new flow();
 my $gpdc                   = new Gpdcreport();
 my $gpprof                 = new Gpprofile();
 my $gphist                 = new Gphistogram();
 my $gpview                 = new Gpviewdcreport();
=pod

 2. Utilize zamin.lsu.edu directory navigation system


=cut

 my ($DATA_SEISMIC_SU) = System_Variables::DATA_SEISMIC_SU();
 my ($GEOPSY) = System_Variables::GEOPSY();


=pod
```

Set Geopsy Directory File System

=cut

```
 my ($GEOPSY_PARAM)    = $GEOPSY.'param/';
 my ($GEOPSY_TARGET)   = $GEOPSY.'target/';
 my ($GEOPSY_ENV)      = $GEOPSY.'env/';
 my ($GEOPSY_REPORTS) = $GEOPSY.'reports/';


my (@flow, @items);
my (@gpdc,@parameters, @report_in, @temp_out);
my (@file_in, @target_in, @inbound, @file_out, @outbound);
my (@gpprof, @gphist, @gpview);

my $t_suffix = '.target';
my $p_suffix = '.param';
my $r_suffix = '.report';
my $start_ep =1;


 print("\n You may need to clear the output profile \n");

#Define EP range, file in names, and file out names
for ( my $ep=$start_ep; $ep <=481; $ep+=1)

{       #Open forloop for ep variable definition


        $file_in[1] = $GEOPSY_REPORTS.'Bueche_New_'.$ep;              #Must Have the
proper .report file name that CURRENTLY exists in the /reports directory
                #Set the input file name
        $report_in[1] = $file_in[1].$r_suffix;
        $inbound[1] = $report_in[1];
#       $parameters[1] = $GEOPSY_PARAM."5lay".$p_suffix;
        $temp_out[1] = $GEOPSY."\.temp_prof";
        $temp_out[2] = $GEOPSY."\.temp_prof2";
        $file_out[1] = $GEOPSY."Profile_moresamples_3000_median_1.7mres.txt";
        #Output File Name. Make Sure this reflections your best sample number and
mean/median.
        $outbound[1] = $file_out[1].$r_suffix;

        print("$ep");
=pod
```

Use this section to define several common variables

1)Number of models to use
2)What depth of investigation to look at
3)How often to sample along the profile according to depth

=cut

```
 my $models          = "3000"; # Number of models to use from report                    #This
should be roughly 10 percent of the total number of valid models from the inversion
 my $depth           = "20";   # Depth of investigation for the bins
 my $depth_interval  = "1.7";   # Sample interval you would like to use in meters
 my $start_depth     = "0";  #Depth to start profile at
 my $grid_population = "40";   # Pertains to number of samples in each bin
##############################################################
 my $x_int      = (($depth/$depth_interval)+(1-($start_depth/$depth_interval)));
 my $xk_limit = ($x_int-1);
#my $x_int     = (($depth/$depth_interval));
#my $xk_limit= ($x_int-1);

$gpdc           -> clear();
$gpdc           -> gm();
$gpdc           -> best($models);
$gpdc           -> file($inbound[1]);
$gpdc[1] = $gpdc->Step();

$gpprof                 ->clear();
$gpprof                 ->vs();
$gpprof                 ->resample();
$gpprof                 ->depth($depth);
$gpprof                 ->samples($grid_population); #Grid Population (number each bin)
$gpprof[1] = $gpprof->Step();

$gphist         ->clear();
$gphist         ->xcount($x_int);
$gphist         ->xmin($start_depth);
$gphist         ->median(); # mean() = mean ; median() = median
$gphist[1] = $gphist->Step();


 @items = ($gpdc[1],$to,$gpprof[1],$to,"grep -v \"#\" $to awk \'{print
\$2,\$1}\'",$to,$gphist[1],"$to grep -v \"#\"",$out,$temp_out[1]);
  $flow[1]      = $run -> modules(\@items);

 #@items = ($gpdc[1],$to,$gpprof[1],$to,"grep -v \"#\" $to awk \'{print
\$2,\$1}\'",$to,$gphist[1],"$to grep -v \"#\"",$out,$temp_out[1]);
 # $flow[1]     = $run -> modules(\@items);
```

```
 $run->flow(\$flow[1]);
# print $flow[1]."\n";

=pod

Create an array from the temp file
Append the ep number onto the array
Create new file that is appended with each profile

=cut



 #Create an array of arrays to handle the profile
 my @AoA;

 for my $i (0..$xk_limit)
{ # open for my $i
        open my $FH, "<" ,"$temp_out[1]" or die "Couldn't open file";
        while (<$FH>) {
                chomp $_;               #chomp default variable
                push (@AoA,[ split(' ')]); #This push just tells the array creator where to end each
string opened from the output of the geopsy modules.
                        }
        close $FH;
#Create new column populated by the ep of the profile
        #for my $i (0..$xk_limit)                        #BTO
        #{                                               #BTO
        push (@{$AoA[$i]}, "$ep");  #ep gets added properly but does not have a space between
it and the column?




} # close for my $i

 #Output the array of array profile to a text file
 open my $OUT, ">>", "$file_out[1]" or die "Couldn't write file";
        for my $j (0..$xk_limit) {
          for my $k (0..4) {
        #print $OUT "$AoA[$j][$k]";
        print $OUT "$AoA[$j][$k] ";          #This works to put the space in between elements!
This prints out the Array of arrays, including the appended EP. the space between the j and k
delimts output columns with spaces
          } #$k
        print $OUT "\n";
```

```
        } #$j
        close $OUT;


} # close for ep for loop

print ("$file_out[1] \n");
```

D.3. Program: Xprof_processor.sh

Program Location: Zamin/home/bodom5/FalseRiver/seismics/geopsy/Bueche/All/H/1

```
#Program:               Xprof_processor.sh
#Author:                Blake Odom
#Date:          Feb 2018
#Purpose:               This Shell Script takes a profile file (.txt) and #multiplies the first column
by -1 so that it appears properly as #depth in the Surfer



#Copies the original Xgreport.pl .txt file to an arhcive folder within the geopsy directory

for  file in bodom5Profile_* ; do

cp "$file"
/home/bodom5/FalseRiver/seismics/geopsy/Bueche/All/H/1/bodom5/SavedProfiles/ArchiveProfi
les ;


done


# 1. Makes Depth Negative
for  file in bodom5Profile_* ; do


awk '{ rev = $1 * -1 ; print rev,$2,$3,$4,$5 }' $file > rev_$file ;


done


# 2. Renames The New File
for  file in rev_bodom5Profile_* ; do
```

```
mv "$file" "${file#rev_bodom5}" ;

done



# 3. Removes The Old file
for  file in bodom5Profile_* ; do

rm -f "$file" ;

done




# 4. Moves newly reversed profile to the SavedProfiles directory in geopsy
for  file in Profile_* ; do

mv "$file" /home/bodom5/FalseRiver/seismics/geopsy/Bueche/All/H/1/bodom5/SavedProfiles ;

done



# 4. Removes the Temp file created by Xgreport.pl
for file in bodom4.temp_prof ; do

rm -f "$file" ;

done



#echo Done;
```

APPENDIX E. CREATION OF PSUEDO 2D PROFILES

For each profile generated by Xgreport.pl and edited by Xprof_processor.sh, should now exist a .txt file containing columns of depth, velocity, velocity range, sampling, and shotpoint. Before this profile can be gridded by the program Surfer, it needs to be corrected for topography. The following matlab script StaticsCorrector.m reads in this profile .txt file, as well as a 2 column file containing a column of ep and a column of the necessary elevation change based on a determined datum that is typically the lowest point on the survey topographically. The elevation numbers and derived corrections were taken from the Louisiana State Lidar project extracting using ArcGIS.

E.1. Program: XstactisCorrector.m

```
% %
% % Applies a statics correction to individual EP's based of a profile when
% given a ep-elevation change file. From datum of the lowest point (~ep200)
% % Author: Blake Odom and Nate Benton
% % Date: Feb 2018
% %
% %
% ----------------------------------------------------------

tic
clc

addpath('C:\Users\bodom5\Documents\MATLAB');
addpath('C:\Users\bodom5\Desktop\SurferProfiles\Bueche');

bigFile=dlmread('Profile_TEST_1000_mean_1.7mres.txt');
littleFile=dlmread('Bueche_Elevation_Correction.txt');

[bF_rs,bF_cs]=size(bigFile);
[lF_rs,lF_cs]=size(littleFile);
total_count=1;

for i1=1:lF_rs,
   for i2=1:bF_rs,
```

```
      if(littleFile(i1,1)==bigFile(i2,5))
         bigFile(total_count,6)=bigFile(total_count,1)+littleFile(i1,2);
         total_count=total_count+1;
      end
   end
end

dlmwrite('Bu_Profile_TEST_1000_mean_1.7mres.txt',bigFile,'delimiter','\t');

toc
```

E.2. Surfer Gridding

The settings for gridding the data and making a pseudo 2D profile are numerous in their scope and specialty. The settings used to grid the data in this study are as follows for the two different surveys:

Bueche Survey:

Gridding: Kriging	Xnodes: 200	Ynodes: 11	Colorbar Range: 50 to 500 m/s

Woody Inline and Crossline Surveys

Gridding Kriging	Xnodes: 40	Ynodes: 20	Colorbar Range 50 to 500 m/s

VITA

A native of Houston, Texas, Blake T. Odom was born in 1993. He graduated from the Kinkaid School in Houston before enrolling in Washington & Lee University in Lexington, Virginia. Under the tutelage of Dr. Christopher Connors, Blake graduated from W&L with a B.S. in Geology in 2016. Seeking a more technical experience with geophysics, Blake decided to enroll at LSU for his Master's, working with Dr. Juan Lorenzo. In his leisure time, Blake enjoys golf, squash, skiing, hunting, and the hallowed Windfall Wednesdays.